

1
2
3
4
5
6
7
8
9
10
11
12
13
14
15
16
17

How many neurons are sufficient for perception of cortical activity?

Henry W. P. Dagleish^{*1,3}, Lloyd E. Russell^{*1}, Adam M. Packer^{*1,2}, Arnd Roth¹, Oliver M. Gauld¹,
Francesca Greenstreet^{1,3}, Emmett J. Thompson^{1,3}, Michael Häusser¹

¹ *Wolfson Institute for Biomedical Research, University College London, Gower Street, London WC1E 6BT, UK*

² *Present address: Department of Physiology, Anatomy and Genetics, University of Oxford, UK*

³ *Present address: UCL Sainsbury Wellcome Centre for Neural Circuits and Behaviour, London, UK*

* These authors contributed equally

Correspondence should be addressed to M.H. (m.hausser@ucl.ac.uk)

18 **Abstract**

19 Many theories of brain function assume that information is encoded and behaviour is
20 controlled through sparse, distributed patterns of activity. It is therefore crucial to
21 place a lower bound on the amount of neural activity that can drive behaviour and to
22 understand how neuronal networks operate within these constraints. We use an all-
23 optical approach to test this lower limit by driving behaviour with targeted two-photon
24 optogenetic activation of small ensembles of L2/3 pyramidal neurons in mouse barrel
25 cortex while using two-photon calcium imaging to record the impact on the local
26 network. By precisely titrating the number of neurons in activated ensembles we
27 demonstrate that the lower bound for detection of cortical activity is ~14 pyramidal
28 neurons. We show that there is a very steep sigmoidal relationship between the
29 number of activated neurons and behavioural output, saturating at only ~37 neurons,
30 and that this relationship can shift with learning. By simultaneously measuring activity
31 in the local network, we show that the activation of stimulated ensembles is balanced
32 by the suppression of neighbouring neurons. This surprising behavioural sensitivity in
33 the face of potent network suppression supports the sparse coding hypothesis and
34 suggests that perception of cortical activity balances a trade-off between minimizing
35 the impact of noise while efficiently detecting relevant signals.

36 **Introduction**

37 How does activity in neural circuits give rise to behaviour? While mammalian brains
38 are composed of many millions (Herculano-Houzel, Mota, & Lent, 2006) or billions
39 (Herculano-Houzel, 2009; Herculano-Houzel, Collins, Wong, & Kaas, 2007) of
40 neurons it has long been postulated that they operate – encoding information and
41 controlling behaviour – through the activity of small subsets of those neurons (Barlow,
42 1972). Indeed, the hypothesis that brains use sparse, distributed activity patterns is
43 supported computationally (Kanerva, 1993; Olshausen & Field, 1996), energetically
44 (Attwell & Laughlin, 2001; Lennie, 2003; Schölvinck, Howarth, & Attwell, 2008) and
45 experimentally (Barth & Poulet, 2012; Olshausen & Field, 2004; Wolfe, Houweling, &
46 Brecht, 2010). A major factor thought to govern such sparse coding is neuronal
47 inhibition (Haider & McCormick, 2009; Isaacson & Scanziani, 2011) which serves to
48 balance and control recurrent excitation (Denève & Machens, 2016; Haider, Häusser,
49 & Carandini, 2013; Murphy & Miller, 2009; Packer & Yuste, 2011; Pehlevan &
50 Sompolinsky, 2014; Sadeh & Clopath, 2020; Tsodyks, Skaggs, Sejnowski, &
51 Mcnaughton, 1997; van Vreeswijk & Sompolinsky, 1996; Wehr & Zador, 2003; Wolf,
52 Engelken, Puelma-Touzel, Weidinger, & Neef, 2014) and shape neuronal output
53 (Borg-Graham, Monier, & Frégnac, 1998; Cardin, Kumbhani, Contreras, & Palmer,
54 2010; Isaacson & Scanziani, 2011; Lee et al., 2012; Wilson, Runyan, Wang, & Sur,
55 2012). Two key questions are therefore: (1) What is the lower bound of activity that
56 can be behaviourally salient? and (2) How does such activity interact with the local
57 network?

58

59 Classical microstimulation experiments have demonstrated that focal activation of
60 cortical regions can influence decision-making, providing a direct causal link between
61 neural activity and behaviour (Cohen & Newsome, 2004; Murasugi, Salzman, &
62 Newsome, 1993; Salzman, Britten, & Newsome, 1990; Salzman, Murasugi, Britten, &
63 Newsome, 1992). This landmark work has been complemented by more recent
64 studies showing that optogenetic activation of dozens to hundreds of cortical
65 neurons can be directly detected (Huber et al., 2008; Histed and Maunsell, 2014). A
66 further refinement of this approach was provided by patch-clamp recording, which
67 revealed that strong electrical stimulation of even a single neuron can be detected in
68 a cell-type and spike timing-dependent manner (Houweling and Brecht, 2008; Doron
69 et al., 2014), to the extent that they can modulate behaviour in sensory-guided tasks
70 (Tanke, Borst and Houweling, 2018). While these studies have provided important
71 approximations of the numbers of neurons required to trigger and manipulate
72 behaviour, they suffered from several important limitations. Firstly, electrical
73 stimulation techniques are ill-suited to titrating the number of neurons stimulated and
74 offer limited targeting specificity, either indiscriminately activating swathes of cortex
75 or activating single neurons. Secondly, one-photon optogenetic approaches, while
76 limiting direct excitation to genetically defined neurons, only offer post-hoc estimation
77 of the number of neurons stimulated from histology (Huber et al., 2008). Finally, in
78 none of these studies has it been possible to carefully assess the impact of the
79 stimulation on the local network, an essential step if we are to understand the link
80 between activity generated by stimulation and behaviour.

81

82 A parallel body of work has investigated the influence of neural activity on local
83 networks *in vivo*, demonstrating that small numbers of active neurons can have a
84 large impact on local network dynamics and brain state. Strong stimulation of single
85 pyramidal neurons in L2/3 has been shown to recruit ~2% of local excitatory neurons
86 and ~30% of local inhibitory neurons (Kwan and Dan, 2012). A single pyramidal
87 neuron spike in L5 is estimated to recruit ~28 post-synaptic neurons (London et al.,
88 2010) and in L2/3 can trigger strong disynaptic inhibition (Jouhanneau, Kremkow and
89 Poulet, 2018). Single neurons can also trigger global switches in brain state (Li, Poo
90 and Dan, 2009), influence network synchronization (Bonifazi et al., 2009) and have a
91 direct impact on motor output (Brecht et al., 2004). However, work investigating the
92 impact of sparse activation on the local network *in vivo* has largely been done under
93 anaesthesia (London et al., 2010; Kwan and Dan, 2012; Jouhanneau, Kremkow and
94 Poulet, 2018) which influences state-dependent cortical processing (Niell and Stryker,
95 2010; Crochet et al., 2011; Harris and Thiele, 2011) and prevents the study of
96 behaviour.

97

98 Combining simultaneous targeted stimulation with readout of effects on the local
99 network during behaviour will allow us to define the local network input-output
100 function. This will yield better understanding of neural network operation, analogously
101 to how measuring single-neuron input-output functions has transformed our
102 understanding of information processing in single neurons (Magee, 2000; Poirazi,
103 Brannon and Mel, 2003; London et al., 2010; Major, Larkum and Schiller, 2013).
104 Moreover, it will allow us to determine how this network input-output function in turn
105 influences the psychometric sensitivity to neural activity, which theoretical work

106 predicts is crucial for understanding the link between neural circuit activity and
107 behaviour (Bernardi, Doron, Brecht, & Lindner, 2020; Bernardi & Lindner, 2017, 2019;
108 Cai et al., 2020). While some studies combining readout with manipulation have made
109 significant progress in this direction (Ceballo, Bourg, et al., 2019; Ceballo,
110 Piwkowska, Bourg, Daret, & Bathellier, 2019; Salzman et al., 1990; Znamenskiy &
111 Zador, 2013) they have lacked spatial resolution and targeting flexibility either on the
112 level of readout or stimulation. Measuring network input-output functions at cellular
113 resolution during perception is likely to yield pivotal insights into how neural
114 populations generate behaviour.

115

116 Here we have activated ensembles of varying numbers of neurons in L2/3 barrel
117 cortex of awake mice trained to detect direct cortical photostimulation. We took
118 advantage of recently developed all-optical approaches combining two-photon
119 calcium imaging and two-photon optogenetics with digital holography to allow us to
120 activate specifically targeted ensembles of neurons while simultaneously recording
121 the response of the local network (Carrillo-Reid et al., 2019; Carrillo-Reid, Yang,
122 Bando, Peterka, & Yuste, 2016; Emiliani, Cohen, Deisseroth, & Hausser, 2015;
123 Mardinly et al., 2018; Marshel et al., 2019; Packer, Russell, Dagleish, & Hausser,
124 2015; Russell et al., 2019; Shemesh et al., 2017). We combined this all-optical
125 approach with an operant conditioning paradigm in which animals were required to
126 report the targeted two-photon activation of arbitrary ensembles of pyramidal
127 neurons in L2/3 barrel cortex to gain rewards. In trained animals we investigated how
128 behaviour and network response vary as a function of the ensemble size stimulated.
129 We show that animals are sensitive to the activation of surprisingly small numbers of

130 neurons (~14) and demonstrate that activating roughly double this number of neurons
131 (~37) is sufficient for detection to saturate. Moreover we show that this perceptual
132 threshold is plastic, and decreases with learning. We also demonstrate that while
133 detection rates increase with increasing stimulation, the surrounding network
134 responds with matched suppression which maintains the balance of activation and
135 suppression at a level consistent with spontaneous epochs.

136 **Results**

137 ***Targeted two-photon optogenetic activation of neural ensembles in L2/3 barrel*** 138 ***cortex can drive behaviour***

139 To investigate both the behavioural and network response to precisely controlled
140 levels of cortical excitation we combined an upgraded version of our previously
141 reported all-optical setup (incorporating 3D volumetric imaging using an ETL, a more
142 powerful two-photon (2P) photostimulation laser and an additional light-path for one-
143 photon (1P) photostimulation; see *Methods*, Packer *et al.*, 2015) with an operant
144 conditioning paradigm whereby mice are trained to report the activation of excitatory
145 neurons in barrel cortex with either 1P or 2P optogenetic stimulation (**Figure 1**). We
146 expressed the calcium indicator GCaMP6s and the two-photon activatable
147 somatically-restricted opsin C1V1 in neurons of L2/3 barrel cortex (**Figure 1a**: inset
148 right, **Figure 1 – figure supplement 1**, see *Methods*). This strategy allows us to
149 flexibly activate specific ensembles of neurons in a given cortical population (**Figure**
150 **1a**: Pixel STA, **Figure 1 – figure supplement 2**) with high spatial resolution (**Figure 1**
151 **– figure supplement 2a**: HWHM 5 μm laterally, 20 μm axially) while performing
152 simultaneous two-photon calcium imaging. Inspired by previous work (Histed &
153 Maunsell, 2014; Huber *et al.*, 2008) we devised a training paradigm in which animals
154 were conditioned to detect bulk activation of barrel cortex via 1P photostimulation.
155 After task acquisition we progressively lowered the 1P stimulation intensity (which
156 reduces the number, reliability and spatial extent of activated neurons (see *Methods*
157 for photostimulation details)), before transitioning animals to detect 2P
158 photostimulation of specific groups of neurons (**Figure 1b**, **Figure 1 – figure**
159 **supplement 3**). We used a simple un-cued go/catch trial design where pseudo-

160 randomly interleaved go trials (1P or 2P photostimulation) or catch trials (no
161 photostimulation) were delivered after animals successfully withheld licking for a
162 variable period (**Figure 1c**: top, see *Methods*). On go trials the presence/absence of
163 licks in the post-stimulus response window was scored as hits/misses, with hits
164 triggering delivery of a sucrose reward (**Figure 1c**: bottom). On catch trials the
165 presence/absence of licks were scored as false alarms/correct rejects and neither
166 outcome was punished or rewarded.

167

168 Animals underwent 3 training phases (**Figure 1c**: bottom, **Figure 1 – figure**
169 **supplement 3a**), beginning with Phase 1 where 1P go trials and catch trials were
170 interleaved in equal proportions. In the first training session (**Figure 1 – figure**
171 **supplement 3b**), go trials of 10 mW 1P photostimuli were delivered and were
172 automatically rewarded irrespective of the animal's response (**Figure 1 – figure**
173 **supplement 3b**, blue line). Animals readily learned to detect photostimulation as
174 shown by an increase in proactive lick responses post-stimulus but before the
175 automatic reward (delivered at 0.5 s post-stimulus onset) and decreases in reaction
176 time mean and s.d. across the first 20 – 100 trials (**Figure 1 – figure supplement 3c**
177 **- e**), often within the first session (**Figure 1 – figure supplement 3b**). Once animals
178 showed evidence of learning, automatic rewards were turned off and the LED power
179 was sequentially reduced across several daily training sessions from 10 – 0.25 mW
180 resulting in an inverted U-shaped profile of performance as behaviour improved but
181 stimulation powers dropped (**Figure 1 – figure supplement 3f,g**). Subsequently,
182 animals were tested on several “high power” psychometric curve sessions (**Figure 1**
183 **– figure supplement 5f** 1.65 ± 1.06 sessions, $N = 26$ mice; 4 mice skipped this step)

184 where intermediate LED powers (250 – 50 μ W) were pseudorandomly interleaved
185 trial-by-trial (**Figure 1 – figure supplement 3h**), finally finishing Phase 1 by
186 undergoing several “low power” psychometric curve sessions (100 – 20 μ W) (**Figure**
187 **1 – figure supplement 3i – k, Figure 1 – figure supplement 5f** 2.12 ± 2.07 sessions,
188 $N = 26$ mice; 4 mice skipped this step). Animals’ response rates decreased with
189 decreasing 1P photostimulation powers (**Figure 1 – figure supplement 3i** P(Lick) for
190 100 μ W 0.94 ± 0.11 vs 20 μ W 0.51 ± 0.29 , $P = 5.96 \times 10^{-5}$ Wilcoxon signed-rank test,
191 $N = 22$ mice) and their reaction times became slower (**Figure 1 – figure supplement**
192 **3j** reaction time for 100 μ W 0.47 ± 0.16 s vs 20 μ W 0.58 ± 0.15 s, $P = 4.61 \times 10^{-5}$
193 Wilcoxon signed-rank test, $N = 22$ mice that did this step) and increasingly variable
194 (**Figure 1 – figure supplement 3k** reaction time s.d. for 100 μ W 0.09 ± 0.04 s vs 20
195 μ W 0.16 ± 0.08 s, $P = 5.46 \times 10^{-4}$ paired t-test, $N = 22$ mice that did this step), though
196 even the lowest LED powers evoked lick rates significantly higher than catch trials
197 (**Figure 1 – figure supplement 3i** P(Lick) for catch trials: 0.12 ± 0.08 vs go trials of
198 20 μ W: 0.51 ± 0.29 , $P = 2.31 \times 10^{-4}$; 40 μ W: 0.77 ± 0.20 , $P = 2.01 \times 10^{-4}$; 60 μ W: 0.90
199 ± 0.11 , $P = 2.01 \times 10^{-4}$; 80 μ W: 0.94 ± 0.07 , $P = 2.01 \times 10^{-4}$; 100 μ W: 0.94 ± 0.11 , $P =$
200 2.01×10^{-4} ; all Wilcoxon signed-rank tests with Bonferroni correction for multiple
201 comparisons, $N = 22$ mice, average over 1 – 3 sessions).

202

203 At this point animals were transitioned to Phase 2 where 1P go trials (50 μ W), 2P go
204 trials (targeted to 200 and subsequently 100 neurons) and catch trials were
205 pseudorandomly interleaved in equal proportion (**Figure 1c,d**). Before each training
206 session we selected 200 neurons based on C1V1-mRuby expression in clearly
207 expressing FOVs in superficial L2/3 barrel cortex (~130 - 230 μ m below pia) and

208 recorded their sensitivity to photostimulation (**Figure 1 – figure supplement 4**). For
209 each animal we selected similarly positioned FOVs across days, but did not
210 specifically target the same neurons (which is challenging due to angular
211 inconsistencies in FOV position across days, see *Methods*). Using these stimulus
212 patterns for 2P go trials we trained animals on Phase 2, and subsequently some
213 animals on Phase 3 (only 2P stim and catch trials), for several sessions (**Figure 1d**
214 single session, **Figure 1 – figure supplement 5a,b,f** 3.40 ± 1.51 Phase 2/3 sessions
215 2P 200/100 neurons, $N = 12$ animals). During this period we also began interleaving
216 2P trials stimulating 100 neurons from the 200 neuron group when animals reliably
217 detected 200 neuron stimulations (typically within a single session; 1.08 ± 0.29
218 sessions to $d\text{-prime} > 1$ on 2P 200 neuron trials, $N = 12$ animals) (**Figure 1 – figure**
219 **supplement 5a,b** performance over time). We found that animals reliably detected
220 2P photostimulation of both 200 and 100 neurons consistently across time, from the
221 first session (**Figure 1 – figure supplement 5c** first 200 neuron $d\text{-prime}$: 2.39 ± 0.86
222 vs 1, $P = 1.70 \times 10^{-4}$ paired t-test; first 100 neuron $d\text{-prime}$: 2.13 ± 0.93 vs 1, $P = 1.4$
223 $\times 10^{-3}$ paired t-test, $N = 12$ mice) to the last session (**Figure 1 – figure supplement**
224 **5c** last 200 neuron $d\text{-prime}$: 2.83 ± 0.62 vs 1, $P = 5.95 \times 10^{-7}$ paired t-test; last 100
225 neuron $d\text{-prime}$: 2.55 ± 0.7 vs 1, $P = 1.00 \times 10^{-5}$ paired t-test, $N = 12$ mice) and only
226 showed a modest improvement over time (**Figure 1 – figure supplement 5c** 200
227 neuron first 2.39 ± 0.86 vs last 2.83 ± 0.62 , $P = 0.07$ paired t-test, $N = 12$ mice; 100
228 neuron first 2.02 ± 1.28 vs last 2.86 ± 0.8 , $P = 0.06$ Wilcoxon signed-rank test, $N = 6$
229 mice with multiple 100 neuron sessions). On their final Phase 2 session (session 2.75
230 ± 1.42 , $N = 12$ animals) animals detected 2P photostimulation of 200 neurons with
231 high response rates that were similar to 1P photostimulation (**Figure 1d** single

232 session, **Figure 1e** group average; $P = 1.82 \times 10^{-5}$ Friedman test; P(Lick) for 1P: 0.99
233 ± 0.02 vs 2P: 0.88 ± 0.10 , $P = 0.19$, Bonferroni correction for multiple comparisons,
234 $N = 12$ mice, 1 session each) and with similar reaction time mean (**Figure 1f** $P = 6.70$
235 $\times 10^{-3}$ one-way repeated measures ANOVA; 1P: 0.49 ± 0.14 s vs 2P: 0.56 ± 0.15 s, P
236 $= 0.77$, Bonferroni correction for multiple comparisons, $N = 11$ mice, 1 session each,
237 only mice with > 2 catch trial responses included) and standard deviation (**Figure 1g**
238 $P = 4.99 \times 10^{-8}$ one-way repeated measures ANOVA; 1P: 0.09 ± 0.05 s vs 2P: $0.13 \pm$
239 0.02 s, $P = 0.25$, Bonferroni correction for multiple comparisons, $N = 11$ mice, 1
240 session each, only mice with > 2 catch trial responses included). Both 2P and 1P
241 photostimulation evoked higher lick rates than catch trials (**Figure 1e** $P = 1.82 \times 10^{-5}$
242 Friedman test; P(Lick) for Catch: 0.11 ± 0.07 vs 2P: 0.88 ± 0.10 , $P = 1.61 \times 10^{-2}$; vs
243 1P: 0.99 ± 0.02 , $P = 1.04 \times 10^{-5}$, Bonferroni correction for multiple comparisons, $N =$
244 12 mice, 1 session each) with less variable reaction times (**Figure 1g** reaction time
245 s.d.; $P = 4.99 \times 10^{-8}$ one-way repeated measures ANOVA; Catch: 0.28 ± 0.09 s vs 2P:
246 0.13 ± 0.02 s, $P = 5.99 \times 10^{-6}$; vs 1P: 0.9 ± 0.05 s, $P = 7.24 \times 10^{-8}$, Bonferroni correction
247 for multiple comparisons, $N = 11$ mice, 1 session each, only mice with > 2 catch trial
248 responses included), though only 1P trials showed quicker reaction times (**Figure 1f**
249 $P = 6.70 \times 10^{-3}$ one-way repeated measures ANOVA; Catch: 0.69 ± 0.11 s vs 1P: 0.49
250 ± 0.14 s, $P = 5.91 \times 10^{-3}$; vs 2P: 0.56 ± 0.15 s, $P = 0.10$, Bonferroni correction for
251 multiple comparisons, $N = 11$ mice, 1 session each, only mice with > 2 catch trial
252 responses included). We also note that we found similar response rates in animals
253 expressing non-somatically-restricted C1V1 (**Figure 1 – figure supplement 6a** catch
254 subtracted P(Lick) for C1V1-Kv2.1 0.77 ± 0.11 vs C1V1 0.79 ± 0.14 , $P = 0.61$ two-
255 sample t-test, $N = 12$ C1V1-Kv2.1 and 19 C1V1 injected mice), though reaction times

256 were significantly slower for somatically-restricted C1V1 (**Figure 1 – figure**
257 **supplement 6** C1V1-Kv2.1 0.55 ± 0.15 s vs C1V1 0.41 ± 0.08 s, $P = 2.09 \times 10^{-3}$ two-
258 sample t-test, $N = 12$ C1V1-Kv2.1 and 19 C1V1 injected mice).

259

260 Thus we have demonstrated that two-photon optogenetic stimulation targeted to
261 small ensembles of cortical neurons can reliably drive behaviour and provides a
262 powerful tool for investigating the perceptual salience of different patterns of neural
263 activity.

264

265 ***Very few cortical neurons are sufficient to drive behaviour***

266 We next tested behavioural sensitivity to the activity of neural ensembles of varying
267 size. To test this we transitioned animals to Phase 3 sessions (2P and catch trials
268 only; **Figure 1c**: bottom) where we precisely titrated the level of activation by targeting
269 different numbers of neurons on a trial by trial basis. We again selected 200 neurons
270 on the basis of C1V1-mRuby expression and sub-divided this group into smaller
271 subsets of 100, 75, 50, 25 10 and 5 neurons (**Figure 2a**). Animals then underwent 2P
272 photostimulation psychometric curve sessions during which, in addition to
273 stimulating the group of 200 neurons, we also pseudorandomly interleaved
274 stimulations of the smaller subsets of neurons (**Figure 2b,c**). We leveraged our ability
275 to simultaneously read out neural activity with calcium imaging to refine our estimate
276 of the number of stimulated neurons according to the number of target neurons that
277 were activated averaged across trials. To quantify activation (and suppression; see
278 later sections) we defined thresholds for each neuron on the basis of their response
279 distribution on correct reject catch trials (**Figure 2 – figure supplement 1b – g**, see
280 *Methods*), where no stimulus or lick occurred, and to differentiate between target and

281 background neurons we defined 3D target zones around each 2P photostimulation
282 target co-ordinate (**Figure 2 – figure supplement 1a,h – j**, see *Methods*). This
283 resulted in numbers of activated target neurons that were 0.46 ± 0.20 times that of
284 the number of target zones (averaged across trial types) and decreased with
285 decreasing number of zones as intended (**Figure 2 – figure supplement 1i**; see
286 *Methods*).

287

288 Animals' response rates increased sigmoidally with increasing numbers of target
289 neurons activated (**Figure 2b** single animal, **Figure 2d** all sessions) and both
290 individual sessions and aggregate data across sessions were well fit by log-normal
291 sigmoid psychometric functions (**Figure 2d** grey dots/lines: individual data/fits, $R^2 =$
292 0.91 ± 0.09 , $N = 11$ sessions, 6 animals, 1 – 2 sessions each; red line: aggregate fit,
293 $R^2 = 0.72$, cross-validated $R^2 = 0.67 \pm 0.23$, $N = 10,000$ permutations, see *Methods*
294 for fit details). Using these fitted psychometric functions we estimate that animals can
295 detect the activation of a minimum of ~14 neurons at their perceptual threshold
296 (**Figure 2e** 10% point of curve: individual fits 14.2 ± 8.96 neurons, $N = 11$ sessions,
297 6 animals, 1 – 2 sessions each; aggregate fit 9.86 [95% CI: 6.09 12.8] neurons), with
298 only roughly double this number of neurons (~37) required to saturate performance
299 (**Figure 2e** 90% point of curve: individual fits 37.0 ± 11.3 neurons, $N = 11$ sessions,
300 6 animals, 1 – 2 sessions each; aggregate fit 45.1 [95% CI: 37.3 63.5 neurons). At the
301 psychometric function's 50% point (**Figure 2e** 50% point of curve: individual fits 21.8
302 ± 8.71 neurons, $N = 11$ sessions, 6 animals, 1 – 2 sessions each; aggregate fit 21.1
303 [95% CI: 17.9 23.9] neurons) this results in a very steep slope, with ~0.05 probability
304 of licking added per neuron stimulated (**Figure 2f** individual fits 0.05 ± 0.03 ; aggregate

305 fit 0.03). This is notably steeper for individual fits than the aggregate fit (0.05 ± 0.03
306 vs 0.03 , $P = 9.77 \times 10^{-3}$ Wilcoxon signed rank test, $N = 11$ sessions, 6 animals, 1 – 2
307 sessions each). Mean reaction times did not vary as fewer neurons were activated
308 (**Figure 2 – figure supplement 2a** $\beta = -0.02$, $R^2 = 0.02$, $P = 0.24$), though they did
309 become more variable (**Figure 2 – figure supplement 2b** $\beta = -0.05$, $R^2 = 0.30$, $P =$
310 1.41×10^{-6}). This demonstrates that animals are exquisitely sensitive to the activation
311 of small numbers of cortical neurons and can read out surprisingly small changes in
312 cortical activity levels.

313

314 We next addressed the question of how flexible this perceptual threshold is and how
315 specific it is to neurons used for training during preceding sessions. After training
316 animals to detect the activation of hundreds of barrel cortex neurons, we asked
317 whether their ability to detect the activation of small subsets of these neurons
318 improved across multiple subsequent days, and whether learning was specific to
319 neurons targeted on each day. In one cohort of animals we identified and activated
320 the same neurons reliably across multiple days (**Figure 2 – figure supplement 3a**)
321 and measured the detection rate across sessions (**Figure 2 – figure supplement 3b**)
322 whereas in a second cohort we moved FOV for each session and stimulated different
323 neurons. Across all animals there was a consistent improvement in detection rate
324 (**Figure 2 – figure supplement 3c** $P(\text{Lick})$ on Session 1: 0.17 ± 0.18 vs Session 2:
325 0.28 ± 0.25 , $P = 6.29 \times 10^{-3}$ paired t-test, $N = 14$ animals testing the same 30 neurons
326 and 5 animals testing different groups of 25 and 50 neurons) which did not differ
327 depending on whether the same or different neurons were stimulated across sessions
328 (**Figure 2 – figure supplement 3d** $P(\text{Lick})$ improvement for same: 0.12 ± 0.18 vs

329 different: 0.09 ± 0.18 , $P = 0.84$ Mann Whitney U-Test, $N = 14$ animals testing the
330 same 30 neurons and 5 animals testing different groups of 25 and 50 neurons).

331

332 These experiments use targeted stimulation of cortical neurons to describe the
333 behavioural input-output function for our task, and suggest that the lower bound for
334 detection is a small number of neurons (~14 neurons) and the psychometric function
335 is very steep (saturating at ~37 neurons). We also demonstrate that animals' ability to
336 detect small numbers of neurons improves with training and that this improvement is
337 not limited to targeted neurons.

338

339 ***Suppression in the local network balances target activation***

340 We took advantage of our ability to simultaneously record activity in both the targeted
341 and untargeted 'background' neurons to investigate how local network activity
342 influences or depends on behavioural performance. Using the same activation
343 thresholds, suppression thresholds and target definitions described earlier (**Figure 2**
344 – **figure supplement 1**, see *Methods*) we calculated the proportion of activated and
345 suppressed neurons on each trial averaged across trials of each type (**Figure 3 –**
346 **figure supplement 1a,e**). Splitting trials by hits and misses we found that hits were
347 associated with more activation (**Figure 3 – figure supplement 1a,b** $P(\text{activated})$
348 background on hits $4.94 \times 10^{-2} \pm 8.63 \times 10^{-3}$ vs misses $3.83 \times 10^{-2} \pm 5.04 \times 10^{-3}$ on 50
349 target trials, $P = 1.95 \times 10^{-3}$ Wilcoxon signed-rank test, $N = 11$ sessions, 6 animals, 1
350 – 2 sessions each) and less suppression (**Figure 3 – figure supplement 1e,f**
351 $P(\text{suppressed})$ background on hits $3.53 \times 10^{-2} \pm 4.84 \times 10^{-3}$ vs misses $3.99 \times 10^{-2} \pm$
352 5.5×10^{-3} on 50 target trials, $P = 2.23 \times 10^{-2}$ paired t-test, $N = 11$ sessions, 6 animals,
353 1 – 2 sessions each) than misses. However, since hits are associated with

354 stereotyped behaviours (licking, whisking, face movements etc.), and significant
355 movement and reward-related activity has been observed in primary sensory cortical
356 areas (Shuler and Bear, 2006; Niell and Stryker, 2010; Musall *et al.*, 2019; Steinmetz
357 *et al.*, 2019; Stringer *et al.*, 2019; Zatka-Haas *et al.*, 2020), we reasoned that such
358 differences might be accounted for by the behaviours themselves irrespective of our
359 manipulations. Indeed we found that in background neurons the level of activation
360 recruited on hits post-photostimulation was not different from false alarms on catch
361 trials where animals licked but no neurons were photostimulated (**Figure 3 – figure**
362 **supplement 1d** $P(\text{activated})$ background on 50 target hit $4.92 \times 10^{-2} \pm 9.05 \times 10^{-3}$ vs
363 catch false alarm $4.83 \times 10^{-2} \pm 1.04 \times 10^{-2}$, $P = 0.52$ paired t-test, $N = 10$ sessions, 6
364 animals, 1 – 2 sessions each, 1 session without any catch false alarms excluded),
365 irrespective of how many neurons we activated (**Figure 3 – figure supplement 1a**).
366 The amount of suppression also did not differ between hits post-photostimulation
367 and false alarms on catch trials (**Figure 3 – figure supplement 1h** 50 neuron hit vs
368 catch false alarm: $3.51 \times 10^{-2} \pm 5.05 \times 10^{-3}$ vs $3.37 \times 10^{-2} \pm 6.99 \times 10^{-3}$, $P = 0.27$ paired
369 t-test, $N = 10$ sessions, 6 animals, 1 – 2 sessions each, 1 session without any catch
370 false alarms excluded), though there was some modulation of this difference with the
371 number of neurons activated (**Figure 3 – figure supplement 1e**). It therefore seemed
372 possible that a significant amount of the stimulus-evoked activity that we read out in
373 background neurons was influenced by lick-related behaviours. In line with this we
374 found that a large fraction of neurons showed activity which was modulated by
375 spontaneous licking (**Figure 3 – figure supplement 1i – k** $46\% \pm 11$ of neurons lick
376 modulated, $N = 11$ sessions, 6 animals, 1 – 2 sessions each, see *Methods*) with
377 neurons showing both positive correlation (**Figure 3 – figure supplement 1j,l,m** 2.83

378 $\times 10^{-2} \pm 1.81 \times 10^{-2}$ lick correlation for all positively lick modulated neurons, $N = 9547$
379 neurons) and negative correlation (**Figure 3 – figure supplement 1j,l,m** -2.52×10^{-2}
380 $\pm 1.51 \times 10^{-2}$ lick correlation for all negatively modulated neurons, $N = 4365$ neurons).
381
382 Unfortunately, the temporal resolution of calcium imaging does allow us to tease
383 apart the direction of causality in our data, i.e. whether this activity causes, or is
384 caused by motor output. However given the literature demonstrating behavioural
385 output-related activity in sensory cortices (Musall et al., 2019; Steinmetz et al., 2019;
386 Stringer et al., 2019), and the fact that manipulating this activity has no effect on
387 behavioural choices (Zatka-Haas et al., 2020), we were concerned that a significant
388 amount of network activity might result from movement rather than causing it. This
389 would be problematic for our interpretation since the amount of lick contamination
390 will vary by trial type (no. neurons activated) in a manner that correlates with the
391 variable under study (due to the increased $P(\text{Lick})$ with no. neurons activated **Figure**
392 **2d**). To take account of this we devised a hit/miss matching procedure which removes
393 the variance in hit:miss ratio across trial types by ensuring that all trial types have a
394 50:50 ratio of hits:misses (**Figure 3 – figure supplement 1o**, see *Methods*). This is
395 achieved for trials of a given type (i.e. a low $P(\text{Lick})$ trial type: 10 activated neurons)
396 by matching the number of trials of the minority response type (i.e. Hits) with random
397 resamples, of the same number, of majority response-type trials (i.e. Misses) and
398 averaging network response metrics across resamples. Following this procedure
399 should ensure that all trial types have the same proportion of data contaminated by
400 lick responses and any variation in network response across trial types remaining
401 should be due to the variation in number of target neurons activated.

402

403 Using this procedure, we investigated how the network response varies as a function
404 of stimulated ensemble size beyond its stereotyped modulation by the behavioural
405 response. Taking the network as a whole (including target neurons) we found that
406 photostimulation causes both activation (**Figure 3a** right inset; $P(\text{activated})$ all
407 neurons on photostimulus $5.91 \times 10^{-2} \pm 1.20 \times 10^{-2}$ vs catch $4.82 \times 10^{-2} \pm 6.65 \times 10^{-3}$
408 trials averaged across all trial types, $P = 1.17 \times 10^{-3}$ paired t-test, $N = 10$ sessions, 6
409 mice, 1 – 2 sessions each) and suppression (**Figure 3b** right inset; $P(\text{suppressed})$ all
410 neurons on photostimulus $4.58 \times 10^{-2} \pm 4.90 \times 10^{-3}$ vs catch $3.97 \times 10^{-2} \pm 4.80 \times 10^{-3}$
411 trials averaged across all trial types, $P = 1.41 \times 10^{-4}$ paired t-test, $N = 10$ sessions, 6
412 mice, 1 – 2 sessions each) and that both scale with the number of neurons activated
413 (**Figure 3a,b** $P(\text{activated})$ all neurons: $\beta = 7.54 \times 10^{-3}$, $R^2 = 0.24$, $P = 2.36 \times 10^{-5}$;
414 $P(\text{suppressed})$ all neurons: $\beta = 3.00 \times 10^{-3}$, $R^2 = 0.25$, $P = 1.54 \times 10^{-5}$, $N = 10$ sessions,
415 6 mice, 1 – 2 sessions each). When we analysed only background neurons (i.e.
416 excluding targets from the calculation) we found that while photostimulation does
417 cause both activation and suppression in the background network (**Figure 3d,e** right
418 insets; $P(\text{activated})$ network on photostimulus $4.40 \times 10^{-2} \pm 6.89 \times 10^{-3}$ vs catch 4.02
419 $\times 10^{-2} \pm 5.60 \times 10^{-3}$ trials, $P = 2.31 \times 10^{-3}$ paired t-test; $P(\text{suppressed})$ background on
420 photostimulation $3.81 \times 10^{-2} \pm 4.60 \times 10^{-3}$ vs catch $3.27 \times 10^{-2} \pm 4.60 \times 10^{-3}$ trials, $P =$
421 1.06×10^{-4} paired t-test, all averaged across trial types, $N = 10$ sessions, 6 mice, 1 –
422 2 sessions each), only background network suppression scales with the number of
423 activated target neurons (**Figure 3e** $\beta = 2.95 \times 10^{-3}$, $R^2 = 0.31$, $P = 7.79 \times 10^{-7}$) whereas
424 activation does not (**Figure 3d** $\beta = 1.70 \times 10^{-3}$, $R^2 = 0.05$, $P = 0.08$). Moreover,
425 activation and suppression have distinct spatial profiles, with significant suppression

426 occurring over a much broader area (**Figure 3 – figure supplement 3**). This suggests
427 that the network reacts to suppress the spread of activation triggered by our
428 photostimulation in a graded manner which tracks the activation strength, whereas
429 network activation changes to a smaller extent. Indeed, across all neurons in the
430 population we see that there is a consistent balance of activation and suppression
431 across all target activation levels (**Figure 3c** $P(\text{Activated})/P(\text{Suppressed})$ across all
432 neurons $\beta = 7.23 \times 10^{-2}$, $R^2 = 0.05$, $P = 0.06$) that remains similar to the rates observed
433 spontaneously during catch trials (**Figure 3c** right inset; $P(\text{Activated})/P(\text{Suppressed})$
434 on photostimulation 1.30 ± 0.28 vs catch 1.24 ± 0.25 trials across all neurons, $P =$
435 0.25 paired t-test, $N = 10$ sessions, 6 mice, 1 – 2 sessions each).

436

437 These results suggest that activating target neurons produces suppression in the
438 surrounding network which maintains homeostasis of background activity.

439

440 ***Behaviour tracks target neuron activity despite constant, matched suppression***
441 ***in the local network***

442 As it has been suggested that both excitation and inhibition of cortical neurons can
443 drive behaviour (Doron, von Heimendahl, Schlattmann, Houweling, & Brecht, 2014),
444 and since target activation and network suppression correlate in our dataset (**Figure**
445 **3e**), we finally asked which of the factors that we have analysed best correlates with
446 animals' behavioural responses. Using the hit:miss matched data described above
447 we modelled behavioural response rates as a function of target activation,
448 background activation and background suppression (**Figure 4a – c**), cross-validating
449 across training and test datasets to assess the goodness and generalisability of the
450 fits (see *Methods*). The strongest and most generalisable predictor of behavioural

451 responses was target neuron activation, which had significantly positive R^2 across
452 both training and test sets during cross-validation (**Figure 4a,d** train R^2 : 0.71 ± 0.06 ,
453 $P = 0$ permutation test vs 0; test R^2 : 0.66 ± 0.23 , $P = 1.68 \times 10^{-2}$ permutation test vs
454 0, $N = 10,000$ train:test splits). Network suppression had mild predictive power on
455 training data, but none on testing data (**Figure 4c,d** train R^2 : 0.16 ± 0.06 , $P = 2.50 \times$
456 10^{-3} permutation test vs 0; test R^2 : 0.01 ± 0.39 , $P = 0.39$ permutation test vs 0, $N =$
457 10,000 train:test splits) which might be explained by its correlation with target
458 activation (**Figure 3e**). Network activation was a poor predictor of both training and
459 testing data, suggesting that it had little influence on behavioural performance (**Figure**
460 **4b,d** train R^2 : -0.05 ± 0.05 , $P = 0.11$ permutation test vs 0; test R^2 : -0.21 ± 0.44 , $P =$
461 0.22 permutation test vs 0, $N = 10,000$ train:test splits). Thus within the cortical region
462 that we can observe and manipulate we have tested three of the main pathways by
463 which activity in cortex could influence downstream circuitry to ultimately drive
464 behaviour: (1) output of directly activated target neurons; (2) output of background
465 neurons synaptically activated by target neurons; (3) suppression of the output of
466 background neurons through disynaptic inhibition by interneurons activated by target
467 neurons (**Figure 4e**). Our results indicate that the most robust effect is the number of
468 activated target neurons (1), with only a minor impact of indirectly modulated neurons
469 in the local network.

470

471 **Discussion**

472 By precisely titrating the number of activated neurons to be detected, we have
473 demonstrated that the psychometric function for detecting cortical activity is
474 sensitive, with only tens of neurons required to drive behaviour, and it is steep, with
475 only an approximate doubling in number sufficient to drive asymptotic behavioural
476 performance. Simultaneous imaging of the surrounding network has allowed us to
477 show that, despite this exquisite behavioural sensitivity, the dominant network
478 response matches the activation of targeted neurons with local suppression,
479 flattening the network input-output function to maintain the level of network activation
480 within the spontaneous range. These results support the sparse coding hypothesis
481 (Barlow, 1972; Barth & Poulet, 2012; Kanerva, 1993; Olshausen & Field, 1996),
482 demonstrate that the local network operates in an inhibition-stabilized regime
483 (Denève & Machens, 2016; Murphy & Miller, 2009; Ozeki, Finn, Schaffer, Miller, &
484 Ferster, 2009; Pehlevan & Sompolinsky, 2014; Sanzeni et al., 2020; Tsodyks et al.,
485 1997; van Vreeswijk & Sompolinsky, 1996; Wolf et al., 2014) and suggest a high
486 storage capacity for recurrent networks (Hopfield, 1982; Lefort *et al.*, 2009; Peron *et*
487 *al.*, 2020). This combination of features likely maximizes perceptual sensitivity while
488 minimizing erroneous detection of background activity, thus avoiding hallucinations
489 (Carbon, 2014; Cassidy et al., 2018; Corlett et al., 2019; Friston, 2005), runaway
490 excitation (Rose & Blakemore, 1974; Treiman, 2001; Ziburkus, Cressman, Barreto, &
491 Schiff, 2006) and reducing cortical energy requirements (Schölvinc et al., 2008). We
492 also show that the lower bound of detectable activity is not fixed, but can improve
493 with training in a way that can generalise to other neurons in the surrounding network.
494 This suggests that perceptual learning can reroute cortical resources to meet even

495 the most stringent task demands and generalise to other potentially relevant neurons,
496 increasing cognitive flexibility. This also demonstrates that the brain's ability to "learn
497 to learn" (Behrens et al., 2018; Harlow, 1949) can extend even to arbitrary activity
498 patterns.

499

500 ***Activation of only a small number of neurons is required to reach perceptual***
501 ***threshold***

502 We leveraged our all-optical system to precisely target different numbers of neurons
503 for two-photon optogenetic activation in order to define the minimum number that is
504 sufficient to drive behaviour. The perceptual threshold we measured is remarkably
505 low: mice can detect the activation of only ~14 cortical neurons. This number is
506 substantially lower than the threshold estimated for one-photon activation of layer
507 2/3 neurons in rodent barrel cortex (~60; Huber *et al.*, 2008). This might be explained
508 by the fact that we tailor our optogenetic stimulus for activation of individual neurons,
509 whereas one-photon stimulation diffusely activates an entire population of neurons
510 (many of which will receive subthreshold levels of photocurrent). Moreover, our stimuli
511 drive double the number of action potentials (~10 in each neuron) which Huber *et al.*
512 show increases detectability, though we note that our minimum threshold of ~140
513 action potentials (10 action potentials in 14 neurons) is still lower than the ~300 that
514 they report. Furthermore, we produce comparatively more clustered activation of
515 stimulated neurons in our ensembles (confined to a ~500 x 500 x 100 μm volume)
516 compared to the more dispersed neuron locations used in Huber *et al.* (potentially
517 across the whole of S1), which may result in different recruitment of both local and
518 downstream targets due to changes in intra- and inter-laminar connection probability

519 with distance (Holmgren, Harkany, Svennenfors, & Zilberter, 2003; Lefort et al., 2009;
520 Perin, Berger, & Markram, 2011; Thomson & Lamy, 2007; Yoshimura, Dantzker, &
521 Callaway, 2005). Finally, the Huber *et al.*, 2008 study relied on post-hoc histological
522 estimates which, as noted by the authors, may have a significant margin of error.

523

524 On the other hand, our estimate of the perceptual threshold is an order of magnitude
525 higher than single-cell patch-clamp experiments demonstrating that strong activation
526 of single neurons can in some cases lead to a behavioural report (Doron et al., 2014;
527 Houweling & Brecht, 2008; Tanke, Borst, & Houweling, 2018). Several key differences
528 could account for this discrepancy. First, these studies mostly stimulated L5 neurons,
529 which serve as the output neurons of the cortical circuit and therefore may drive
530 behaviour more reliably compared to the L2/3 ensembles we target. Indeed, such a
531 dichotomy is confirmed by a recent study comparing the behavioural influence of
532 functionally defined ensembles in L2/3 with those in L5 (Marshel et al., 2019).
533 Secondly, these studies report significant variability in the ability of single neurons to
534 drive behaviour, with many neurons having no effect, and with the most potent
535 behavioural effects being limited mainly to fast-spiking putative interneurons (Doron
536 et al., 2014). Additional factors which may play a role include differences in level of
537 stimulation of individual neurons, differences in the training protocol, or species
538 differences between mice and rats.

539

540 Interestingly, the reaction times to optogenetic stimuli that we report (0.4 – 0.7 s) are
541 comparable to, though slightly slower than, those reported for detection of whisker
542 stimuli in mice (0.3 – 0.4 s; J. L. Chen, Carta, Soldado-Magraner, Schneider, &

543 Helmchen, 2013; Hires, Gutnisky, Yu, O'Connor, & Svoboda, 2015; O'Connor et al.,
544 2010; Sachidhanandam, Sreenivasan, Kyriakatos, Kremer, & Petersen, 2013)
545 suggesting that they may be processed differently. This could be because sensory
546 stimuli more robustly recruit many neurons distributed over several parallel thalamo-
547 cortical pathways which provide input to multiple cortical layers (Feldmeyer et al.,
548 2013; Petersen, 2007), including direct projections from thalamus to cortical output
549 L5 (Constantinople & Bruno, 2013), whereas our optogenetic stimuli will only activate
550 small numbers of neurons in L2/3. Moreover, sensory stimuli will likely drive patterns
551 of activity that respect cortical wiring for transmission of sensory information and so
552 may propagate more potently downstream. Future work comparing reaction times to
553 targeted activation of sensory-evoked or random ensembles of neurons in the same
554 animal will yield insight into any distinction between naturalistic and artificial neural
555 activity in driving behaviour. Our results also reveal reduced reaction time for non-
556 somatically-restricted C1V1 with little difference in response rate. This difference in
557 reaction time may be due to increased off-target activation via processes traversing
558 the photostimulation volume as well as larger photocurrent in target neurons through
559 activation of opsin in neuronal compartments in addition to the soma
560 (dendrites/axon). It is possible that this does not result in an increased response rate
561 because animals' performance is saturated at its upper bound (allowing for a lapse
562 rate that is independent of the salience of stimuli).

563

564 What are the functional implications of the perceptual threshold we have defined?
565 The fact that in our study (see also Daie, Svoboda, & Druckmann, 2019; Gill et al.,
566 2020; Marshel et al., 2019) the lower perceptual bound is well above a single neuron

567 suggests that perceptual thresholds are tuned to minimize conscious perception of
568 the spontaneous neural activity which often co-exists alongside stimulus activity
569 (Bernander, Douglas, Martin, & Koch, 1991; Destexhe & Pare, 1999; Destexhe,
570 Rudolph, & Paré, 2003; London, Roth, Beeren, Häusser, & Latham, 2010; Musall et
571 al., 2019; Shadlen & Newsome, 1994; Stringer et al., 2019; Tolhurst, Movshon, & Dean,
572 1983; Waters & Helmchen, 2006). If the perceptual apparatus is sensitive to single-
573 neuron activation this may lead to erroneous detection of background cortical
574 activity. While the stimuli in our study do not explicitly mimic sensory evoked activity,
575 such false positives in our behavioural paradigm may be related to the hypothesized
576 role of false sensory percepts in generating hallucinations, which impair normal
577 cognitive function and are associated with an array of pathological conditions
578 (Chaudhury, 2010; Kumar, Soren, & Chaudhury, 2009; Llorca, Pereira, Jardri,
579 Brousse, & Misdrahi, 2016). The threshold of ~14 neurons could therefore be
580 important for avoiding perceptual false positives caused by spontaneous background
581 network activity.

582

583 The relatively low perceptual threshold may also have significant computational
584 advantages. A large body of theoretical work has suggested that the brain may use
585 a sparse coding scheme to represent information (Barlow, 1972; Kanerva, 1993;
586 Olshausen and Field, 1996). Our demonstration that the perceptual threshold (~14
587 neurons) is much lower than the dimensionality of barrel cortex (~400,000 neurons in
588 barrel cortex; Hooks *et al.*, 2011; Meyer *et al.*, 2013; ~2000 neurons in superficial
589 layers of a barrel; Lefort *et al.*, 2009), but also significantly higher than a single neuron,
590 is consistent with computational theories proposing that individual items are

591 represented sparsely compared to the dimensionality of the space, but also that they
592 are not represented by single elements of that space (Baum, Moody, & Wilczek, 1988;
593 Kanerva, 1993; Olshausen & Field, 2004; Palm, 1980). Our work is also consistent
594 with work suggesting that barrel cortex can use ensembles on this scale to robustly
595 encode sensory information (Hires et al., 2015; Mayrhofer, Haiss, Helmchen, &
596 Weber, 2015; Panzeri, Ince, Diamond, & Kayser, 2014; Stüttgen & Schwarz, 2008).
597 Such sensitivity is beneficial as it suggests that recurrent networks like cortical L2/3
598 have a high storage capacity (Hopfield, 1982; Lefort *et al.*, 2009; Ko *et al.*, 2011; Harris
599 and Mrsic-Flogel, 2013; Cossell *et al.*, 2015; Peron *et al.*, 2020) allowing the brain to
600 represent many patterns independently (Amit, Gutfreund and Sompolinsky, 1985a;
601 Amit, Gutfreund and Sompolinsky, 1985b; McEliece *et al.*, 1987; Brunel, 2016; Folli,
602 Leonetti and Ruocco, 2017).

603

604 ***The network input-output function for perception is steep***

605 By recording the response of the local network while carefully titrating the number of
606 targeted neurons we have defined the network input-output function for perception
607 in our task. This function is sigmoidal and remarkably steep, saturating at only ~37
608 neurons. These results echo similarly steep perceptual input-output functions found
609 in other systems (Gill et al., 2020; Marshel et al., 2019) but are much steeper than
610 estimated in barrel cortex for one-photon optogenetic stimulation (Huber et al. 2008).
611 Again, this discrepancy may be due to a range of factors associated with one-photon
612 photostimulation, from the spatially diffuse (and largely subthreshold) nature of the
613 activation to differences in network cooperativity associated with our more clustered
614 stimulation patterns. Indeed, the highly synergistic activation of a local network of

615 densely interconnected excitatory neurons (Cossell et al., 2015; Douglas, Koch,
616 Mahowald, Martin, & Suarez, 1995; Ko et al., 2011), rapidly followed by suppression
617 in the local network (London et al. 2010; Kwan & Dan, 2012; Chettih & Harvey, 2019)
618 likely mediated by disynaptic inhibition (Jouhanneau, Kremkow, & Poulet, 2018;
619 Mateo et al., 2011; Silberberg & Markram, 2007), may be the basis for the steep and
620 saturating input-output function we have observed.

621

622 This steep input-output function may have significant functional consequences. While
623 allowing rejection of noise due to spontaneous activity (see the previous section), it
624 also enables perceptual detection of relevant activity with high sensitivity and
625 efficiency, and yet avoids further unnecessary engagement of the network with
626 additional stimulation. This may represent a circuit mechanism for optimizing the
627 canonical trade-off in a sensory system subject to noise (Bialek, 2012) between
628 minimizing false positives (a response when there is no signal: a “false alarm”) and
629 minimizing false negatives (missing a signal when there is one present). The
630 steepness of the input-output function and the low number of neurons at saturation
631 are also consistent with optimal energy efficiency (Attwell & Laughlin, 2001; Lennie,
632 2003). Indeed, our results offer cellular-resolution support for the proposal that the
633 energy associated with conscious perception is surprisingly low (Schölvinck et al.,
634 2008), since our data predict that the number of additional neurons required to allow
635 a subconsciously processed sensory stimulus to be consciously perceived will be
636 low.

637

638 While our behavioural paradigm relies on stimulation of artificially defined ensembles
639 of neurons, we maintain that our results add general insight as to how neural activity
640 can underlie flexible behaviour in barrel cortex since: (1) bulk optogenetic activation
641 of pyramidal neurons in sensory areas can readily replace trained sensory stimuli with
642 minimal behavioural impact (Ceballo, Piwkowska, et al., 2019; O'Connor et al., 2013;
643 Sachidhanandam et al., 2013), suggesting that the activity evoked is not so alien as
644 to confuse behavioural processing; (2) the order of magnitude of the numbers that we
645 report corresponds closely with the estimated number of barrel cortex neurons
646 required to decode tactile stimuli of various types (Hires et al., 2015; Mayrhofer et al.,
647 2015; Stüttgen & Schwarz, 2008) suggesting that there is limit to this system's
648 sensitivity that can be found through both observation and causal manipulation; (3)
649 irrespective of the exact numbers, the steepness of the psychometric function
650 suggests a fine distinction between whether neural activity is perceptible or not which
651 is indicative of a highly sensitive yet specific sensory system, as has also been shown
652 for optogenetic stimuli mimicking sensory (visual) percepts (Marshel et al., 2019); (4)
653 the unique ability of two-photon optogenetics to specifically target the same, or
654 different, ensembles of neurons throughout learning has explicitly demonstrated the
655 flexibility of this perceptual threshold and how this flexibility can generalise; (5) our
656 ability to image background neurons in the surrounding network has added a further
657 layer of understanding to seminal papers in the field (Houweling & Brecht, 2008;
658 Huber et al., 2008) and demonstrates that cortical networks largely balance
659 increasing levels of activation with matched suppression.

660

661 Nevertheless it is important to keep in mind caveats inherent to current all-optical
662 approaches that may influence these results, such as limitations in spike readout with
663 calcium indicators (T.-W. Chen et al., 2013; Pachitariu, Stringer, & Harris, 2018), the
664 photostimulation efficiency of two-photon optogenetic activation (reported here and
665 in Mardinly et al., 2018; Marshel et al., 2019; Shemesh et al., 2017) and the fact that
666 calcium imaging subsamples the full extent of neural activity involved in complex
667 behaviours. It is also likely that our results will be influenced by the exact stimulation
668 parameters, such as stimulus duration, strength and timing, as has been noted for
669 the detectability of direct cortical activation in the past (Doron et al., 2014; Gill et al.,
670 2020; Histed & Maunsell, 2014; Huber et al., 2008). Additionally, as with all studies
671 using trained non-naturalistic behaviour, it is worth considering how training duration
672 might influence our results. We note that animals learn our basic task very quickly
673 and that they continue to quickly generalise learning to new, harder stimuli over time
674 as is often observed in trained sensory paradigms (Andermann, Kerlin, & Reid, 2010;
675 Gerdjikov, Bergner, Stüttgen, Waiblinger, & Schwarz, 2010; O'Connor et al., 2010).
676 This quick learning means that their performance is stable and effectively saturated
677 by the time we test their perceptual sensitivity, in line with the way in which sensitivity
678 to sensory stimuli is tested in many systems (Britten, Newsome, Shadlen, Celebrini,
679 & Movshon, 1996; Busse et al., 2011; Carandini & Churchland, 2013; Morita, Kang,
680 Wolfe, Jadhav, & Feldman, 2011). Therefore, our results are interpretable within this
681 standard framework of testing perceptual sensitivity in animals that have learned a
682 non-naturalistic task close to saturation (though see next section), be it contingent on
683 sensory or artificial stimulation. Moreover, as we explore in the next section, we
684 demonstrate that this threshold can change with training, suggesting that the more

685 pertinent feature to consider in relation to perception more generally may be the
686 steepness of animals' psychometric curves. Indeed, our results using artificial
687 ensembles complement the psychometric functions reported in recent studies driving
688 behaviour by optogenetically mimicking sensory ensembles (Carrillo-Reid et al.,
689 2019; Marshel et al., 2019). Finally, an additional factor influencing our experiments
690 is that bulk 1P optogenetic activation over long training periods may change activity
691 and connectivity patterns, as has been suggested for repeated exposure to 2P
692 optogenetic stimulation of the same neurons over time in the absence of behaviour
693 (Carrillo-Reid et al., 2016) and for repeated exposure to the same sensory stimuli over
694 behavioural training (J. L. Chen et al., 2015; Khan et al., 2018; Peron, Freeman, Iyer,
695 Guo, & Svoboda, 2015; Poort et al., 2015; Wiest, Thomson, Pantoja, & Nicolelis,
696 2020). Future work recording neural responses in the population before, during and
697 after 1P/2P behavioural training will yield important insight into this process and it will
698 be crucial to compare the changes observed between animals trained on optogenetic
699 stimuli and sensory stimuli.

700

701 ***The perceptual threshold is plastic and can generalise***

702 We have used our ability to specifically target the same (or different) neurons across
703 multiple days to show that the perceptual threshold is not fixed and depends on
704 learning in a neuron-agnostic manner. This suggests that the perceptual apparatus
705 can flexibly adapt in order to adjust the trade-offs between different kinds of errors
706 while maximizing sensitivity (e.g. minimizing false positives vs false negatives). It also
707 underscores the brain's ability to reroute its resources (J. L. Chen et al., 2015; Hong,
708 Lacefield, Rodgers, & Bruno, 2018; Huber et al., 2012; Kawai et al., 2015; Law & Gold,

709 2008; Ölveczky, Otchy, Goldberg, Aronov, & Fee, 2011) to adaptively meet task
710 demands with ever increasing sensitivity and accuracy (Carandini & Churchland,
711 2013; Fahle, 2002; Gilbert, Sigman, & Crist, 2001; Sasaki, Nanez, & Watanabe, 2009).
712 Previous studies addressing this question in the context of sensory tasks have
713 suggested that such learning is associated with changes in the representation of
714 sensory stimuli in primary sensory areas (J. L. Chen et al., 2015; Khan et al., 2018;
715 Peron et al., 2015; Poort et al., 2015; Wiest et al., 2020). However in our case animals
716 learn despite the stimulus (direct stimulation) being held constant in sensory cortex.
717 We therefore hypothesise that, in our task, such learning-related changes likely occur
718 in downstream regions like S2 (J. L. Chen et al., 2015; Kwon, Yang, Minamisawa, &
719 O'Connor, 2016), motor cortex (J. L. Chen et al., 2015; Huber et al., 2012) or striatum
720 (Sippy, Lapray, Crochet, & Petersen, 2015; Xiong, Znamenskiy, & Zador, 2015).

721

722 The fact that the learning we observe during the 2P training phase generalizes to
723 neurons that are not stimulated during this period suggests that animals can “learn
724 to learn” (Harlow, 1949) within the context of detecting arbitrary cortical activity
725 patterns, similar to that observed in tasks relying on more naturalistic neural
726 processing (Fahle, 2002; Rudebeck & Murray, 2011; Tse et al., 2007; Walton,
727 Behrens, Buckley, Rudebeck, & Rushworth, 2010). Such generalization of knowledge
728 acquired from one learning epoch to another is a hallmark of the type of powerful
729 statistical learning systems that could underlie some of the brain’s most complex,
730 flexible behaviours (Behrens et al., 2018; Eichenbaum & Cohen, 2014; Fahle, 2002;
731 Gustafson & Daw, 2011; Stachenfeld, Botvinick, & Gershman, 2018; Tolman, 1948;
732 Tolman, Ritchie, & Kalish, 1946; Whittington, Muller, Barry, & Behrens, 2018;

733 Whittington et al., 2019). Our results, and the experimental paradigm that we present,
734 could provide a useful framework to further investigate how learning and credit are
735 assigned to ensembles of neurons in an appropriate yet generalizable way.

736

737 The relationship between the perceptual threshold that we measure and how much
738 learning can generalise also merits further investigation. It would be interesting to
739 investigate how nearby stimulated neurons have to be to previously trained neurons,
740 either physically or in terms of tuning similarity, for learning to generalise to them.
741 Indeed another all-optical study hints that generalisation is limited to neurons that
742 share stimulus tuning congruent with ensembles of neurons that have been previously
743 trained (Marshel et al., 2019) implying that generalisation is not a universal property.
744 Moreover, it would also be interesting to see whether the strength of generalisation
745 scales with the amount of uncertainty in the preceding trained stimulus set. One could
746 imagine that learning would be more likely to generalise if different neurons were
747 activated on each training day (as in our experiments), or even each trial, than if just
748 one pattern was trained for the same duration. Such volatility in the learning
749 environment is indeed thought to change learning dynamics (Behrens, Woolrich,
750 Walton, & Rushworth, 2007; Massi, Donahue, & Lee, 2018; Mcguire, Nassar, Gold, &
751 Kable, 2014) and by extension may influence the level of generalisation at the neural
752 level, as has recently been suggested for hippocampal representations (Plitt &
753 Giocomo, 2019; Sanders, Wilson, & Gershman, 2020).

754

755 How might such generalisability of learning arise? It could in part result from
756 increased connectivity between opsin-expressing neurons through plasticity induced

757 during their synchronous activation during 1P training phases, equivalent to how
758 artificial subnetworks might be generated by 2P all-optical methods (Carrillo-Reid et
759 al., 2016; Zhang, Russell, Packer, Gauld, & Häusser, 2018, though see also Alejandre-
760 García et al., 2020 for alternative non-Hebbian mechanisms). In this case, subsequent
761 2P photostimulation of opsin-expressing neurons on a given day might preferentially
762 recurrently excite other non-targeted opsin-expressing neurons on that day to a
763 greater extent than non-opsin-expressing neurons, as is thought to happen with 2P
764 optogenetic recall of artificially generated subnetworks (Carrillo-Reid et al., 2016).
765 This could cause them to become active and “bound into” the learning process on
766 that day, despite not being directly targeted, and allow them to better drive
767 behaviours when targeted on subsequent days. This would be an intriguing
768 mechanism and, while such changes in connectivity in our task would be “artificial”,
769 other work suggests that similar changes might underlie generalisation in more
770 natural sensory guided tasks. Neurons sharing functional tuning to sensory stimuli
771 tend to form recurrently connected subnetworks (Carrillo-Reid et al., 2019; Chettih &
772 Harvey, 2019; Cossell et al., 2015; Jennings et al., 2019; Ko et al., 2013; Marshel et
773 al., 2019; Peron et al., 2020; Russell et al., 2019; Znamenskiy et al., 2018), which
774 result in non-targeted members being recruited when a subset are targeted for
775 photostimulation (Carrillo-Reid et al., 2019; Jennings et al., 2019; Marshel et al., 2019;
776 Russell et al., 2019), and learning can preferentially generalise across neurons within
777 such subnetworks in sensory-guided tasks (Marshel et al., 2019). Thus while the
778 subnetworks that might be generated through our 1P training may be artificial, the
779 process of learning generalisation that we observe may also occur in more naturalistic
780 sensory-driven tasks. Indeed, the fact that this mechanism can extend beyond

781 naturalistic stimuli to aid in detection of arbitrary stimulus patterns speaks to how
782 pivotal it may be in helping the brain generate flexible behaviour.

783

784 The combination of sensitivity and flexibility that we report also raises the question of
785 whether animals could be rapidly trained to detect the activity of small numbers of
786 neurons *de novo*, without prior conditioning. This may be difficult to demonstrate in
787 a realistic experimental timeframe given that animals have a tendency to adopt easy
788 but sub-optimal strategies, such as timing licks to coincide with the mean of the trial-
789 time distribution, when they are faced both with non-naturalistic task design and
790 stimuli that are hard to detect/discriminate. Once these strategies are adopted, such
791 local optima tend to be very hard to train away and are thus better avoided in the first
792 place. Indeed, studies testing perceptual sensitivity to or discrimination of sensory
793 stimuli overwhelmingly begin with easier stimulus types to habituate the animal to the
794 novel task at hand and learning continues as more difficult stimuli are introduced
795 (Abraham et al., 2004; Andermann et al., 2010; Busse et al., 2011; Carandini &
796 Churchland, 2013; Gerdjikov et al., 2010; Histed, Carvalho, & Maunsell, 2012; Lee et
797 al., 2012; Morita et al., 2011; O'Connor et al., 2010). These features of sensory-
798 evoked behavioural performance are analagous to how animals in our task constantly
799 adapt over time to reductions in stimulus strength, even down to the lowest stimulus
800 levels tested. Furthermore, all previous studies using all-optical techniques to
801 influence behaviour with cellular resolution optogenetics have incorporated some
802 kind of conditioning phase using either sensory or optogenetic stimuli of
803 progressively lower strength (Carrillo-Reid et al., 2019; Gill et al., 2020; Jennings et

804 al., 2019; Marshel et al., 2019; Russell et al., 2019) again implying that this may be
805 necessary when probing the limits of perception.

806

807 ***Perception is sensitive despite matched network suppression***

808 The matched suppression that we observed in the local L2/3 network is in
809 accordance with the general net inhibitory effect of pyramidal neuron stimulation
810 observed *in vivo* (Chettih & Harvey, 2019; Kwan & Dan, 2012; Mateo et al., 2011;
811 Russell et al., 2019) and in detailed network models of cortex (Cai et al., 2020). This
812 supports the idea that such networks operate in an inhibition-stabilized regime where
813 one role of inhibition is to control strong recurrent excitation (Denève & Machens,
814 2016; Murphy & Miller, 2009; Ozeki et al., 2009; Pehlevan & Sompolinsky, 2014;
815 Sanzeni et al., 2020; Tsodyks et al., 1997; van Vreeswijk & Sompolinsky, 1996; Wolf
816 et al., 2014), though since our perturbations are not targeted to inhibitory neurons
817 with specific tuning we cannot assess how functionally specific this architecture
818 might be (Sadeh & Clopath, 2020). However, these results also seemingly challenge
819 recent work demonstrating that activation of co-tuned ensembles in V1
820 predominantly activates other similarly tuned neurons in the surrounding network
821 (Carrillo-Reid et al., 2019; Marshel et al., 2019) and that ablation of some neurons
822 within functional sub-groups reduces activity in the spared neurons (Peron et al.,
823 2020). This discrepancy is likely explained by the fact that recurrent excitation is
824 known to increase with tuning similarity such that neurons sharing functional tuning
825 tend to recurrently excite each other (Cossell et al., 2015; Ko et al., 2011) whereas
826 inhibition is generally less tuned and structured (Kerlin *et al.*, 2010; Bock *et al.*, 2011;
827 Fino and Yuste, 2011; Hofer *et al.*, 2011; Packer and Yuste, 2011; Scholl *et al.*, 2015,

828 though see Ye *et al.*, 2015; Znamenskiy *et al.*, 2018). Indeed, Marshel *et al.*, 2019
829 specifically use a V1 network model relying on recurrent excitation between co-tuned
830 neurons and strong general inhibition, which keeps activity in check, to explain the
831 low threshold and steepness of their psychometric functions. The subset of neurons
832 we targeted, which may not share functional tuning, are unlikely to benefit from such
833 preferential recurrent connectivity but they will likely recruit general inhibition (though
834 as mentioned above some form of enhanced connectivity or intrinsic excitability may
835 have been induced during early 1P training). Therefore, the matched suppression and
836 steep psychometric functions that we observe are consistent with this model.

837

838 Since it has not been possible up until very recently to assess the impact of such
839 titrated activation of cortical neurons on the local network during behaviour (Doron *et al.*,
840 2014; Histed & Maunsell, 2014; Houweling & Brecht, 2008; Huber *et al.*, 2008;
841 Tanke *et al.*, 2018, though see recent work Gill *et al.*, 2020; Marshel *et al.*, 2019),
842 recent theoretical work inspired by previous behavioural results has explored how
843 simulated neural networks can detect the activation of single neurons (Bernardi *et al.*,
844 2020; Bernardi & Lindner, 2017, 2019). These studies make three key predictions: (1)
845 the pool of readout neurons must be biased in favour of connecting with the
846 stimulated neuron (Bernardi & Lindner, 2017), (2) the readout network must include
847 local recurrent inhibition to mitigate noise-inducing neuronal cross-correlations
848 (Bernardi & Lindner, 2019) and (3) inhibition must lag excitation in the readout network
849 (Bernardi *et al.*, 2020). Since our paradigm allows us to simultaneously monitor the
850 local network response during behavioural detection of similarly sparse activity, we
851 can assess the validity of such predictions *in vivo*. The strong suppression recruited

852 by our stimulation suggests that powerful inhibition is at work in the network and
853 therefore supports prediction (2). The activity we induce drives behaviour despite this
854 strong local suppression, suggesting that excitation might be transmitted to
855 downstream circuits responsible for driving behaviour before inhibition has a chance
856 to quell it locally. This supports prediction (3). Our results concerning prediction (1)
857 are more mixed. Bernardi and Lindner, 2017 suggest that the predicted bias could
858 arise due to Hebbian plasticity between stimulated and readout neurons during the
859 initial microstimulation phase of training. They take as evidence for this the fact that
860 naïve animals cannot detect single neurons, something which both we and other
861 similar studies also see (Carrillo-Reid et al., 2019; Gill et al., 2020; Histed & Maunsell,
862 2014; Huber et al., 2008; Marshel et al., 2019). The fact that animals generally require
863 initial one-photon priming before being able to detect targeted two-photon stimuli
864 therefore lends some support to prediction (1). However, somewhat contradictory to
865 this prediction is our finding that the amount by which animals improve in their
866 detection of threshold stimuli across sessions is similar irrespective of whether the
867 same or different neurons were stimulated. The bias in connectivity that supposedly
868 develops between target neurons and readout neurons should not extend to other
869 neurons that are not targeted on that day. The fact that we observe such a transfer,
870 manifested in a similar learning rate across different neurons targeted across days,
871 suggests that this bias may be more general than hypothesized above and may apply
872 across most neurons contained within the area where learning has taken place,
873 potentially via recurrent lateral connectivity (either existing or induced during 1P
874 training).

875

876 **Outlook**

877 The combination of techniques that we have deployed provide a powerful
878 experimental framework that can be used to test how more nuanced features of
879 cellular identity and specific patterns of cortical activity influence perception. This will
880 bring us closer to the goal of testing precisely which of the candidate features of the
881 neural code underlie the considerable flexibility and processing power of the brain
882 (Jazayeri & Afraz, 2017; Panzeri, Harvey, Piasini, Latham, & Fellin, 2017).

883

884 **Materials and Methods**

885 All experimental procedures were carried out under Project Licence 70/14018
886 (PCC4A4ECE) issued by the UK Home Office in accordance with the UK Animals
887 (Scientific Procedures) Act (1986) and were also subject to local ethical review. All
888 surgical procedures were carried out under isoflurane anaesthesia (5% for induction,
889 1.5% for maintenance), and every effort was made to minimize suffering.

890

891 *Animal preparation*

892 4 – 6 week old wild-type (C57/BL6) and transgenic GCaMP6s mice (Emx1-
893 Cre;CaMKIIa-tTA;Ai94) of both sexes were used. A calibrated injection pipette (15 µm
894 inner diameter) bevelled to a sharp point was mounted on an oil-filled hydraulic
895 injection system (Harvard apparatus) and front-loaded with virus (either a 1:10 mixture
896 of AAV1-Syn-GCaMP6s-WPRE-SV40 and AAVdj-CaMKIIa-C1V1(E162T)-TS-P2A-
897 mCherry-WPRE or a 1:8 mixture of AAV1-Syn-GCaMP6s-WPRE-SV40 and either
898 AAV2/9-CaMKII-C1V1(t/t)-mScarlett-Kv2.1 or AAV2/9-CaMKII-C1V1(t/t)-mRuby2-
899 Kv2.1). AAV2/9-CaMKII-C1V1(t/t)-mScarlett-Kv2.1 and AAV2/9-CaMKII-C1V1(t/t)-
900 mRuby2-Kv2.1 virus was diluted in virus buffer solution (20 mM Tris, pH 8.0, 140 mM
901 NaCl, 0.001% Pluronic F-68) 10-fold relative to stock concentration ($\sim 6.9 \times 10^{14}$ gc/ml).
902 These constructs were as in Chettih and Harvey, 2019. One of the latter two
903 somatically restricted (Kv2.1) opsins was used for all experiments except those
904 targeting the same neurons across days (**Figure 2 – figure supplement 3**) where
905 non-restricted opsin was used. Of the 22 mice initially trained on 1P stimulation, 4
906 were opsin-injected GCaMP6s transgenics and 18 were opsin/indicator-injected WT
907 mice. Of these, 6 mice were used for 2P psychometric curve experiments (**Figure 2**

908 – 4), 4 of these were opsin-injected GCaMP6s transgenics and 2 were
909 opsin/indicator-injected WT mice (see *Behavioural training* below for details of mice
910 used for each training phase). Mice were given a peri-operative sub-cutaneous
911 injection of 0.3 mg/mL buprenorphine hydrochloride (Vetergesic). They were then
912 anaesthetized with isoflurane (5% for induction, 1.5% for maintenance) and the scalp
913 above the dorsal surface of the skull was removed. A metal headplate with a 7 mm
914 diameter circular imaging well was fixed to the skull over right S1 (2 mm posterior and
915 3.5 mm lateral from bregma) using dental cement. A 3 mm craniotomy was drilled
916 (NSK UK Ltd.) in the centre of the headplate well and the dura removed. Virus was
917 then injected at a depth of 300 μ m below the pia either as a single 750 nL injection at
918 200 nL/min or as ~5 injections of 150 nL virus at 50 nL/min spaced ~300 μ m apart.
919 The pipette was left in the brain for 2 minutes after each injection. Following the final
920 retraction of the injection pipette, a two-tiered 4 mm/3 mm circle/circle chronic
921 window (UQG Optics cover-glass bonded with UV optical cement, NOR-61, Norland
922 Optical Adhesive) was press-fit into the craniotomy, sealed with cyanoacrylate
923 (Vetbond) and fixed in place with dental cement. After surgery, animals were
924 monitored and allowed to recover for at least 6 days during which they received water
925 and food *ad libitum*.

926

927 *Two-photon imaging*

928 For most experiments (**Figure 2 – 4**) two-photon imaging was performed using a
929 resonant scanning (30 Hz) microscope (Ultima II, Bruker Corporation) driven by
930 PrairieView and a Chameleon Ultra II laser (Coherent). For these experiments a
931 16x/0.8-NA water-immersion objective (Nikon) and an ETL (Optotune EL-10-30-TC,

932 Gardosoft driver) were used to collect 100 μm z-depth imaging volumes (4 planes,
933 33.3 μm spacing) with FOV sizes ranging from 600 x 600 μm to 850 x 850 μm (due to
934 ETL magnification changes) at a constant image size of 512 x 512 pixels and plane-
935 rate of ~ 7 Hz. The number of neurons recorded in each 2P psychometric curve
936 experiment was 2809 ± 704 , $N = 11$ sessions, 6 animals, 1 – 2 sessions each. For
937 these experiments we used an orbital nosepiece that allows pitch, roll and yaw to
938 vary in order to get the light-path through the objective orthogonal to the plane of the
939 cranial window to ensure optimal imaging conditions (via the following procedure:
940 <https://github.com/l1erussell/MONPangle>). Due to inconsistencies in the window
941 position across days and inaccuracies in the orbital nosepiece positioning and
942 readout, pitch, roll and yaw can vary significantly across days making it difficult to
943 image the same planes, and thus same neurons, in a volume. We therefore chose to
944 reacquire new volumes each day and target new sets of neurons. For some
945 experiments (some in **Figure 1**, some **Supplementary Figures**) two-photon imaging
946 was performed using a resonant scanning (30 Hz) microscope (custom-build, Bruker
947 Corporation) driven by PrairieView and a Chameleon Ultra II laser (Coherent). For
948 these experiments a 25x/0.95-NA water-immersion objective (Leica) and an ETL
949 (Optotune EL-10-30-TC, Optotune driver) were used to collect either 490 x 490 x 100
950 μm imaging volumes (4 planes with ~ 33 μm spacing) at an image size of 512 x 512
951 pixels and plane-rate of ~ 7 Hz or single planes of FOV size 490 x 490 μm and image
952 size 512 x 512 pixels at 30 Hz. GCaMP6s was imaged at 920 nm and mCherry was
953 imaged at 765 nm. For functional volumetric GCaMP6s imaging at 920nm the
954 maximum power on sample was 50 mW at the shallowest plane (~ 130 μm below pia),
955 increasing linearly to 80 mW at the deepest plane (~ 230 μm) to maintain image quality

956 across the volume (maximum 120 mins total duration per experiment). For single
957 plane GCaMP6s imaging a maximum power of 50 mW was used for all depths. Power
958 on sample for mCherry/mRuby2/mScarlett (conjugated to C1V1), imaged at 765 nm,
959 was 50 – 100 mW (maximum 1 minute continuous duration).

960

961 *Two-photon optogenetic stimulation*

962 Two-photon photostimulation was carried out using a femto-second pulsed laser at
963 1030 nm (Satsuma, Amplitude Systèmes, 2 MHz rep-rate, 20 W). The single laser
964 beam was split via a reflective spatial light modulator (SLM) (7.68 x 7.68 mm active
965 area, 512 x 512 pixels, optimized for 1064nm, OverDrive Plus SLM, Meadowlark
966 Optics/Boulder Nonlinear Systems) which was installed in-line of the
967 photostimulation path. Phase masks used to generate beamlet patterns at the focal
968 plane were calculated from photostimulation target xy co-ordinates centred on cell-
969 bodies of interest via the weighted Gerchberg-Saxton (GS) algorithm. These targets
970 were weighted according to their location relative to the centre of the SLM's
971 addressable FOV to compensate for the decrease in diffraction efficiency when
972 directing beamlets to peripheral positions. The transformation between SLM co-
973 ordinates and imaging pixel co-ordinates was mapped by burning arbitrary spots in
974 the FOV and calculating an affine transformation between SLM pixel targets and burn
975 targets imaged in 2P. Calibration routines are available here
976 <https://github.com/l1erussell/SLMTransformMaker3D>. Spiral patterns were generated
977 by moving all beamlets simultaneously with a pair of galvanometer mirrors. Each
978 spiral consisted of 3 rotations (i.e. from centre to edge of spiral), 10 µm diameter, 20
979 ms duration. Powers were adjusted to maintain 6 mW per target neuron. Due to

980 constraints on the total power output of the photostimulation laser to stimulate 200
981 neurons we randomly divided all targeted neurons into 2 groups of 100 which were
982 stimulated as an alternating pair such that each group of 100 neurons was stimulated
983 10 times at 20 Hz (stimulate first group with 20 ms spiral, 5 ms inter-spiral interval,
984 stimulate second group with 20 ms spiral, 5 ms inter-spiral interval, then return to first
985 group and repeat a further 9 times; each group therefore receives 10 x 20 ms spirals
986 with an effective inter-spiral interval, for that group, of 25 ms; ~500 ms total stimulus
987 duration). To stimulate 100 neurons or less all neurons were stimulated
988 simultaneously 10 times at 40 Hz (10 x 20 ms spirals, 5 ms inter-spiral interval, ~250
989 ms stimulus duration). From our previous work we expect a single spiral to produce
990 ~1 action potential (Packer et al., 2015), thus all 2P stimuli should drive ~10 action
991 potentials. Spiral timing and positioning protocols were generated by a custom
992 MATLAB software suite called Naparm and executed by the photostimulation
993 modules of the microscope software (PrairieView, Bruker Corporation), the
994 MeadowLark SLM software and our synchronisation software (PackIO; see below).

995

996 *One-photon optogenetic stimulation*

997 For Phase 1 of behavioural training an amber LED (590 nm peak wavelength,
998 ThorLabs M590D2) was fixed to a manipulatable arm (DTI clamp, RS components)
999 and press-fit onto the chronic window surface. For subsequent training phases an
1000 amber LED (595 nm peak wavelength, ThorLabs M595L3) was mounted in the
1001 lightpath above the two-photon microscope objective. LED powers ranged from 0.02
1002 mW - 10 mW. Power and timing of LED photostimulation was controlled by custom
1003 MATLAB software through National Instruments data acquisition cards (NI USB-

1004 6351, NI USB-6211). All LED stimuli consisted of 5 x 20 ms pulses at 25 Hz of varying
1005 powers ranging from 10 – 0.02 mW (measured with PM100A power meter/S130C
1006 photodiode sensor, ThorLabs). We did not record activity while animals were learning
1007 to detect 1P photostimulation. We thus roughly estimate the spatial extent, number
1008 and rate of spiking evoked by pulses of this power, duration and frequency from the
1009 literature as follows. Blue light emitted from an LED shows a ~1 mm HWHM spatial
1010 spread in brain tissue and ChR2-based pyramidal neuron activation shows relatively
1011 little variation with depth (Huber et al., 2008), though this could be due to activation
1012 of superficial processes. C-fos expression also shows that recruitment by optic fibre
1013 stimulation of ChR2-expressing pyramidal neurons is limited to a ~0.7 mm³ volume
1014 around the fibre tip (Gradinaru, Mogri, Thompson, Henderson, & Deisseroth, 2009).
1015 Blue and orange light photoactivation of PV interneurons with moderate powers (10
1016 mW) show similar lateral recruitment (~0.5 – 0.8 mm HWHM) (Li et al., 2019), as does
1017 orange light Arch-mediate inhibition of pyramidal neurons (~0.5 – 0.8 mm HWHM)
1018 (Babl, Rummell, & Sigurdsson, 2019). However, high power photobleaching indicates
1019 that orange light excitation has a two-fold larger lateral extent than blue light and
1020 extends across all cortical layers to form a roughly symmetric excitation volume (Li et
1021 al., 2019), as would be expected from the reduced scattering of red-shifted light in
1022 cortical tissue (Helmchen & Denk, 2005). Given the fact that we are using an LED
1023 instead of a fibre and we are using orange light, we suggest that our excitation volume
1024 has a roughly two-fold larger lateral extent than that measured for a blue LED (Huber
1025 et al., 2008) and for orange light from a fibre/laser (Babl et al., 2019; Li et al., 2019)
1026 and is roughly symmetric. With respect to stimulus frequency, C1V1 should be able
1027 to faithfully follow a 25 Hz pulse train with ~90% fidelity though our stimulus pulses

1028 are longer than those used with C1V1 (Yizhar et al., 2011) or ChR2 (Huber et al., 2008).
1029 With respect to pulse duration, for ChR2 a doubling in pulse duration roughly
1030 corresponds to a doubling in spike probability (Histed & Maunsell, 2014) suggesting
1031 that our ten-fold increase in pulse duration relative to the literature (Yizhar et al., 2011)
1032 might correspond to a ten-fold increase in the number of evoked spikes. Though this
1033 might be an overestimate for C1V1 as it has slower channel kinetics than ChR2
1034 (Yizhar et al., 2011), it is certainly likely we are driving multiple spikes with each pulse
1035 with an upper limit defined by C1V1's inability to reliably follow trains of > 50 Hz.
1036 These data, in combination with our observation that < 25% of neurons express C1V1
1037 **(Figure 1 – figure supplement 1f)** and ~50% of C1V1-expressing neurons are
1038 photoactivatable, suggest that our initial training powers (10 mW) will drive > 5 spikes
1039 at between 25 – 50 Hz in ~10% of pyramidal neurons in a 1.5 – 2 mm³ volume. The
1040 lowest powers at the behavioural threshold will likely recruit progressively fewer
1041 neurons over smaller cortical volumes with longer spike latencies (Huber et al., 2008)
1042 and these neurons will fire fewer spikes per pulse with lower reliability (Histed &
1043 Maunsell, 2014).

1044

1045 *Synchronisation*

1046 For synchronisation of imaging frames, photostimulation spirals, sensory stimulation
1047 epochs and behavioural trial data during experiments, analogue triggers and
1048 waveforms were recorded with National Instruments DAQ cards controlled by PackIO
1049 (Watson, Yuste, & Packer, 2016). Behavioural trial timing and licking response
1050 contingency analyses were done online by an Arduino Mega microcontroller board
1051 controlled by PyBehaviour (Russell et al., 2019).

1052

1053 *Online design and execution of photostimulation protocols*

1054 To quickly design photostimulation ensembles online during experiments we used
1055 our custom controls software, Naparm (<https://github.com/l1erussell/Naparm>).
1056 Briefly, this software allows users to import images of neuronal populations of interest
1057 (i.e. C1V1 expression images) and semi-automatically detect the xyz centroids of
1058 neuron bodies. These potential target neurons can then be divided into different
1059 stimulation groups and the photostimulation protocol defined. Once defined this
1060 software saves out all files necessary to synchronise the microscope, lasers, SLM
1061 and master clock software PackIO. For behavioural training experiments we
1062 combined this with our custom two-photon behavioural training software (TPBS)
1063 which allows users to import a directory of phasemasks and associate one or more
1064 phasemasks with trial types that can be read into and executed by our behavioural
1065 control software PyBehaviour (see below).

1066

1067 *Behavioural training*

1068 Training began ~21 days post virus injection/window installation. Animals were water-
1069 restricted to 85 – 90% of their pre-training weight throughout the training period and
1070 their weight was monitored daily. The majority of each animal's daily water was
1071 consumed during behavioural training, topped-up if necessary with additional water
1072 post-training. Early one-photon training sessions took place in closed, soundproofed
1073 and unlit behavioural training boxes. During training, animals were head-fixed via their
1074 headplates and housed in Perspex tubes. A metal reward delivery spout, connected
1075 to an electronic lickometer circuit, was positioned within easy reach of the mouse's

1076 tongue to record licks and deliver sugar-water rewards (5 μ L, 10% sucrose v/v). Mice
1077 were adapted to this procedure over a day or two during which rewards were
1078 randomly delivered manually. All subsequent behavioural training was controlled by
1079 Arduino-based behavioural control software written in Python (PyBehaviour:
1080 <https://github.com/llerussell/PyBehaviour>). This software acted as the master clock,
1081 dictating the sequence and timing of behavioural trials, and recording and scoring
1082 licking behaviour. The power and temporal characteristics of LED photostimulation
1083 patterns were controlled by custom-written MATLAB software and National
1084 Instruments hardware (see “One-photon optogenetic stimulation” section).
1085 PyBehaviour controlled the output of this LED software via TTL pulses. At the
1086 beginning of each behavioural session the LED, mounted on a manipulatable arm
1087 (DTI clamp, RS components), was press-fit onto the surface of the chronic window.
1088 This region was then sealed with tape to minimize direct visual stimulation.
1089 Throughout all training sessions and phases the basic task structure was the same.
1090 Trials were triggered after animals withheld licking for 7 ± 3 s. Each trial consisted of
1091 a response window during which licking behaviour was scored, followed by a 5 s
1092 post-stimulus period. The response window lasted for 2 s in training Phase 1 and 1 s
1093 in training Phase 2 and 3, though for all behavioural analyses a 1 s window beginning
1094 at 0.15 s (0.15 – 1.15 s) post stimulus was used to exclude unrealistically quick
1095 reaction times and ensure consistency of metrics across analyses of different phases
1096 (this window is indicated on all behavioural plots). Sessions consisted of 100 – 400
1097 trials of two types: go trials and catch trials. During go trials, some form of optogenetic
1098 stimulus was delivered, and animals were required to lick. Licking was scored as a
1099 hit and was rewarded by delivery of a sugar water reward (see above), non-licking

1100 was scored as a miss and was unpunished. During catch trials, no stimulus was
1101 delivered and animals were required not to lick. Licking was scored as a false alarm,
1102 and was unpunished, non-licking was scored as a correct reject and was
1103 unrewarded. Neither of these two trial types were cued. Stimulus trials therefore test
1104 an animal's detection rate on particular stimuli and catch trials assess an animal's
1105 chance response rate. All trial types were pseudorandomly interleaved with a 3 trial
1106 upper limit on consecutive trials of the same type. During the first few sessions go
1107 trials were auto-rewarded 500 ms following the stimulus to encourage learning. As
1108 soon as animals reliably began licking in anticipation of the auto-reward it was turned
1109 off for all subsequent sessions. Animals were initially trained on Phase 1 to detect 10
1110 mW. Performance was then manually assessed and the LED power was dropped by
1111 half multiple times within a session until animals could detect very low powers (0.05
1112 mW). This usually took ~4 days. Animals then underwent psychometric curve
1113 sessions to assess their performance on the lowest LED powers (0.1, 0.08, 0.06, 0.04,
1114 0.02 mW). Animals that could detect 0.1 mW stimuli with $d\text{-prime} > 1$ were eligible for
1115 transitioning to subsequent experiments (all animals tested achieved this criterion),
1116 however only the subset with clearest expression were transitioned to two-photon
1117 training phases to allow for sufficient training time on the all-optical system. These
1118 animals were transitioned to Phases 2 and 3 where two-photon stimuli were
1119 introduced. For these phases animals were head-fixed under the microscope on a
1120 cylindrical treadmill and the LED was directed through the light-path. Note we expect
1121 that animals could be trained from the offset under the microscope using the LED
1122 through the objective, however we opted against this due to time constraints on the
1123 all-optical system. An objective well/baffle was used to minimize light leakage. A

1124 white-noise mask was played continuously throughout all subsequent training
1125 sessions to mask any auditory cues emitted by the galvos during photostimulation.
1126 Following selection of neurons for 2P photostimulation (see below) animals began
1127 training on Phase 2 where 1P and 2P optogenetic stimuli were interleaved along with
1128 catch trials in equal proportions. Initial 2P stimuli targeted 200 neurons and animals
1129 required ~1 day to reach good performance. Once animals could reliably detect 200
1130 neurons, we interleaved 2P stimuli targeting a 100 neuron subset of the original 200
1131 neurons. Once animals could reliably detect 100 neurons they were transitioned to
1132 Phase 3 where only 2P optogenetic stimulation of those 100 neurons and catch trials
1133 were delivered in equal proportions. On some trials in a few Phase 2/3 sessions auto-
1134 rewards were delivered at 0.5, 1 or 1.5 s following the stimulus (depending on the
1135 animal's reaction time) to encourage transition to detecting two-photon stimuli. These
1136 trials were scored as hits if the animal licked before the auto-reward, otherwise they
1137 were conservatively scored as misses (even if they fell within the response window)
1138 (see *Behavioural data analysis* below). For the above phases we used the same FOV
1139 across days but didn't specifically target the same neurons (see *Two-photon imaging*
1140 section of *Methods*) except in the "Same" condition in **Figure 2 – figure supplement**
1141 **3**. Following this, a subset of animals were transitioned to 2P psychometric curve
1142 sessions with the remaining subset used for other experiments not reported here (for
1143 details, see: <https://discovery.ucl.ac.uk/id/eprint/10095170/>). During two-photon
1144 psychometric curve sessions trial types were pseudorandomly interleaved to ensure
1145 an even distribution of trial types across the behavioural session. Trial-type ratios
1146 were as follows: 15% catch trials, 15% "easy" 200 neuron trials, 70% trials
1147 stimulating smaller numbers of neurons (~12% each for 100, 75, 50, 25, 10 and 5

1148 neurons). All psychometric curve sessions had an initial 10-trial buffer of “easy” 200
1149 neurons trials to allow the animal to warm up. Multiple FOVs were tested in each
1150 animal, but each FOV was tested only once. Mice were eligible for transfer from Phase
1151 2 to Phase 3 and from Phase 3 to psychometric curve sessions once they’d achieved
1152 $d\text{-prime} > 1$ for detecting 2P stimulation of 200 neurons. This did not always happen
1153 immediately due to time constraints on the all-optical system. If transition was
1154 delayed, in the intervening days mice were often trained to keep them familiar with
1155 the task. Summary of N for behavioural training: 26 mice did 1P training and of these
1156 18 mice did both high power and low power 1P psychometric curves and 4 did just
1157 high power and 4 did just low power (these tended to be the best mice which were
1158 rushed to later training phases) (**Figure 1, Figure 1 – figure supplement 3**). From
1159 these, 12 mice with the clearest expression were transitioned onto 2P training (**Figure**
1160 **1, Figure 1 – figure supplement 5**) and from these 6 mice were used for 2P
1161 psychometric curve sessions (**Figures 2 – 4**) and the remaining 6 were used for other
1162 2P experiments not reported here.

1163

1164 *Image processing*

1165 All offline data were analysed using custom software and toolboxes in MATLAB.
1166 PackIO data acquired during experiments was used to synchronise imaging frames
1167 with photostimulation and behavioural epochs. To avoid the large imaging artefacts
1168 caused by 2P photostimulation, we implemented a “stimulus artefact exclusion
1169 epoch” whereby all imaging frames acquired during photostimulation periods were
1170 excluded from all processing, analyses and plotting. This is described below. Since
1171 it takes 500 ms to stimulate 200 neurons (see *Two-photon optogenetic stimulation*

1172 above), and since we wanted the amount of data (volume scans) excluded to be the
1173 same for all trial types (to facilitate comparison across them), we need to exclude at
1174 least 0 - 500 ms of imaging data post-stimulus onset on all trials (even though stimuli
1175 targeting ≤ 100 neurons take ~ 250 ms). In reality we actually have to remove a
1176 slightly longer period of imaging data (5 full volumes peri-stimulus; ~ 750 ms of
1177 imaging data) due to how the photostimulus epoch overlaps with the time-course of
1178 imaging volume acquisition. We explain this below. Photostimulation onsets are not
1179 synchronized to begin at the same time as the first plane in a given volume (i.e. they
1180 can occur during any plane within a volume). Our volumes contain 4 planes and if any
1181 plane is corrupted by the stimulus artifact then that volume must be discarded. Our
1182 imaging frame (plane) rate is 26.8 Hz and, since we acquire 4 planes per volume, our
1183 volume rate is 6.69 Hz. This means it takes ~ 150 ms to acquire the four planes
1184 constituting one volume. Thus, given that the maximum photostimulus duration is
1185 ~ 500 ms (see above), even if photostimulus onset was synchronized to always begin
1186 with the first plane of a given volume, the minimum number of volumes we could
1187 discard post-stimulus onset would be 4 ($4 * 150$ ms = 600 ms). However, since the
1188 photostimulus onset can occur at any time during a volume acquisition, it can also
1189 occur during the last plane of the volume immediately preceding the stimulus onset.
1190 This volume must also be discarded in addition to the subsequent 4 volumes which
1191 must also be discarded as they will also all contain at least one frame corrupted by
1192 the photostimulus. This means that on some trials 5 volumes will need to be
1193 discarded (~ 750 ms of imaging data). Since we always want to discard the same
1194 amount of imaging data across trials to facilitate comparison between them, we have
1195 to exclude this maximum value of 5 volumes (~ 750 ms) peri-stimulus on all trials.

1196 Since most reaction times occur before this (560 ± 150 ms reaction time for 2P 200
1197 neuron trials) we are unable to analyse data in the absence of response-related
1198 activity (licking, whisking, facial movements). Thus we had to control for this in our
1199 subsequent analyses (see *Neurometric curve analyses* section of *Methods*). Imaging
1200 time-series were registered and segmented into ROIs using the Python version of
1201 Suite2P (Pachitariu et al., 2016). ROIs were manually curated. Neuropil subtracted
1202 neuron traces were calculated as:

$$1203 \quad F_{cell} = F_{ROI} - c * F_{neuropil}$$

1204 where the neuropil subtraction coefficient c was estimated separately for each ROI
1205 by robust regression between F_{ROI} and $F_{neuropil}$ (T.-W. Chen et al., 2013). For this
1206 estimation process, all photostimulation epochs were excluded and F_{ROI} and $F_{neuropil}$
1207 were downsampled by a factor of 10 (to 0.7 Hz). Coefficients were post-hoc bounded
1208 between 0.5 and 1 and any coefficients that could not be reliably estimated were set
1209 to the median of all reliably estimated coefficients in that dataset (usually ~ 0.7). Once
1210 $F_{neuropil}$ had been subtracted from F_{ROI} , F_{cell} was then re-baselined to the 33rd
1211 percentile of F_{ROI} values to ensure accuracy in subsequent $\Delta F/F_0$ and $\Delta F/\sigma F$
1212 calculations. Neuropil subtraction had a small but significant effect on trial-wise
1213 response amplitude, however we observed a large fraction of negative responses
1214 even without neuropil subtraction and response classifications (activated,
1215 suppressed and no response) were largely consistent between raw and neuropil
1216 subtracted trial-wise responses (**Figure 3 – figure supplement 2**). To detect neurons
1217 expressing C1V1 offline post experiment (**Figure 1 – figure supplement 1**) we used
1218 the Cellpose algorithm followed by manual curation (Stringer, Wang, Michaelos, &
1219 Pachitariu, 2020) using the *cytoplasm* model with diameter = 15 μm .

1220

1221 *Neuronal response analysis*

1222 For trial-wise analyses, F_{cell} traces were divided into epochs triggered on
1223 photostimulation onset for stimulus trials and catch trial response window onset for
1224 catch trials (stimulus-triggered averages – STAs). All STAs had a 1 s baseline period.
1225 STAs for each trial were converted to $\Delta F/\sigma F$ by subtracting the baseline mean from
1226 the STA trace (ΔF) and dividing the result by the baseline standard deviation (σF).
1227 Responses on both photostimulation and catch trials were quantified as the average
1228 response $\sim 0.7 - 1$ s following photostimulus onset so as to avoid photostimulation
1229 artefacts (see *Image processing* section above for full description of the stimulus
1230 artefact exclusion epoch). For our analyses we wanted to be able to assess neural
1231 responses on single trials as our procedure for mitigating potential lick response
1232 artefacts requires trial-wise analyses. Moreover we cannot assume that the same
1233 background neurons will be recruited by photostimulation of a given set of target
1234 neurons on each trial due to the high variability and low probability of synaptic
1235 transmission (London et al., 2010). This therefore precludes the use of a standard
1236 statistical test comparing a neuron's stimulus trial response distribution to its catch
1237 trial response distribution to assess responsivity. We therefore sought to define
1238 activation and suppression thresholds that we could apply to responses on individual
1239 trials. We used each neuron's response distribution on correct reject (CR) catch trials,
1240 when no stimulus or lick response occurred, to define its separate activation and
1241 suppression thresholds (since activation and suppression are readout differently by
1242 calcium indicators; see Otis et al., 2017) (**Figure 2 – figure supplement 1b – g**). For
1243 each neuron we defined its activation threshold as:

1244
$$Threshold_{activation} = Mean_{catch} + S.D._{catch} * Scaling\ Factor_{activation}$$

1245 and its suppression threshold as:

1246
$$Threshold_{suppression} = Mean_{catch} - S.D._{catch} * Scaling\ Factor_{suppression}$$

1247 Where $Mean_{catch}$ and $S.D._{catch}$ are the mean and standard deviation of the
1248 distribution of CR catch trial responses respectively (**Figure 2 – figure supplement**
1249 **1b**). We estimated the activation and suppression scaling factors separately for each
1250 session (i.e. each session will have a single activation and single suppression scaling
1251 factor applied to all neurons), and separately from each other, using a cross-validated
1252 empirical procedure where the objective was to ensure that only 5% of neurons were
1253 activated and 5% of neurons were suppressed on catch trials, effectively fixing the
1254 false positive (FP) rate at 5% for each session (**Figure 2 – figure supplement 1c**).
1255 For data recorded on each session and for each response type (i.e. in the following
1256 example for activation) we swept through a series of potential activation scaling
1257 factors (range 1 – 3 in increments of 0.1). At each scaling factor we ran 10,000
1258 permutations of an 80:20 train:test split over CR catch trials. On each permutation
1259 we used the training CR catch trials to define each neuron’s activation threshold
1260 (using the equation above with the current scaling factor) and then used these
1261 thresholds to calculate the proportion of neurons crossing their threshold on each
1262 testing CR catch trial and averaged this across trials to get the average proportion
1263 activated across testing trials. We then took the median proportion activated across
1264 all permuted train:test splits. We plot this median value for all scaling factors resulting
1265 in a distinct curve for each session (**Figure 2 – figure supplement 1d,e** data points).
1266 We fit each session’s curve with cubic interpolation (**Figure 2 – figure supplement**
1267 **1d,e** curves) and then used this to infer the s.d. scaling factor that yields a 5% FP

1268 rate across permuted train:test splits for each session and for each response type
1269 (**Figure 2 – figure supplement 1d,e** box plots). These scaling factors can then be
1270 used in conjunction with the full CR catch response distribution as described in the
1271 equations above to define an activation threshold and a suppression threshold for
1272 each neuron in each session. For subsequent analyses, to quantify the number of
1273 target neurons activated we simply calculated the number of neurons in target zones
1274 that passed their activation threshold on each trial and averaged this across trials of
1275 the same type. To quantify P(Activated) and P(Suppressed) in all neurons (**Figure 3a**
1276 – **c**) we divided the total number of activated or suppressed neurons on each trial,
1277 irrespective of whether they were in target zones or not, by the total number of
1278 neurons (targets and background) and averaged across trials of the same type. To
1279 quantify P(Activated) and P(Suppressed) in background neurons (**Figure 3d,e**) we
1280 divided the total number of activated or suppressed background neurons on each
1281 trial (target neurons excluded) and divided this by the total number of neurons (targets
1282 and background) and averaged across trials of the same type. Note that all neural
1283 response data in **Figure 3** and **4** are hit:miss matched (see below *Hit:miss matching*).

1284

1285 *Classifying target neurons and background neurons*

1286 Since the spatial resolution of two-photon photostimulation is not perfect we defined
1287 conservative 3D photostimulation zones around each targeted location in the imaging
1288 volume. These had a 10 μm radius, which is $\sim 2\times$ the lateral resolution of our 2P
1289 photostimulation (**Figure 1 – figure supplement 2a**), and extended through the entire
1290 axial range of the volume (99 μm) (**Figure 2 – figure supplement 1a**). Thus we
1291 considered all ROIs with a centroid $\leq 10 \mu\text{m}$ from any target location to be a potential

1292 target neuron, irrespective of their axial displacement relative to the target location.
1293 ROIs outside these zones were considered background neurons. Since these
1294 exclusion zones are conservative, many neurons fell within them (**Figure 2 – figure**
1295 **supplement 1h**), though only a fraction were responsive to photostimulation (**Figure**
1296 **2 – figure supplement 1i,j** 0.18 ± 0.1 fraction activated across neurons within target
1297 zones, averaged across trial types, $N = 11$ sessions, 6 animals, 1 – 2 sessions each).
1298 Nevertheless this fraction was far above the fraction responsive on catch trials
1299 (**Figure 2 – figure supplement 1j** stimulus trials: 0.18 ± 0.1 vs catch trials: $0.04 \pm$
1300 0.01 averaged across trial types $P = 4.92 \times 10^{-4}$ paired t-test, $N = 11$ sessions, 6
1301 animals, 1 – 2 sessions each) and resulted in numbers of activated target neurons
1302 that were 0.46 ± 0.20 times that of the number of target zones (averaged across trial
1303 types) and decreased with decreasing number of zones as intended (**Figure 2 – figure**
1304 **supplement 1i**).

1305

1306 *Hit:miss matching*

1307 We are interested in how the number of target neurons activated modulates
1308 responses in the local network (**Figure 3,4**). The number of target neurons activated
1309 increases the probability of licking (**Figure 2**). Licking itself activates responses in the
1310 background network irrespective of photostimulation of target neurons (**Figure 3 –**
1311 **figure supplement 1**). Therefore we sought to minimize the chance that any
1312 modulation in background network activity we observe in response to changes in the
1313 number of target neurons activated is due to increased recruitment of licking, and
1314 lick-evoked activity, by more salient target stimulation. Thus we fixed a 50:50 ratio of
1315 hits:misses (lick:no-lick trials) on every trial type (number of target zones) (**Figure 3 –**

1316 **figure supplement 1o**). In this way we can ensure that the proportion of lick
1317 corruption in hard to detect stimuli (5 target zones), which mainly result in misses, is
1318 similar to that of easy to detect stimuli (100 target zones), which mainly result in hits.
1319 Below we describe this procedure using the least salient trial type (5 target zones) of
1320 a given session as an example. First we count the number of trials of this trial type
1321 with the minority response type which, in this case, is hits since animals rarely detect
1322 5 target site stimulations. This number is logged as the number of trials to match with
1323 trials of the majority response type which, in this case, is misses (as animals often fail
1324 to detect 5 target zone stimulations). We then run 100 permutations where we take
1325 all the minority trial type trials (hits) and random resamples, of the same number, of
1326 the majority trial type trials (misses). For example if there were 2 hits and 15 misses
1327 overall then on each permutation we would take the same 2 hit trials and a random 2
1328 miss trials (sampled from the 15 misses) and calculate our neural metrics across these
1329 trials. We then average these metrics across all permutations to get final values
1330 reported in network response figures. This procedure was not possible for a few trial
1331 types as there only trials of one response type (i.e. only hits or only misses). These
1332 trial types were excluded from analysis.

1333

1334 *Lick analysis*

1335 To correlate spontaneous fluorescence traces with spontaneous licking we removed
1336 photostimulation trial periods (0 – 4 s post-stimulus) and analysed the remaining
1337 periods of lick and fluorescence traces spanning the time between the first and last
1338 spontaneous lick. We smoothed the lick trace with a Gaussian kernel (sigma = 0.5 s)
1339 and calculated the Pearson's correlation coefficient (and associated *P*-values)

1340 between the smoothed lick trace and each neuron's fluorescence trace. To detect
1341 spontaneous lick bouts for lick-triggered STA analysis we excluded all trial periods (0
1342 – 4 s post-stimulus onset) and found groups of at least 3 licks that occurred with a
1343 minimum 0.5 s inter-lick interval that were separated from preceding licks by at least
1344 1 s.

1345

1346 *Behavioural data analysis*

1347 All behavioural trials with ≤ 0.15 s reaction time were excluded from analysis.
1348 Response windows for analysis of all Phases extended for 1 s following this period
1349 (i.e. 0.15 – 1.15 s post-stimulus onset). This is indicated in all raster plots. Behavioural
1350 trials during imaging experiments which occurred so close to the beginning/end of
1351 imaging epochs that the requisite analysis windows were truncated were excluded
1352 from analyses. For calculations of reaction time standard deviation we only included
1353 sessions where all trial types had responses on > 2 trials. For sessions including some
1354 auto-rewarded trials (early Phase 1 and Phase 2 sessions) we scored auto-rewarded
1355 trials with response times $< t_{\text{auto-reward}} + 0.15$ s as hits and scored auto-rewarded trials
1356 with responses after this time, or no response at all, as misses. The basic behavioural
1357 response metric used throughout was the $P(\text{response})$ for each stimulation type,
1358 calculated as:

$$1359 \quad P(\text{response}) = \frac{n_{\text{lick}}}{n_{\text{lick}} + n_{\text{no lick}}}$$

1360 Where n_{lick} and $n_{\text{no lick}}$ are the number of trials where the animal licked and did not
1361 lick respectively. For some analyses the catch trial $P(\text{response})$ was subtracted from
1362 the $P(\text{response})$ on go trials. This has been indicated where relevant as “Catch
1363 subtracted”. For some behavioural analyses where learning relative to our

1364 behavioural response criterion ($d\text{-prime} > 1$) was relevant we report performance in
1365 terms of $d\text{-prime}$ which we computed as:

$$1366 \quad \text{norminv}(\text{Hit rate}) - \text{norminv}(\text{False alarm rate})$$

1367 where *norminv* is the inverse of the normal cumulative distribution function. We
1368 corrected for hit rates/false alarm rates of 1 and 0 according to Macmillan & Kaplan,
1369 1985.

1370

1371 *Psychometric curve fitting*

1372 We used the MATLAB *psignifit* toolbox (Schütt, Harmeling, Macke, & Wichmann,
1373 2016; <https://github.com/wichmann-lab/psignifit>) to fit log-normal beta-binomial
1374 psychometric curves of the following form:

$$1375 \quad \psi(x) = \gamma + (1 + \lambda - \gamma) S(x; m, w)$$

$$1376 \quad S(x; m, w) = \Phi\left(c \frac{\log(x) - m}{w}\right)$$

$$1377 \quad c = \Phi^{-1}(0.95) - \Phi^{-1}(0.05)$$

1378 For which we fit the width (w) and threshold (m) and fixed the lapse rate (λ) and guess
1379 rate (γ). \log is the natural logarithm. The lapse rate was fixed as $1 - \max(\text{P(Lick)}_{\text{stim}})$
1380 where $\max(\text{P(Lick)}_{\text{stim}})$ is the maximum response rate to any stimulus trial-type (this
1381 was always either 100 or 200 target zone stimulation trials). The guess rate was fixed
1382 as the catch trial response rate. Only go (stimulus) trials were used for fitting. For fits
1383 aggregating across sessions (**Figure 2d** red curve) the lapse rate and guess rate were
1384 fixed using values averaged across sessions. For fits during train/test permutations
1385 (**Figure 4d**) the lapse rate and guess rate were fixed at values computed from all data
1386 and fixed for all permutations whereas the width and threshold were re-fit for every
1387 permutation.

1388

1389 *Data exclusion criteria*

1390 Some animals were removed from analysis of reaction time variability in Phase 1
1391 behavioural sessions as they did not show enough responses in catch trials to
1392 compute the standard deviation of reaction time (**Figure 1f**). Some trial types for some
1393 sessions were excluded from **Figure 3** and **4** as the procedure required to match the
1394 number of Hit and Miss trials resulted in no trials of certain trial types (see *Hit:miss*
1395 *matching* section of the *Methods*). Some trial types were removed from network
1396 response analyses (**Figure 3**) as the number of targets activated was < 1 on average.
1397 No data were removed as outliers. Trials with reaction times ≤ 0.15 s were excluded
1398 from all figures (except for illustrative purposes in **Figure 1 – figure supplement 3b**)
1399 and analyses as this was deemed to be too quick to be a reaction to the stimulus. In
1400 the latter half of each training session if the response probability on the easiest trial
1401 type for that session fell below 0.7 (calculated in a 10-trial sliding window centred on
1402 each trial) the animal was deemed to be “sated” and trials beyond this point were
1403 excluded from all analyses.

1404

1405 *Statistical procedures*

1406 No statistical procedures were used to estimate sample sizes. Appropriate sample
1407 sizes were estimated from previous experiments of a similar type. Experiments were
1408 not randomized and experimenters were not blinded with respect to experiment and
1409 outcome. All data were analysed with custom routines and toolboxes in MATLAB
1410 except for psychometric curve fitting which was done using the MATLAB *psignifit*
1411 toolbox (see *Psychometric curve fitting* section of *Methods*). All error bars are given

1412 as mean \pm s.e.m and all values in the text are mean \pm s.d. unless otherwise stated.
1413 All boxplots show median and 25th/75th percentile boxes with whiskers extending to
1414 the most extreme data not considered outliers (outliers defined as data $> q_3 +$
1415 $1.5 \times (q_3 - q_1)$ or $< q_1 - 1.5 \times (q_3 - q_1)$ where q_3 and q_1 are the 75th and 25th
1416 percentiles respectively). Regression coefficients and psychometric function
1417 parameters are reported \pm 95% confidence intervals where appropriate. Datasets of
1418 $N > 8$ were tested for normality with D'Agostino-Pearson's K2 test and analysed
1419 according to the result. Datasets of $N \leq 8$ were analysed as non-parametric. Multiple
1420 comparisons were corrected using the Bonferroni correction. All tests were two-
1421 tailed. Relevant tests are reported in the text.

1422

1423 *Data availability*

1424 Import, processing, analysis and figure code is available on Github (Dalglish, 2020;
1425 <https://github.com/alloptical/Dalglish-eLife-2020>) for use with analysed data
1426 (<https://doi.org/10.6084/m9.figshare.13135505>) and/or unprocessed behavioural
1427 session data (<https://doi.org/10.6084/m9.figshare.13128950>). Raw calcium imaging
1428 movies are ~1TB in size and are thus available upon reasonable request.

1429

1430 **Acknowledgements**

1431 We thank Mehmet Fişek for useful discussions about experiments and analysis;
1432 Selmaan Chettih and Christopher Harvey for developing and sharing the somatically-
1433 restricted C1V1 opsin; Soyon Chun and Agnieszka Jucht for mouse breeding; Sarolta
1434 Gabulya for behavioural training during pilot experiments; and Bruker Corporation for
1435 technical support. This work was supported by grants from the Wellcome Trust,
1436 Gatsby Charitable Foundation, ERC, MRC and the BBSRC.

1437

1438 **Competing interests**

1439 The authors declare no competing interests.

1440

1441 **References**

- 1442 Abraham, N. M., Spors, H., Carleton, A., Margrie, T. W., Kuner, T., & Schaefer, A. T. (2004).
1443 Maintaining Accuracy at the Expense of Speed: Stimulus Similarity Defines Odor
1444 Discrimination Time in Mice. *Neuron*, *44*, 865–876.
- 1445 Alejandro-García, T., Kim, S., Pérez-Ortega, J., & Yuste, R. (2020). Intrinsic excitability
1446 mechanisms of neuronal ensemble formation. *BioRxiv*, 1–43.
- 1447 Amit, D., Gutfreund, H., & Sompolinsky, H. (1985a). Spin-glass models of neural networks.
1448 *Physical Review A*, *32*(2), 1007–1018.
- 1449 Amit, D., Gutfreund, H., & Sompolinsky, H. (1985b). Storing infinite numbers of patterns in a
1450 Spin-Glass model of neural networks. *Physical Review Letters*, *55*(14), 1530–1533.
- 1451 Andermann, M. L., Kerlin, A. M., & Reid, R. C. (2010). Chronic cellular imaging of mouse visual
1452 cortex during operant behavior and passive viewing. *Front Cellular Neuroscience*,
1453 *4*(March), 3. <https://doi.org/10.3389/fncel.2010.00003>
- 1454 Attwell, D., & Laughlin, S. B. (2001). An Energy Budget for Signaling in the Grey Matter of the
1455 Brain. *Journal of Cerebral Blood Flow and Metabolism*, *21*, 1133–1145.
- 1456 Babl, S. S., Rummell, B. P., & Sigurdsson, T. (2019). The Spatial Extent of Optogenetic
1457 Silencing in Transgenic Mice Expressing Channelrhodopsin in Inhibitory Interneurons.
1458 *Cell Reports*, *29*, 1381–1395. <https://doi.org/10.1016/j.celrep.2019.09.049>
- 1459 Barlow, H. B. (1972). Single units and sensation: A neuron doctrine for perceptual
1460 psychology? *Perception*, *1*, 371–394.
- 1461 Barth, A. L., & Poulet, J. F. a. (2012). Experimental evidence for sparse firing in the neocortex.
1462 *Trends in Neurosciences*, *35*(6), 345–355. <https://doi.org/10.1016/j.tins.2012.03.008>
- 1463 Baum, E. B., Moody, J., & Wilczek, F. (1988). Internal representations for associative memory.
1464 *Biological Cybernetics*, *228*, 217–228.
- 1465 Behrens, T. E. J., Muller, T. H., Whittington, J. C. R., Mark, S., Baram, A. B., Stachenfeld, K.
1466 L., & Kurth-nelson, Z. (2018). What is a cognitive map? Organizing knowledge for flexible
1467 behavior. *Neuron*, *100*(2), 490–509. <https://doi.org/10.1016/j.neuron.2018.10.002>
- 1468 Behrens, T. E. J., Woolrich, M. W., Walton, M. E., & Rushworth, M. F. S. (2007). Learning the
1469 value of information in an uncertain world. *Nature Neuroscience*, *10*(9), 1214–1221.
1470 <https://doi.org/10.1038/nn1954>
- 1471 Bernander, O., Douglas, R., Martin, K., & Koch, C. (1991). Synaptic background activity
1472 influences spatiotemporal integration in single pyramidal cells. *Proceedings of the*
1473 *National Academy of Sciences of the United States of America*, *88*(December), 11569–
1474 11573.
- 1475 Bernardi, D., Doron, G., Brecht, M., & Lindner, B. (2020). A network model of the barrel cortex
1476 combined with a differentiator detector reproduces features of the behavioral response
1477 to single-neuron stimulation. *BioRxiv*, 1–35.
- 1478 Bernardi, D., & Lindner, B. (2017). Optimal Detection of a Localized Perturbation in Random
1479 Networks of Integrate-and-Fire Neurons. *Physical Review Letters*, *118*(268301), 1–5.
1480 <https://doi.org/10.1103/PhysRevLett.118.268301>
- 1481 Bernardi, D., & Lindner, B. (2019). Detecting single-cell stimulation in a large network of
1482 integrate-and-fire neurons. *Physical Review E*, *99*(032304), 1–18.
1483 <https://doi.org/10.1103/PhysRevE.99.032304>
- 1484 Bialek, W. (2012). *Biophysics: Searching for Principles*. Princeton University Press. Retrieved

- 1485 from <https://books.google.co.uk/books?id=MLYJ5Rz3GLwC>
- 1486 Bock, D. D., Lee, W. A., Kerlin, A. M., Andermann, M. L., Hood, G., Wetzel, A. W., ... Reid, R.
1487 C. (2011). Network anatomy and in vivo physiology of visual cortical neurons. *Nature*,
1488 471, 177–182. <https://doi.org/10.1038/nature09802>
- 1489 Borg-Graham, L. J., Monier, C., & Frégnac, Y. (1998). Visual input evokes transient and strong
1490 shunting inhibition in visual cortical neurons. *Nature*, 7603(1979), 619–623.
- 1491 Britten, K. H., Newsome, W. T., Shadlen, M. N., Celebrini, S., & Movshon, J. a. (1996). A
1492 relationship between behavioral choice and the visual responses of neurons in macaque
1493 MT. *Visual Neuroscience*, 13(1), 87–100. Retrieved from
1494 <http://www.ncbi.nlm.nih.gov/pubmed/8730992>
- 1495 Brunel, N. (2016). Is cortical connectivity optimized for storing information? *Nature*
1496 *Neuroscience*, 19(5). <https://doi.org/10.1038/nn.4286>
- 1497 Busse, L., Ayaz, A., Dhruv, N. T., Katzner, S., Saleem, A. B., Scho, M. L., ... Carandini, M.
1498 (2011). The Detection of Visual Contrast in the Behaving Mouse. *The Journal of*
1499 *Neuroscience*, 31(31), 11351–11361. [https://doi.org/10.1523/JNEUROSCI.6689-](https://doi.org/10.1523/JNEUROSCI.6689-10.2011)
1500 10.2011
- 1501 Cai, B., Billeh, Y. N., Chettih, S. N., Harvey, C. D., Koch, C., Arkhipov, A., & Mihalas, S. (2020).
1502 Modeling robust and efficient coding in the mouse primary visual cortex using
1503 computational perturbations. *BioRxiv*, 1–37.
- 1504 Carandini, M., & Churchland, A. K. (2013). Probing perceptual decisions in rodents. *Nature*
1505 *Neuroscience*, 16(7), 824–831. <https://doi.org/10.1038/nn.3410>
- 1506 Carbon, C.-C. (2014). Understanding human perception by human-made illusions. *Frontiers*
1507 *in Human Neuroscience*, 8(July), 1–6. <https://doi.org/10.3389/fnhum.2014.00566>
- 1508 Cardin, J. A., Kumbhani, R. D., Contreras, D., & Palmer, L. A. (2010). Cellular Mechanisms of
1509 Temporal Sensitivity in Visual Cortex Neurons. *The Journal of Neuroscience*, 30(10),
1510 3652–3662. <https://doi.org/10.1523/JNEUROSCI.5279-09.2010>
- 1511 Carrillo-Reid, L., Han, S., Yang, W., Akrouh, A., Carrillo-reid, L., Han, S., ... Yuste, R. (2019).
1512 Controlling Visually Guided Behavior by Holographic Recalling of Cortical Ensembles.
1513 *Cell*, 178, 1–11. <https://doi.org/10.1016/j.cell.2019.05.045>
- 1514 Carrillo-Reid, L., Yang, W., Bando, Y., Peterka, D. S., & Yuste, R. (2016). Imprinting and
1515 recalling cortical ensembles. *Science*, 353, 691–694.
1516 <https://doi.org/10.1126/science.aaf7560>
- 1517 Cassidy, C. M., Balsam, P. D., Rosengard, R. J., Slifstein, M., Daw, N. D., Abi-dargham, A.,
1518 & Horga, G. (2018). A Perceptual Inference Mechanism for Hallucinations Linked to
1519 Striatal Dopamine. *Current Biology*, 28(4), 503–514.
1520 <https://doi.org/10.1016/j.cub.2017.12.059>
- 1521 Ceballo, S., Bourg, J., Kempf, A., Piwkowska, Z., Daret, A., Pinson, P., ... Bathellier, B. (2019).
1522 Cortical recruitment determines learning dynamics and strategy. *Nature*
1523 *Communications*, 10, 1–12. <https://doi.org/10.1038/s41467-019-09450-0>
- 1524 Ceballo, S., Piwkowska, Z., Bourg, J., Daret, A., & Bathellier, B. (2019). Targeted Cortical
1525 Manipulation of Auditory Perception. *Neuron*, 104, 1168–1179.
1526 <https://doi.org/10.1016/j.neuron.2019.09.043>
- 1527 Chaudhury, S. (2010). Hallucinations: Clinical aspects and management. *Industrial Psychiatry*
1528 *Journal*, 19(1), 5–12. <https://doi.org/10.4103/0972-6748.77625>
- 1529 Chen, J. L., Carta, S., Soldado-Magraner, J., Schneider, B. L., & Helmchen, F. (2013).

- 1530 Behaviour-dependent recruitment of long-range projection neurons in somatosensory
1531 cortex. *Nature*, 499(7458), 336–340. <https://doi.org/10.1038/nature12236>
- 1532 Chen, J. L., Margolis, D. J., Stankov, A., Sumanovski, L. T., Schneider, B. L., & Helmchen, F.
1533 (2015). Pathway-specific reorganization of projection neurons in somatosensory cortex
1534 during learning. *Nature Neuroscience*, 18(8), 1101–1108.
1535 <https://doi.org/10.1038/nn.4046>
- 1536 Chen, T.-W., Wardill, T. J., Sun, Y., Pulver, S. R., Renninger, S. L., Baohan, A., ... Kim, D. S.
1537 (2013). Ultrasensitive fluorescent proteins for imaging neuronal activity. *Nature*,
1538 499(7458), 295–300. <https://doi.org/10.1038/nature12354>
- 1539 Chettih, S. N., & Harvey, C. D. (2019). Single-neuron perturbations reveal feature-specific
1540 competition in V1. *Nature*, 567, 334–340. <https://doi.org/10.1038/s41586-019-0997-6>
- 1541 Cohen, M. R., & Newsome, W. T. (2004). What electrical microstimulation has revealed about
1542 the neural basis of cognition. *Current Opinion in Neurobiology*, 14, 169–177.
1543 <https://doi.org/10.1016/j.conb.2004.03.016>
- 1544 Constantinople, C. M., & Bruno, R. M. (2013). Deep Cortical Layers Are Activated Directly by
1545 Thalamus. *Science*, 1591(June), 1591–1594. <https://doi.org/10.1126/science.1236425>
- 1546 Corlett, P. R., Horga, G., Fletcher, P. C., Alderson-day, B., Schmack, K., & Powers III, A. R.
1547 (2019). Hallucinations and Strong Priors. *Trends in Cognitive Sciences*, 23(2), 114–127.
1548 <https://doi.org/10.1016/j.tics.2018.12.001>
- 1549 Cossell, L., Iacaruso, M. F., Muir, D. R., Houlton, R., Sader, E. N., Ko, H., ... Mrsic-flogel, T.
1550 D. (2015). Functional organization of excitatory synaptic strength in primary visual
1551 cortex. *Nature*, 518(00), 399–403. <https://doi.org/10.1038/nature14182>
- 1552 Daie, K., Svoboda, K., & Druckmann, S. (2019). Targeted photostimulation uncovers circuit
1553 motifs supporting short-term memory. *BioRxiv*.
- 1554 Dagleish, H. W. P. (2020). Dagleish-eLife-2020. *GitHub*.
1555 <https://github.com/alloptical/Dagleish-eLife-2020.7e47864>.
- 1556 Denève, S., & Machens, C. K. (2016). Efficient codes and balanced networks. *Nature*
1557 *Neuroscience*, 19(3), 375–382. <https://doi.org/10.1038/nn.4243>
- 1558 Destexhe, A., & Pare, D. (1999). Impact of Network Activity on the Integrative Properties of
1559 Neocortical Pyramidal Neurons In Vivo. *Journal of Neurophysiology*, 81(4), 1531–1547.
- 1560 Destexhe, A., Rudolph, M., & Paré, D. (2003). The high-conductance state of neocortical
1561 neurons in vivo. *Nature Reviews Neuroscience*, 4(September), 739–751.
1562 <https://doi.org/10.1038/nrn1198>
- 1563 Doron, G., von Heimendahl, M., Schlattmann, P., Houweling, A. R., & Brecht, M. (2014).
1564 Spiking Irregularity and Frequency Modulate the Behavioral Report of Single-Neuron
1565 Stimulation. *Neuron*, 81(3), 653–663. <https://doi.org/10.1016/j.neuron.2013.11.032>
- 1566 Douglas, R. J., Koch, C., Mahowald, M., Martin, K. A. C., & Suarez, H. H. (1995). Recurrent
1567 Excitation in Neocortical Circuits. *Science*, 269(August), 981–986.
- 1568 Eichenbaum, H., & Cohen, N. J. (2014). Can we reconcile the declarative memory and spatial
1569 navigation views on hippocampal function? *Neuron*, 83(4), 764–770.
1570 <https://doi.org/10.1016/j.neuron.2014.07.032>
- 1571 Emiliani, V., Cohen, A. E., Deisseroth, K., & Hausser, M. (2015). All-Optical Interrogation of
1572 Neural Circuits. *The Journal of Neuroscience*, 35(41), 13917–13926.
1573 <https://doi.org/10.1523/JNEUROSCI.2916-15.2015>
- 1574 Fahle, M. (2002). Perceptual learning: specificity versus generalization. *Current Opinion in*

- 1575 *Neurobiology*, 15, 154–160. <https://doi.org/10.1016/j.conb.2005.03.010>
- 1576 Feldmeyer, D., Brecht, M., Helmchen, F., Petersen, C. C. H., Poulet, J. F. A., Staiger, J. F., ...
 1577 Schwarz, C. (2013). Barrel cortex function. *Progress in Neurobiology*, 103, 3–27.
 1578 <https://doi.org/10.1016/j.pneurobio.2012.11.002>
- 1579 Fino, E., & Yuste, R. (2011). Dense Inhibitory Connectivity in Neocortex. *Neuron*, 69(6), 1188–
 1580 1203. <https://doi.org/10.1016/j.neuron.2011.02.025>
- 1581 Folli, V., Leonetti, M., & Ruocco, G. (2017). On the Maximum Storage Capacity of the Hopfield
 1582 Model. *Frontiers in Computational Neuroscience*, 10(January), 1–9.
 1583 <https://doi.org/10.3389/fncom.2016.00144>
- 1584 Friston, K. (2005). Hallucinations and perceptual inference. *Behavioral and Brain Sciences*,
 1585 28(May 2020), 764–766.
- 1586 Gerdjikov, T. V., Bergner, C. G., Stüttgen, M. C., Waiblinger, C., & Schwarz, C. (2010).
 1587 Discrimination of Vibrotactile Stimuli in the Rat Whisker System: Behavior and
 1588 Neurometrics. *Neuron*, 65, 530–540. <https://doi.org/10.1016/j.neuron.2010.02.007>
- 1589 Gilbert, C. D., Sigman, M., & Crist, R. E. (2001). The Neural Basis of Perceptual Learning.
 1590 *Neuron*, 31, 681–697.
- 1591 Gill, J. V., Lerman, G. M., Zhao, H., Stetler, B. J., Rinberg, D., & Shoham, S. (2020). Precise
 1592 Holographic Manipulation of Olfactory Circuits Reveals Coding Features Determining
 1593 Perceptual Detection. *Neuron*, 108, 1–12. <https://doi.org/10.1016/j.neuron.2020.07.034>
- 1594 Gradinaru, V., Mogri, M., Thompson, K. R., Henderson, J. M., & Deisseroth, K. (2009). Optical
 1595 Deconstruction of Parkinsonian Neural Circuitry. *Science*, 324(April), 354–360.
- 1596 Gustafson, N. J., & Daw, N. D. (2011). Grid Cells, Place Cells, and Geodesic Generalization
 1597 for Spatial Reinforcement Learning. *PLoS Computational Biology*, 7(10), e1002235.
 1598 <https://doi.org/10.1371/journal.pcbi.1002235>
- 1599 Haider, B., Häusser, M., & Carandini, M. (2013). Inhibition dominates sensory responses in
 1600 the awake cortex. *Nature*, 493(7430), 97–100. <https://doi.org/10.1038/nature11665>
- 1601 Haider, B., & McCormick, D. A. (2009). Rapid Neocortical Dynamics: Cellular and Network
 1602 Mechanisms. *Neuron*, 62(2), 171–189. <https://doi.org/10.1016/j.neuron.2009.04.008>
- 1603 Harlow, H. F. (1949). The formation of learning sets. *Psychological Review*, 56(1), 51–65.
- 1604 Harris, K. D., & Mrsic-Flogel, T. D. (2013). Cortical connectivity and sensory coding. *Nature*,
 1605 503(7474), 51–58. <https://doi.org/10.1038/nature12654>
- 1606 Helmchen, F., & Denk, W. (2005). Deep tissue two-photon microscopy. *Nature Methods*,
 1607 2(12), 932–940. <https://doi.org/10.1038/NMETH818>
- 1608 Herculano-Houzel, S. (2009). The human brain in numbers: a linearly scaled-up primate brain.
 1609 *Frontiers in Human Neuroscience*, 3(November), 1–11.
 1610 <https://doi.org/10.3389/neuro.09.031.2009>
- 1611 Herculano-Houzel, S., Collins, C. E., Wong, P., & Kaas, J. H. (2007). Cellular scaling rules for
 1612 primate brains. *Proceedings of the National Academy of Sciences*, 104(9), 3562–3567.
- 1613 Herculano-Houzel, S., Mota, B., & Lent, R. (2006). Cellular scaling rules for rodent brains.
 1614 *Proceedings of the National Academy of Sciences*, 103(32), 12138–12143.
- 1615 Hires, S. A., Gutnisky, D. A., Yu, J., O'Connor, D. H., & Svoboda, K. (2015). Low-noise
 1616 encoding of active touch by layer 4 in the somatosensory cortex. *ELife*, 4, e06619.
 1617 <https://doi.org/10.7554/eLife.06619>
- 1618 Histed, M. H., Carvalho, L. A., & Maunsell, J. H. R. (2012). Psychophysical measurement of

- 1619 contrast sensitivity in the behaving mouse. *Journal of Neurophysiology*, 107, 758–765.
1620 <https://doi.org/10.1152/jn.00609.2011>
- 1621 Histed, M. H., & Maunsell, J. H. R. (2014). Cortical neural populations can guide behavior by
1622 integrating inputs linearly, independent of synchrony. *Proceedings of the National*
1623 *Academy of Sciences*, 111(1), E178-87. <https://doi.org/10.1073/pnas.1318750111>
- 1624 Hofer, S. B., Ko, H., Pichler, B., Vogelstein, J., Ros, H., Zeng, H., ... Mrcic-Flogel, T. D. (2011).
1625 Differential connectivity and response dynamics of excitatory and inhibitory neurons in
1626 visual cortex. *Nature Neuroscience*, 14(8), 1045–1052. <https://doi.org/10.1038/nn.2876>
- 1627 Holmgren, C., Harkany, T., Svennenfors, B., & Zilberter, Y. (2003). Pyramidal cell
1628 communication within local networks in layer 2/3 of rat neocortex. *Journal of Physiology*,
1629 551(1), 139–153. <https://doi.org/10.1113/jphysiol.2003.044784>
- 1630 Hong, Y. K., Lacefield, C. O., Rodgers, C. C., & Bruno, R. M. (2018). Sensation, movement
1631 and learning in the absence of barrel cortex. *Nature*, 561, 542–546.
1632 <https://doi.org/10.1038/s41586-018-0527-y>
- 1633 Hooks, B. M., Hires, S. A., Zhang, Y., Huber, D., Petreanu, L., & Shepherd, G. M. G. (2011).
1634 Laminar Analysis of Excitatory Local Circuits in Vibrissal Motor and Sensory Cortical
1635 Areas. *PLoS Biology*, 9(1), e10000572. <https://doi.org/10.1371/journal.pbio.1000572>
- 1636 Hopfield, J. J. (1982). Neural networks and physical systems with emergent collective
1637 computational abilities. *Proceedings of the National Academy of Sciences of the United*
1638 *States of America*, 79(8), 2554–2558. <https://doi.org/10.1073/pnas.79.8.2554>
- 1639 Houweling, A. R., & Brecht, M. (2008). Behavioural report of single neuron stimulation in
1640 somatosensory cortex. *Nature*, 451(7174), 1–8. <https://doi.org/10.1038/nature0>
- 1641 Huber, D., Gutnisky, D. A., Peron, S., O'Connor, D. H., Wiegert, J. S., Tian, L., ... Svoboda,
1642 K. (2012). Multiple dynamic representations in the motor cortex during sensorimotor
1643 learning. *Nature*, 484(7395), 473–478. <https://doi.org/10.1038/nature11039>
- 1644 Huber, D., Petreanu, L., Ghitani, N., Ranade, S., Hromádka, T., Mainen, Z., & Svoboda, K.
1645 (2008). Sparse optical microstimulation in barrel cortex drives learned behaviour in freely
1646 moving mice. *Nature*, 451(7174), 61–64. <https://doi.org/10.1038/nature06445>
- 1647 Isaacson, J. S., & Scanziani, M. (2011). How inhibition shapes cortical activity. *Neuron*, 72(2),
1648 231–243. <https://doi.org/10.1016/j.neuron.2011.09.027>
- 1649 Jazayeri, M., & Afraz, A. (2017). Navigating the Neural Space in Search of the Neural Code.
1650 *Neuron*, 93(5), 1003–1014. <https://doi.org/10.1016/j.neuron.2017.02.019>
- 1651 Jennings, J. H., Kim, C. K., Marshel, J. H., Raffiee, M., Ye, L., Quirin, S., ... Deisseroth, K.
1652 (2019). Interacting neural ensembles in orbitofrontal cortex for social and feeding
1653 behaviour. *Nature*, 565, 645–649. <https://doi.org/10.1038/s41586-018-0866-8>
- 1654 Jouhanneau, J.-S., Kremkow, J., & Poulet, J. F. A. (2018). Single synaptic inputs drive high-
1655 precision action potentials in parvalbumin expressing GABA-ergic cortical neurons in
1656 vivo. *Nature Communications*, 9(1), 1540. <https://doi.org/10.1038/s41467-018-03995-2>
- 1657 Kanerva, P. (1993). Sparse Distributed Memory and Related Models. In M. H. Hassoun (Ed.),
1658 *Associative Neural Memories: Theory and Implementation* (pp. 50–76). Oxford University
1659 Press Inc.
- 1660 Kawai, R., Markman, T., Poddar, R., Ko, R., Fantana, A. L., Dhawale, A. K., ... Ölveczky, B.
1661 P. (2015). Motor Cortex Is Required for Learning but Not for Executing a Motor Skill.
1662 *Neuron*, 800–812. <https://doi.org/10.1016/j.neuron.2015.03.024>
- 1663 Kerlin, A. M., Andermann, M. L., Berezovskii, V. K., & Reid, R. C. (2010). Broadly Tuned

- 1664 Response Properties of Diverse Inhibitory Neuron Subtypes in Mouse Visual Cortex.
1665 *Neuron*, 67(5), 858–871. <https://doi.org/10.1016/j.neuron.2010.08.002>
- 1666 Khan, A. G., Poort, J., Chadwick, A., Blot, A., Sahani, M., Mrsic-flogel, T. D., & Hofer, S. B.
1667 (2018). Distinct learning-induced changes in stimulus selectivity and interactions of
1668 GABAergic interneuron classes in visual cortex. *Nature Neuroscience*, 21(June).
1669 <https://doi.org/10.1038/s41593-018-0143-z>
- 1670 Ko, H., Cossell, L., Baragli, C., Antolik, J., Clopath, C., Hofer, S. B., & Mrsic-Flogel, T. D.
1671 (2013). The emergence of functional microcircuits in visual cortex. *Nature*, 496(7443),
1672 96–100. <https://doi.org/10.1038/nature12015>
- 1673 Ko, H., Hofer, S. B., Pichler, B., Buchanan, K. a, Sjöström, P. J., & Mrsic-Flogel, T. D. (2011).
1674 Functional specificity of local synaptic connections in neocortical networks. *Nature*,
1675 473(7345), 87–91. <https://doi.org/10.1038/nature09880>
- 1676 Kumar, S., Soren, S., & Chaudhury, S. (2009). Hallucinations: Etiology and clinical
1677 implications. *Industrial Psychiatry Journal*, 18(2), 119–126.
1678 <https://doi.org/10.4103/0972-6748.62273>
- 1679 Kwan, A. C., & Dan, Y. (2012). Dissection of cortical microcircuits by single-neuron stimulation
1680 in vivo. *Current Biology*, 22(16), 1459–1467. <https://doi.org/10.1016/j.cub.2012.06.007>
- 1681 Kwon, S. E., Yang, H., Minamisawa, G., & O'Connor, D. H. (2016). Sensory and decision-
1682 related activity propagate in a cortical feedback loop during touch perception. *Nature*
1683 *Neuroscience*, 19(9), 1243–1252. <https://doi.org/10.1038/nn.4356>
- 1684 Law, C.-T., & Gold, J. I. (2008). Neural correlates of perceptual learning in a sensory-motor,
1685 but not a sensory, cortical area. *Nature Neuroscience*, 11(4), 505–513.
1686 <https://doi.org/10.1038/nn2070>
- 1687 Lee, S.-H., Kwan, A. C., Zhang, S., Phoumthippavong, V., Flannery, J. G., Masmanidis, S.
1688 C., ... Dan, Y. (2012). Activation of specific interneurons improves V1 feature selectivity
1689 and visual perception. *Nature*, 488(7411), 379–383.
1690 <https://doi.org/10.1038/nature11312>
- 1691 Lefort, S., Tómm, C., Sarria, J., & Petersen, C. C. H. (2009). The Excitatory Neuronal Network
1692 of the C2 Barrel Column in Mouse Primary Somatosensory Cortex. *Neuron*, 61(2), 301–
1693 316. <https://doi.org/10.1016/j.neuron.2008.12.020>
- 1694 Lennie, P. (2003). The Cost of Cortical Computation. *Current Biology*, 13, 493–497.
1695 <https://doi.org/10.1016/S>
- 1696 Li, N., Chen, S., Guo, Z. V, Chen, H., Huo, Y., Inagaki, H. K., ... Svoboda, K. (2019).
1697 Spatiotemporal constraints on optogenetic inactivation in cortical circuits. *ELife*, 8,
1698 e48622.
- 1699 Llorca, P. M., Pereira, B., Jardri, R., Brousse, G., & Misdrahi, D. (2016). Hallucinations in
1700 schizophrenia and Parkinson's disease: an analysis of sensory modalities involved and
1701 the repercussion on patients. *Scientific Reports*, 6(December), 31852.
1702 <https://doi.org/10.1038/srep38152>
- 1703 London, M., Roth, A., Beeren, L., Häusser, M., & Latham, P. E. (2010). Sensitivity to
1704 perturbations in vivo implies high noise and suggests rate coding in cortex. *Nature*,
1705 466(7302), 123–127. <https://doi.org/10.1038/nature09086>
- 1706 Macmillan, N. A., & Kaplan, H. L. (1985). Detection theory analysis of group data: Estimating
1707 sensitivity from average hit and false-alarm rates. *Psychological Bulletin*, 98, 185–199.
- 1708 Mardinly, A. R., Oldenburg, I. A., Pégard, N. C., Sridharan, S., Lyall, E. H., Chesnov, K., ...
1709 Adesnik, H. (2018). Precise multimodal optical control of neural ensemble activity.

- 1710 *Nature Neuroscience*. <https://doi.org/10.1038/s41593-018-0139-8>
- 1711 Marshel, J. H., Kim, Y. S., Machado, T. A., Quirin, S., Benson, B., Kadmon, J., ... Deisseroth,
1712 K. (2019). Cortical layer-specific critical dynamics triggering perception. *Science*, *365*,
1713 1–12. <https://doi.org/10.1126/science.aaw5202>
- 1714 Massi, B., Donahue, C. H., & Lee, D. (2018). Volatility Facilitates Value Updating in the
1715 Prefrontal Cortex. *Neuron*, *99*(3), 598–608.
1716 <https://doi.org/10.1016/j.neuron.2018.06.033>
- 1717 Mateo, C., Avermann, M., Gentet, L. J., Zhang, F., Deisseroth, K., & Petersen, C. C. H. (2011).
1718 In vivo optogenetic stimulation of neocortical excitatory neurons drives brain-state-
1719 dependent inhibition. *Current Biology*, *21*(19), 1593–1602.
1720 <https://doi.org/10.1016/j.cub.2011.08.028>
- 1721 Mayrhofer, J. M., Haiss, F., Helmchen, F., & Weber, B. (2015). Sparse, reliable, and long-term
1722 stable representation of periodic whisker deflections in the mouse barrel cortex.
1723 *NeuroImage*, *115*, 52–63. <https://doi.org/10.1016/j.neuroimage.2015.04.045>
- 1724 McEliece, R., Posner, E. C., Rodemich, E. R., & Venkatesh, S. S. (1987). The Capacity of the
1725 Hopfield Associative Memory. *IEEE Transactions on Information Theory*, *33*(4), 461–482.
- 1726 Mcguire, J. T., Nassar, M. R., Gold, J. I., & Kable, J. W. (2014). Functionally Dissociable
1727 Influences on Learning Rate in a Dynamic Environment. *Neuron*, *84*(4), 870–881.
1728 <https://doi.org/10.1016/j.neuron.2014.10.013>
- 1729 Meyer, H. S., Egger, R., Guest, J. M., Foerster, R., Reissl, S., & Oberlaender, M. (2013).
1730 Cellular organization of cortical barrel columns is whisker-specific. *Proceedings of the*
1731 *National Academy of Sciences*, *110*(47), 19113–19118.
1732 <https://doi.org/10.1073/pnas.1312691110>
- 1733 Morita, T., Kang, H., Wolfe, J., Jadhav, S. P., & Feldman, D. E. (2011). Psychometric Curve
1734 and Behavioral Strategies for Whisker-Based Texture Discrimination in Rats. *PLoS ONE*,
1735 *6*(6), e20437. <https://doi.org/10.1371/journal.pone.0020437>
- 1736 Murasugi, C. M., Salzman, C. D., & Newsome, W. T. (1993). Microstimulation in visual area
1737 MT: effects of varying pulse amplitude and frequency. *The Journal of Neuroscience*,
1738 *13*(4), 1719–1729. Retrieved from <http://www.ncbi.nlm.nih.gov/pubmed/8463847>
- 1739 Murphy, B. K., & Miller, K. D. (2009). Balanced Amplification: A New Mechanism of Selective
1740 Amplification of Neural Activity Patterns. *Neuron*, *61*(4), 635–648.
1741 <https://doi.org/10.1016/j.neuron.2009.02.005>
- 1742 Musall, S., Kaufman, M. T., Juavinett, A. L., Gluf, S., & Churchland, A. K. (2019). Single-trial
1743 neural dynamics are dominated by richly varied movements. *Nature Neuroscience*,
1744 *22*(October), 1677–1686. <https://doi.org/10.1038/s41593-019-0502-4>
- 1745 Niell, C. M., & Stryker, M. P. (2010). Modulation of visual responses by behavioral state in
1746 mouse visual cortex. *Neuron*, *65*(4), 472–479.
1747 <https://doi.org/10.1016/j.neuron.2010.01.033>
- 1748 O'Connor, D. H., Clack, N. G., Huber, D., Komiyama, T., Myers, E. W., & Svoboda, K. (2010).
1749 Vibrissa-based object localization in head-fixed mice. *The Journal of Neuroscience*,
1750 *30*(5), 1947–1967. <https://doi.org/10.1523/JNEUROSCI.3762-09.2010>
- 1751 O'Connor, D. H., Hires, S. A., Guo, Z. V, Li, N., Yu, J., Sun, Q., ... Svoboda, K. (2013). Neural
1752 coding during active somatosensation revealed using illusory touch. *Nature*
1753 *Neuroscience*, *16*(7), 958–965. <https://doi.org/10.1038/nn.3419>
- 1754 Olshausen, B. A., & Field, D. J. (1996). Emergence of simple-cell receptive field properties by
1755 learning a sparse code for natural images. *Nature*, *381*(June), 607–609.

- 1756 Olshausen, B. A., & Field, D. J. (2004). Sparse coding of sensory inputs. *Current Opinion in*
1757 *Neurobiology*, 14(4), 481–487. <https://doi.org/10.1016/j.conb.2004.07.007>
- 1758 Ölveczky, B. P., Otchy, T. M., Goldberg, J. H., Aronov, D., & Fee, M. S. (2011). Changes in
1759 the neural control of a complex motor sequence during learning. *Journal of*
1760 *Neurophysiology*, 106, 386–397. <https://doi.org/10.1152/jn.00018.2011>
- 1761 Otis, J. M., Namboodiri, V. M. K., Matan, A. M., Voets, E. S., Mohorn, E. P., Kosyk, O., ...
1762 Stuber, G. D. (2017). Prefrontal cortex output circuits guide reward seeking through
1763 divergent cue encoding. *Nature*, 543(7643), 103–107.
1764 <https://doi.org/10.1038/nature21376>
- 1765 Ozeki, H., Finn, I. M., Schaffer, E. S., Miller, K. D., & Ferster, D. (2009). Inhibitory Stabilization
1766 of the Cortical Network Underlies Visual Surround Suppression. *Neuron*, 62(4), 578–592.
1767 <https://doi.org/10.1016/j.neuron.2009.03.028>
- 1768 Pachitariu, M., Stringer, C., & Harris, K. D. (2018). Robustness of Spike Deconvolution for
1769 Neuronal Calcium Imaging. *The Journal of Neuroscience*, 38(37), 7976–7985.
1770 <https://doi.org/10.1523/JNEUROSCI.3339-17.2018>
- 1771 Pachitariu, M., Stringer, C., Schröder, S., Dipoppa, M., Rossi, L. F., Carandini, M., & Harris,
1772 K. D. (2016). Suite2p: beyond 10,000 neurons with standard two-photon microscopy.
1773 *BioRxiv*. <https://doi.org/10.1101/061507>
- 1774 Packer, A. M., Russell, L. E., Dalgleish, H. W. P., & Hausser, M. (2015). Simultaneous all-
1775 optical manipulation and recording of neural circuit activity with cellular resolution in
1776 vivo. *Nature Methods*, 12(2), 140–146. <https://doi.org/10.1038/nmeth.3217>
- 1777 Packer, A. M., & Yuste, R. (2011). Dense, Unspecific Connectivity of Neocortical
1778 Parvalbumin-Positive Interneurons: A Canonical Microcircuit for Inhibition? *The Journal*
1779 *of Neuroscience*, 31(37), 13260–13271. <https://doi.org/10.1523/JNEUROSCI.3131-11.2011>
- 1781 Palm, G. (1980). On associative memory. *Biological Cybernetics*, 31, 19–31.
- 1782 Panzeri, S., Harvey, C. D., Piasini, E., Latham, P. E., & Fellin, T. (2017). Cracking the neural
1783 code for sensory perception by combining statistics, intervention and behavior. *Neuron*,
1784 93(3), 491–507. <https://doi.org/10.1111/gcb.13051>
- 1785 Panzeri, S., Ince, R. A. A., Diamond, M. E., & Kayser, C. (2014). Reading spike timing without
1786 a clock: intrinsic decoding of spike trains. *Philosophical Transactions of the Royal*
1787 *Society B*, 369, 1–11.
- 1788 Pehlevan, C., & Sompolinsky, H. (2014). Selectivity and Sparseness in Randomly Connected
1789 Balanced Networks. *PLoS ONE*, 9(2). <https://doi.org/10.1371/journal.pone.0089992>
- 1790 Perin, R., Berger, T. K., & Markram, H. (2011). A synaptic organizing principle for cortical
1791 neuronal groups. *Proceedings of the National Academy*, 108(13), 5419–5424.
1792 <https://doi.org/10.1073/pnas.1016051108>
- 1793 Peron, S., Freeman, J., Iyer, V., Guo, C., & Svoboda, K. (2015). A Cellular Resolution Map of
1794 Barrel Cortex Activity during Tactile Behavior. *Neuron*, 86(3), 783–799.
1795 <https://doi.org/10.1016/j.neuron.2015.03.027>
- 1796 Peron, S., Pancholi, R., Voelcker, B., Wittenbach, J. D., Ólafsdóttir, H. F., Freeman, J., &
1797 Svoboda, K. (2020). Recurrent interactions in local cortical circuits. *Nature*, (October
1798 2016), 1–4. <https://doi.org/10.1038/s41586-020-2062-x>
- 1799 Petersen, C. C. H. (2007). The functional organization of the barrel cortex. *Neuron*, 56(2), 339–
1800 355. <https://doi.org/10.1016/j.neuron.2007.09.017>

- 1801 Plitt, M. H., & Giocomo, L. M. (2019). Experience dependent contextual codes in the
1802 hippocampus. *BioRxiv*, 1–30.
- 1803 Poort, J., Khan, A. G., Pachitariu, M., Nemri, A., Orsolich, I., Krupic, J., ... Hofer, S. B. (2015).
1804 Learning Enhances Sensory and Multiple Non-sensory Representations in Primary
1805 Visual Cortex. *Neuron*, 86(6), 1478–1490. <https://doi.org/10.1016/j.neuron.2015.05.037>
- 1806 Rose, D., & Blakemore, C. (1974). Effects of bicuculline on functions of inhibition in visual
1807 cortex. *Nature*, 249, 375–377.
- 1808 Rudebeck, P. H., & Murray, E. A. (2011). Dissociable Effects of Subtotal Lesions within the
1809 Macaque Orbital Prefrontal Cortex on Reward-Guided Behavior. *The Journal of*
1810 *Neuroscience*, 31(29), 10569–10578. [https://doi.org/10.1523/JNEUROSCI.0091-](https://doi.org/10.1523/JNEUROSCI.0091-11.2011)
1811 [11.2011](https://doi.org/10.1523/JNEUROSCI.0091-11.2011)
- 1812 Russell, L. E., Yang, Z., Tan, P. L., Fişek, M., Packer, A. M., Dalgleish, H. W. P., ... Häusser,
1813 M. (2019). The influence of visual cortex on perception is modulated by behavioural
1814 state. *BioRxiv*.
- 1815 Sachidhanandam, S., Sreenivasan, V., Kyriakatos, A., Kremer, Y., & Petersen, C. C. H. (2013).
1816 Membrane potential correlates of sensory perception in mouse barrel cortex. *Nature*
1817 *Neuroscience*, (October), 1–9. <https://doi.org/10.1038/nn.3532>
- 1818 Sadeh, S., & Clopath, C. (2020). Patterned perturbation of inhibition can reveal the dynamical
1819 structure of neural processing. *ELife*, 9, e52757.
- 1820 Salzman, C. D., Britten, K. H., & Newsome, W. T. (1990). Cortical microstimulation influences
1821 perceptual judgements of motion direction. *Nature*, 346, 174–176.
1822 [https://doi.org/10.1016/0021-9797\(80\)90501-9](https://doi.org/10.1016/0021-9797(80)90501-9)
- 1823 Salzman, C. D., Murasugi, C. M., Britten, K. H., & Newsome, W. T. (1992). Microstimulation
1824 in Visual Area MT: Effects on Direction Discrimination Performance. *The Journal of*
1825 *Neuroscience*, 12(6), 2331–2355.
- 1826 Sanders, H., Wilson, M. A., & Gershman, S. J. (2020). Hippocampal remapping as hidden
1827 state inference. *ELife*, 9, e51140.
- 1828 Sanzeni, A., Akitake, B., Goldback, H., Leedy, C., Brunel, N., & Histed, M. (2020). Inhibition
1829 stabilization is a widespread property of cortical networks. *BioRxiv*.
- 1830 Sasaki, Y., Nanez, J. E., & Watanabe, T. (2009). Advances in visual perceptual learning and
1831 plasticity. *Nature Reviews Neuroscience*, 11(1), 53–60. <https://doi.org/10.1038/nrn2737>
- 1832 Scholl, B., Pattadkal, J. J., Dilly, G. A., Priebe, N. J., & Zemel, B. V. (2015). Local
1833 Integration Accounts for Weak Selectivity of Mouse Neocortical Parvalbumin
1834 Interneurons. *Neuron*, 87(2), 424–436. <https://doi.org/10.1016/j.neuron.2015.06.030>
- 1835 Schölvinck, M. L., Howarth, C., & Attwell, D. (2008). The cortical energy needed for conscious
1836 perception. *NeuroImage*, 40, 1460–1468.
1837 <https://doi.org/10.1016/j.neuroimage.2008.01.032>
- 1838 Schütt, H. H., Harmeling, S., Macke, J. H., & Wichmann, F. A. (2016). Painfree and accurate
1839 Bayesian estimation of psychometric functions for (potentially) overdispersed data.
1840 *Vision Research*, 122, 105–123. <https://doi.org/10.1016/j.visres.2016.02.002>
- 1841 Shadlen, M. N., & Newsome, W. T. (1994). Noise, neural codes and cortical organization.
1842 *Current Opinion in Neurobiology*, 4, 569–579. Retrieved from
1843 <http://www.ncbi.nlm.nih.gov/pubmed/7812147>
- 1844 Shemesh, O. A., Tanese, D., Zampini, V., Linghu, C., Piatkevich, K., Ronzitti, E., ... Emiliani,
1845 V. (2017). Temporally precise single-cell-resolution optogenetics. *Nature Neuroscience*,

- 1846 20(12), 1796–1806. <https://doi.org/10.1038/s41593-017-0018-8>
- 1847 Shuler, M. G., & Bear, M. F. (2006). Reward timing in the primary visual cortex. *Science*,
1848 311(March), 1606–1610.
- 1849 Silberberg, G., & Markram, H. (2007). Disynaptic Inhibition between Neocortical Pyramidal
1850 Cells Mediated by Martinotti Cells. *Neuron*, 53, 735–746.
1851 <https://doi.org/10.1016/j.neuron.2007.02.012>
- 1852 Sippy, T., Lapray, D., Crochet, S., & Petersen, C. C. H. (2015). Cell-Type-Specific
1853 Sensorimotor Processing in Striatal Projection Neurons during Goal-Directed Behavior
1854 Supplemental Information. *Neuron*, 1–8. <https://doi.org/10.1016/j.neuron.2015.08.039>
- 1855 Stachenfeld, K. L., Botvinick, M. M., & Gershman, S. J. (2018). The hippocampus as a
1856 predictive map. *Nature Neuroscience*, 20(11), 1643–1653.
1857 <https://doi.org/10.1038/nn.4650>
- 1858 Steinmetz, N. A., Zatzka-haas, P., Carandini, M., & Harris, K. D. (2019). Distributed coding of
1859 choice, action and engagement across the mouse brain. *Nature*, 576(December), 266–
1860 273. <https://doi.org/10.1038/s41586-019-1787-x>
- 1861 Stringer, C., Pachitariu, M., Steinmetz, N., Reddy, C. B., Carandini, M., & Harris, K. D. (2019).
1862 Spontaneous behaviors drive multidimensional, brainwide activity. *Science*, 364(255),
1863 1–11. <https://doi.org/10.1126/science.aav7893>
- 1864 Stringer, C., Wang, T., Michaelos, M., & Pachitariu, M. (2020). Cellpose: a generalist algorithm
1865 for cellular segmentation. *BioRxiv*, 1–19.
- 1866 Stüttgen, M., & Schwarz, C. (2008). Psychophysical and neurometric detection performance
1867 under stimulus uncertainty. *Nature Neuroscience*, 11(9), 1091–1099.
1868 <https://doi.org/10.1038/nn.2162>
- 1869 Tanke, N., Borst, J. G. G., & Houweling, A. R. (2018). Single-cell stimulation in barrel cortex
1870 influences psychophysical detection performance. *The Journal of Neuroscience*, 38(8),
1871 2057–2068. <https://doi.org/10.1523/JNEUROSCI.2155-17.2018>
- 1872 Thomson, A. M., & Lamy, C. (2007). Functional maps of neocortical local circuitry. *Frontiers*
1873 *in Neuroscience*, 1(1), 19–42.
- 1874 Tolhurst, D. J., Movshon, J. A., & Dean, A. F. (1983). The statistical reliability of signals in single
1875 neurons in cat and monkey visual cortex. *Vision Research*, 23(8), 775–785.
- 1876 Tolman, E. C. (1948). Cognitive maps in rats and men. *Psychological Review*, 55(4), 189–208.
- 1877 Tolman, E. C., Ritchie, B. F., & Kalish, D. (1946). Studies in spatial learning. I. Orientation and
1878 the short-cut. *Journal of Experimental Psychology*, 6(1), 13–24.
- 1879 Treiman, D. M. (2001). GABAergic Mechanisms in Epilepsy. *Epilepsia*, 42(2), 8–12.
- 1880 Tse, D., Langston, R. F., Kakeyama, M., Bethus, I., Spooner, P. A., Wood, E. R., ... Morris, R.
1881 G. M. (2007). Schemas and Memory Consolidation. *Science*, 316(7489), 76–82.
- 1882 Tsodyks, M. V., Skaggs, W. E., Sejnowski, T. J., & McNaughton, B. L. (1997). Paradoxical
1883 Effects of External Modulation of Inhibitory Interneurons. *The Journal of Neuroscience*,
1884 17(11), 4382–4388.
- 1885 van Vreeswijk, C., & Sompolinsky, H. (1996). Chaos in Neuronal Networks with Balanced
1886 Excitatory and Inhibitory Activity. *Science*, 274(December), 1724–1726.
- 1887 Walton, M. E., Behrens, T. E. J., Buckley, M. J., Rudebeck, P. H., & Rushworth, M. F. S.
1888 (2010). Separable Learning Systems in the Macaque Brain and the Role of Orbitofrontal
1889 Cortex in Contingent Learning. *Neuron*, 65(6), 927–939.

- 1890 <https://doi.org/10.1016/j.neuron.2010.02.027>
- 1891 Waters, J., & Helmchen, F. (2006). Background synaptic activity is sparse in neocortex. *The*
1892 *Journal of Neuroscience*, *26*(32), 8267–8277.
1893 <https://doi.org/10.1523/JNEUROSCI.2152-06.2006>
- 1894 Watson, B. O., Yuste, R., & Packer, A. M. (2016). PackIO and EphysViewer: software tools
1895 for acquisition and analysis of neuroscience data. *BioRxiv*.
1896 <https://doi.org/https://doi.org/10.1101/054080>
- 1897 Wehr, M., & Zador, A. M. (2003). Balanced inhibition underlies tuning and sharpens spike
1898 timing in auditory cortex. *Nature*, *426*(November), 860–863.
- 1899 Whittington, J. C. R., Muller, T. H., Barry, C., & Behrens, T. E. J. (2018). Generalisation of
1900 structural knowledge in the Hippocampal-Entorhinal system. *ArXiv*.
- 1901 Whittington, J. C. R., Muller, T. H., Mark, S., Chen, G., Barry, C., Burgess, N., & Behrens, T.
1902 E. J. (2019). The Tolman-Eichenbaum Machine: Unifying space and relational memory
1903 through generalisation in the hippocampal formation. *BioRxiv*.
- 1904 Wiest, M. C., Thomson, E., Pantoja, J., & Nicolelis, M. A. L. (2020). Changes in S1 Neural
1905 Responses During Tactile Discrimination Learning. *Journal of Neurophysiology*, *104*,
1906 300–312. <https://doi.org/10.1152/jn.00194.2010>.
- 1907 Wilson, N. R., Runyan, C. A., Wang, F. L., & Sur, M. (2012). Division and subtraction by distinct
1908 cortical inhibitory networks in vivo. *Nature*, *488*(7411), 343–348.
1909 <https://doi.org/10.1038/nature11347>
- 1910 Wolf, F., Engelken, R., Puelma-Touzel, M., Weidinger, J. D. F., & Neef, A. (2014). Dynamical
1911 models of cortical circuits. *Current Opinion in Neurobiology*, *25*, 228–236.
1912 <https://doi.org/10.1016/j.conb.2014.01.017>
- 1913 Wolfe, J., Houweling, A. R., & Brecht, M. (2010). Sparse and powerful cortical spikes. *Current*
1914 *Opinion in Neurobiology*, *20*(3), 306–312. <https://doi.org/10.1016/j.conb.2010.03.006>
- 1915 Xiong, Q., Znamenskiy, P., & Zador, A. M. (2015). Selective corticostriatal plasticity during
1916 acquisition of an auditory discrimination task. *Nature*.
1917 <https://doi.org/10.1038/nature14225>
- 1918 Ye, Z., Mostajo-Radji, M. A., Brown, J. R., Rouaux, C., Tomassy, G. S., Hensch, T., & Arlotta,
1919 P. (2015). Instructing Perisomatic Inhibition by Direct Lineage Reprogramming of
1920 Neocortical Projection Neurons. *Neuron*, *88*(3), 475–483.
1921 <https://doi.org/10.1016/j.neuron.2015.10.006>
- 1922 Yizhar, O., Fenno, L. E., Prigge, M., Schneider, F., Davidson, T. J., Shea, D. J. O., ...
1923 Deisseroth, K. (2011). Neocortical excitation/inhibition balance in information processing
1924 and social dysfunction. *Nature*, *477*(7363), 171–178.
1925 <https://doi.org/10.1038/nature10360>
- 1926 Yoshimura, Y., Dantzker, J. L. M., & Callaway, E. M. (2005). Excitatory cortical neurons from
1927 fine-scale functional networks. *Nature*, *5*(February), 2005–2005.
1928 <https://doi.org/10.1038/nature03291.1>.
- 1929 Zátka-Haas, P., Steinmetz, N. A., Carandini, M., & Harris, K. D. (2020). A perceptual decision
1930 requires sensory but not action coding in mouse cortex. *BioRxiv*.
- 1931 Zhang, Z., Russell, L. E., Packer, A. M., Gauld, O. M., & Häusser, M. (2018). Closed-loop all-
1932 optical interrogation of neural circuits in vivo. *Nature Methods*, *15*(December), 1037–
1933 1040. <https://doi.org/10.1038/s41592-018-0183-z>
- 1934 Ziburkus, J., Cressman, J. R., Barreto, E., & Schiff, S. J. (2006). Interneuron and Pyramidal

1935 Cell Interplay During In Vitro Seizure-Like Events. *Journal of Neurophysiology*, 95, 3948–
1936 3954. <https://doi.org/10.1152/jn.01378.2005>.

1937 Znamenskiy, P., Kim, M., Muir, D. R., Iacaruso, F., Hofer, S. B., & Mrsic-flogel, T. D. (2018).
1938 Functional selectivity and specific connectivity of inhibitory neurons in primary visual
1939 cortex. *BioRxiv*.

1940 Znamenskiy, P., & Zador, A. M. (2013). Corticostriatal neurons in auditory cortex drive
1941 decisions during auditory discrimination. *Nature*, 497(7450), 482–485.
1942 <https://doi.org/10.1038/nature12077>

1943

1944

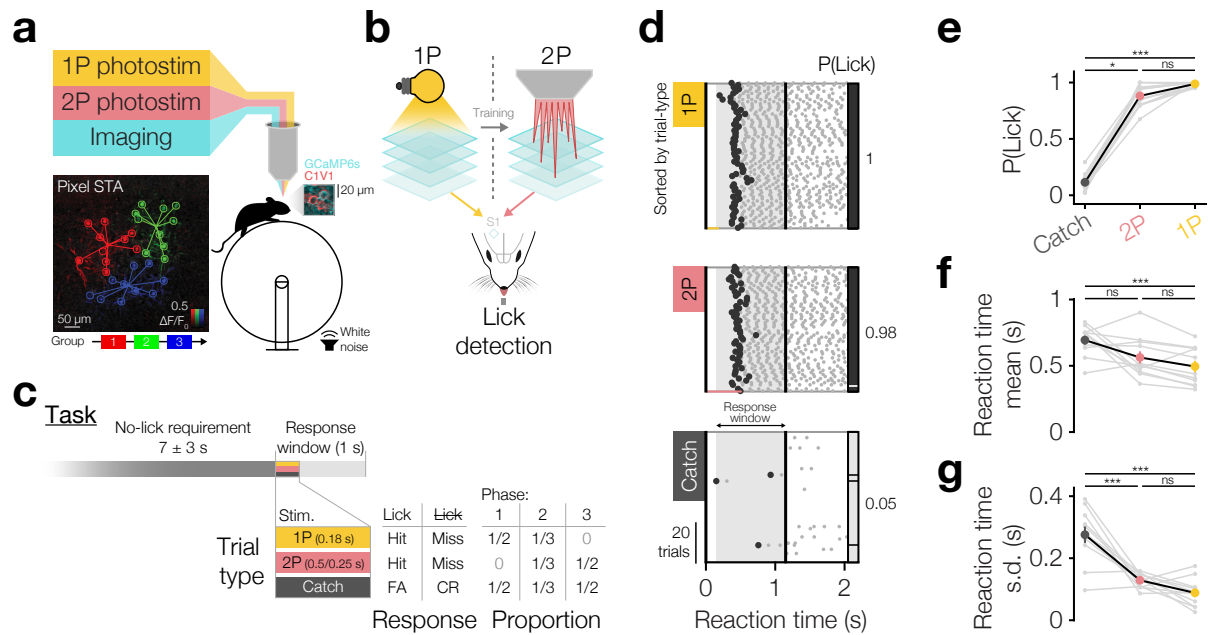
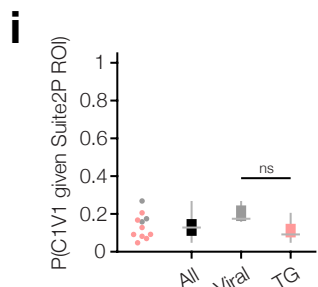
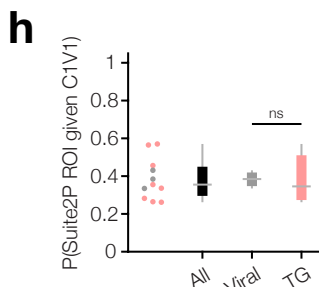
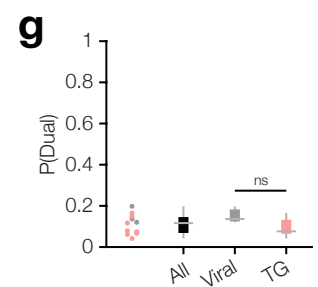
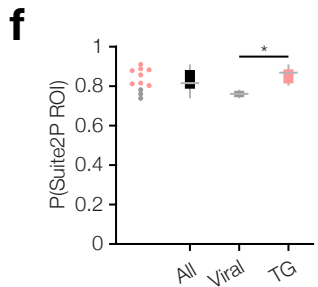
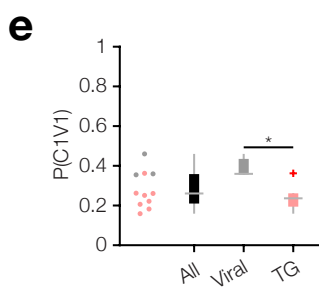
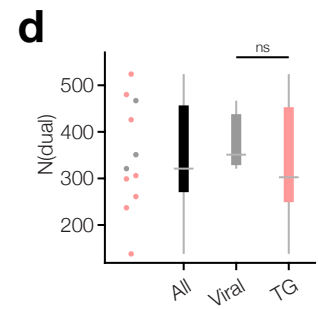
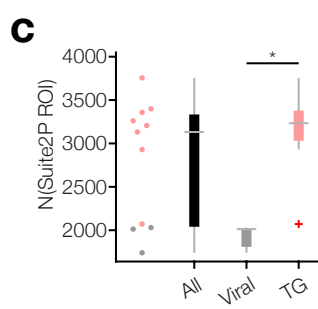
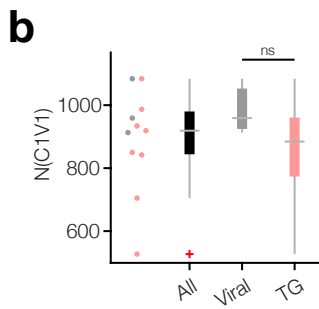
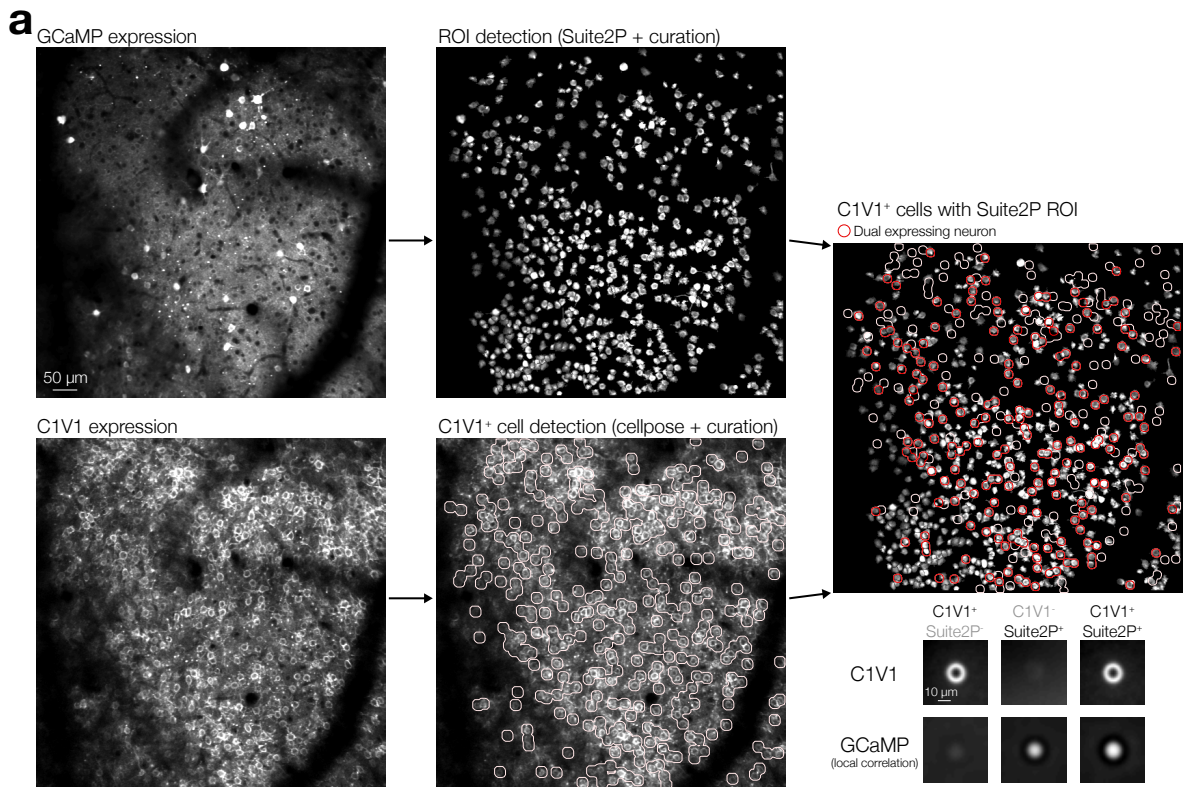


Figure 1 | Driving behaviour with two-photon optogenetics targeted to ensembles of neurons in L2/3 barrel cortex.

a, Schematic of all-optical setup. *Bottom left*: Example of flexible ensemble photostimulation. Three 10 neuron groups in barrel cortex (red, green, blue circles joined by group centroids) were photostimulated sequentially (sequence below Pixel STA). Pixel STA is maximum intensity projection across photostimulus groups of activity in post-photostimulation epoch averaged across trials ($N = 3$ photostimulus groups, 10 trials each). *Inset right*: sub-region of a full imaging FOV in L2/3 barrel cortex expressing GCaMP6s/C1V1-mRuby. **b**, Schematic summarizing the strategy used to train animals to respond to two-photon optogenetic (2P) stimulation. Mice are first trained to respond to one-photon optogenetic (1P) stimulation of barrel cortex (S1) by licking at an electronic lickometer. The power of 1P illumination is reduced until they can be transitioned onto 2P stimulation targeted to specific ensembles of barrel cortex neurons. **c**, Structure of the behavioural task (top) and stimulus probabilities, response type contingencies and training phase structures (bottom). Note that stimulus durations, which vary across stimulus types, are not to scale. **d**, Lick raster from an example Phase 2 behavioural training session during which a mouse received 2P stimulation trials (pink: 200 neurons), catch trials (grey, no stimulus) and 1P stimulation trials (amber: 0.05 mW, untargeted). Trials were delivered pseudo-randomly (see *Methods*) but have been sorted by trial-type for display. All licks shown in grey with first lick highlighted in black. Hits (black) and misses (grey) are indicated as the vertical bar on the right-hand side. Stimulus durations indicated as coloured bars below lick rasters. Behavioural response window indicated as grey shading, label and arrows. **e – g**, Response rates and reaction time mean and standard deviation for different trial types in final Phase 2 session. Animals detect 1P photostimulation and 2P stimulation targeted to 200 neurons to similar extents, at a level far above chance (catch trials), with similar reaction time mean and standard deviation. ($N = 12$ mice, 1 session each). Note only animals which responded on > 2 Catch trials are included for reaction time panels (*f* and *g*) ($N = 11$ animals, 1 session each). All error bars are s.e.m.



1972
 1973
 1974
 1975
 1976

Figure 1 – figure supplement 1 | Indicator and opsin expression overlap analysis.
a, Detection of indicator/opsin expression overlap. Suite2P followed by manual curation was used to detect functional GCaMP expressing neurons from time-series data (*top row*) and Cellpose followed by manual curation was used to detect C1V1 expression from static images (*bottom row*). GCaMP

1977 (top left) and C1V1 (bottom left) expression in an example plane from a volumetric FOV with
1978 corresponding Suite2P ROIs (top middle) and detected C1V1⁺ neurons (bottom middle). C1V1⁺
1979 neurons with a Suite2P ROI are circled in red (right; see *Methods*) and the average expression pattern
1980 in both C1V1 expression and GCaMP local correlation images is shown for each of the 3 possible
1981 expression configurations (bottom right insets). $N = 6250$ C1V1⁺/Suite2P⁻ neurons, 27084 C1V1⁻
1982 /Suite2P⁺ neurons and 3810 C1V1⁺/Suite2P⁺ neurons across 11 volumetric FOVs from 6 animals, 1 –
1983 2 volumetric FOVs each. **b**, Number of C1V1⁺ neurons in each volumetric FOV in all mice (black), dual
1984 injected WT mice (grey) and opsin injected transgenic GCaMP mice (pink). See below and *Methods*
1985 for details. **c**, Number of Suite2P ROIs in each volumetric FOV. **d**, Number of dual expressing neurons
1986 in each volumetric FOV (C1V1⁺ neurons with Suite2P ROI). **e**, Proportion of C1V1⁺ neurons out of total
1987 number of neurons that have a Suite2P ROI and/or are C1V1⁺. **f**, Proportion of neurons with a Suite2P
1988 ROI out of total number of neurons (same denominator as e). **g**, Proportion of dual expressing neurons
1989 (C1V1⁺ with Suite2P ROI) out of total number of neurons (same denominator as e). **h**, Proportion of
1990 C1V1⁺ neurons with a Suite2P ROI. **i**, Proportion of Suite2P ROIs that are C1V1⁺. For all group data
1991 panels $N = 11$ volumetric FOVs from the 2P psychometric curve sessions (**Figure 2 – 4**), 3 FOVs from
1992 WT (C57/BL6) mice co-injected with hSyn-GCaMP6s/CaMKII-C1V1-Kv2.1 (grey in all plots) and 8
1993 FOVs from transgenic (Emx1Cre;CaMKIIa-tTA;Ai94) mice injected with CaMKII-C1V1-Kv2.1 (pink in all
1994 plots). Aggregate data across expression strategies are black in all plots.
1995

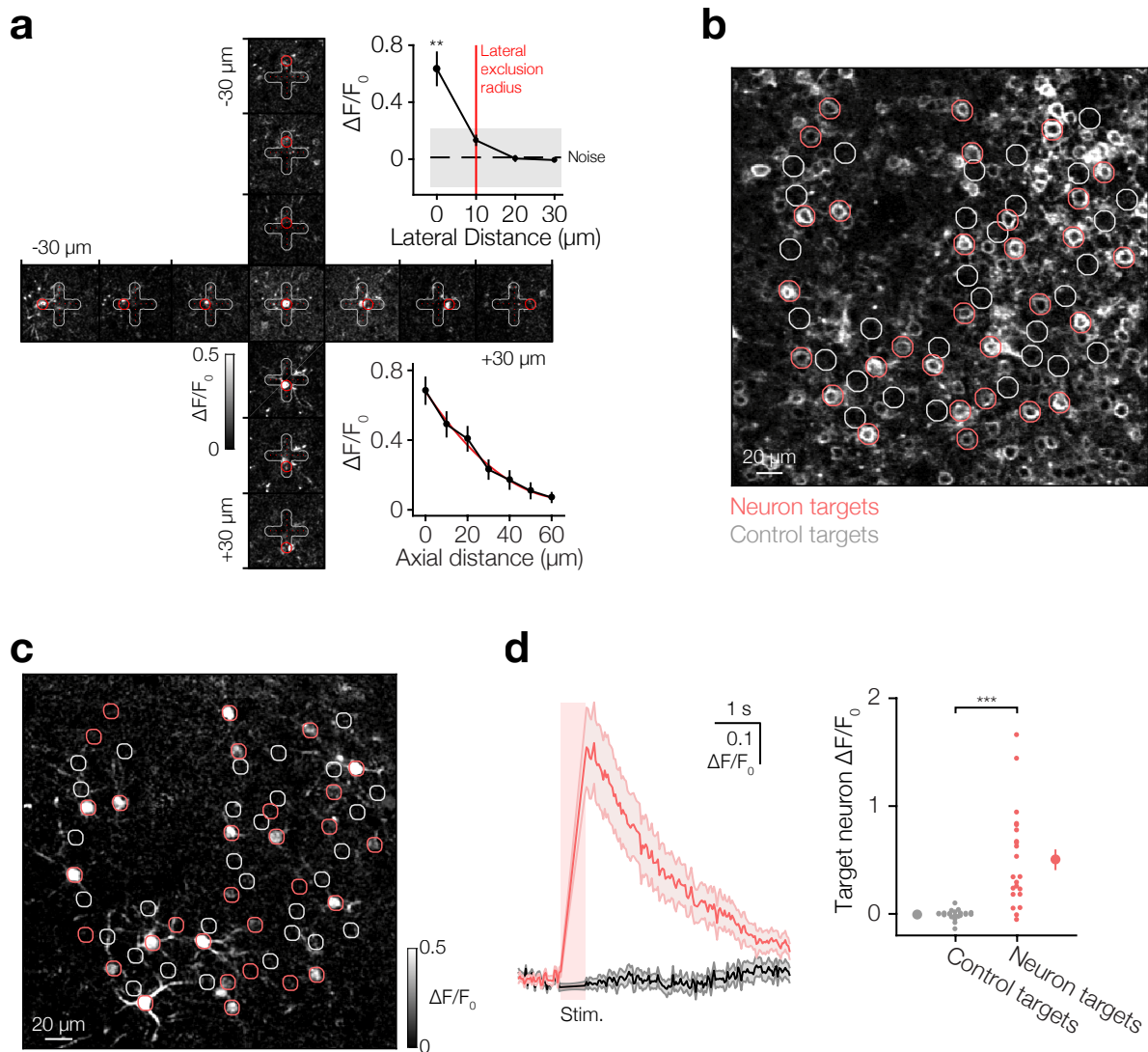
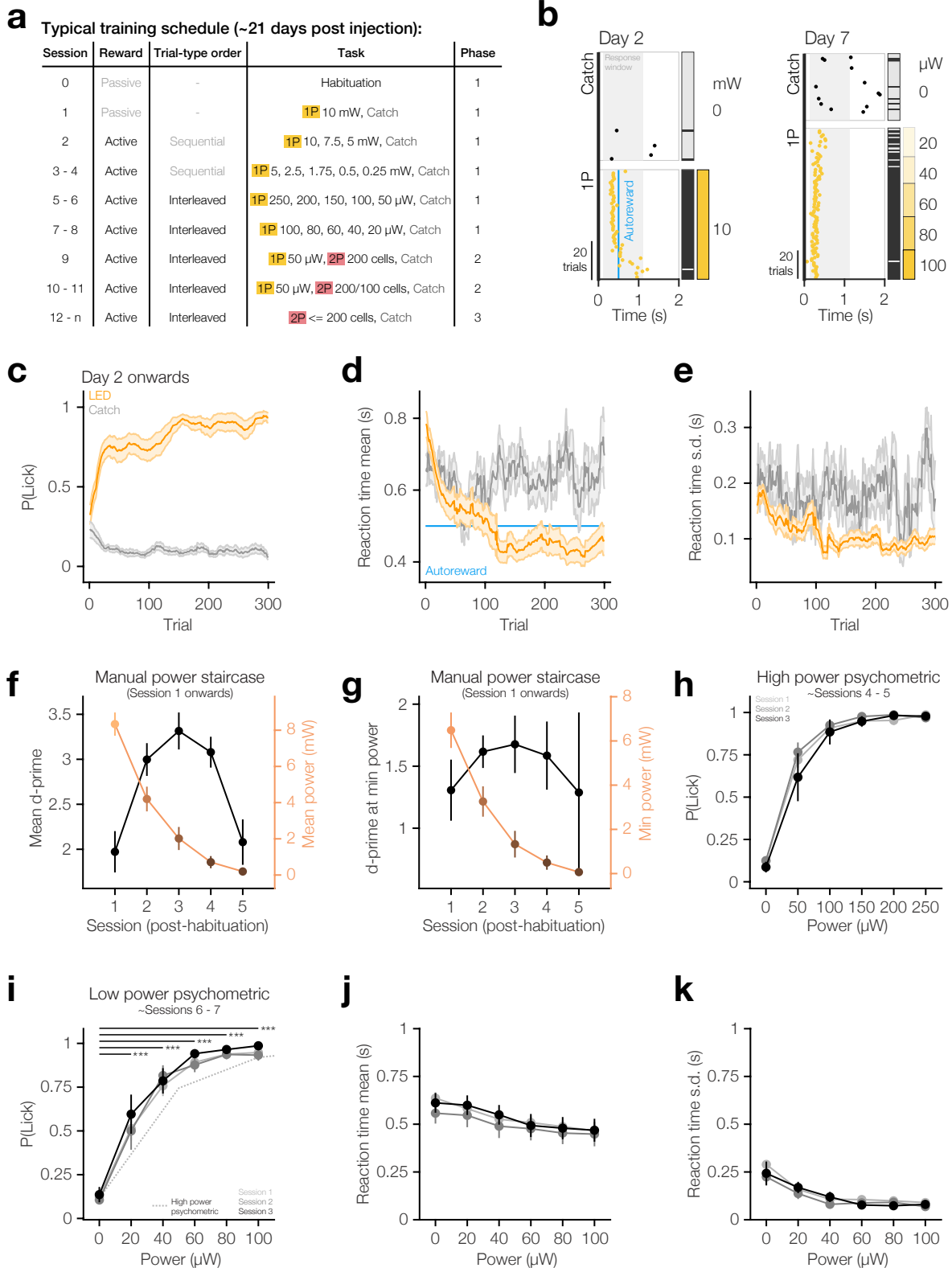


Figure 1 – figure supplement 2 | Spatial resolution of spiral-scanned two-photon optogenetic activation of Kv2.1-C1V1.

a, Left: A cross-shaped grid of photostimulation targets was centred on a single target neuron and each photostimulation target was activated 10 times in random order (10 μm inter-target distance, 30 μm maximum distance from centre, 10 s inter-trial interval, 10 x 20 ms spirals at 20 Hz, 6 mW/neuron). **Top right inset:** Lateral (xy) resolution of photostimulation of the central target neuron. Only the target position centred over the target neuron result in significant activation. Lateral HWHM = 5 μm (2-degree polynomial fit). $N = 1$ neuron, 10 trials per stimulation site. Note the lateral exclusion radius (10 μm) used to define target neurons in subsequent analyses is plotted in red. All neurons within this region were considered potential target neurons (see *Methods*). **Bottom right inset:** Axial (z) resolution of photostimulation. Photostimulation targets were axially translated from 60 μm above target neurons down onto their cell-body locations in the objective focal plane in 10 μm steps using SLM-based axial displacement while the target neuron responses were consistently imaged at the objective focal plane (separate experiments from lateral resolution). HWHM = 20 μm (2-degree polynomial fit). $N = 20$ neurons, 10 trials per axial offset. To account for these considerable axial off-target effects we defined all neurons within the lateral exclusion zone of 10 μm (see above) to be potential target neurons irrespective of their axial displacement. **b,** Example Kv2.1-C1V1-mScarlet expression image with neuron (pink) and control (grey) targets overlaid as circles. **c,** Maximum intensity projection across two pixel-wise STAs triggered off neuron and control site stimulation. Neuron stimulation results in robust activation of targeted neurons, control stimulation results in no activation. $N = 10$ trials. **d, Left:** Extracted traces from target neuron ROIs during both neuron site stimulation (pink) and control site stimulation (grey). **Right:** post-stimulus $\Delta F/F_0$ from target neuron ROIs. Transients evoked in target

1996
1997
1998
1999
2000
2001
2002
2003
2004
2005
2006
2007
2008
2009
2010
2011
2012
2013
2014
2015
2016
2017
2018

2019 neuron ROIs during neuron site stimulation are completely absent during stimulation of adjacent
2020 control sites, resulting in no recorded $\Delta F/F_0$ response. $N = 20$ neurons, 10 trials each. All error bars
2021 and shading are s.e.m.
2022

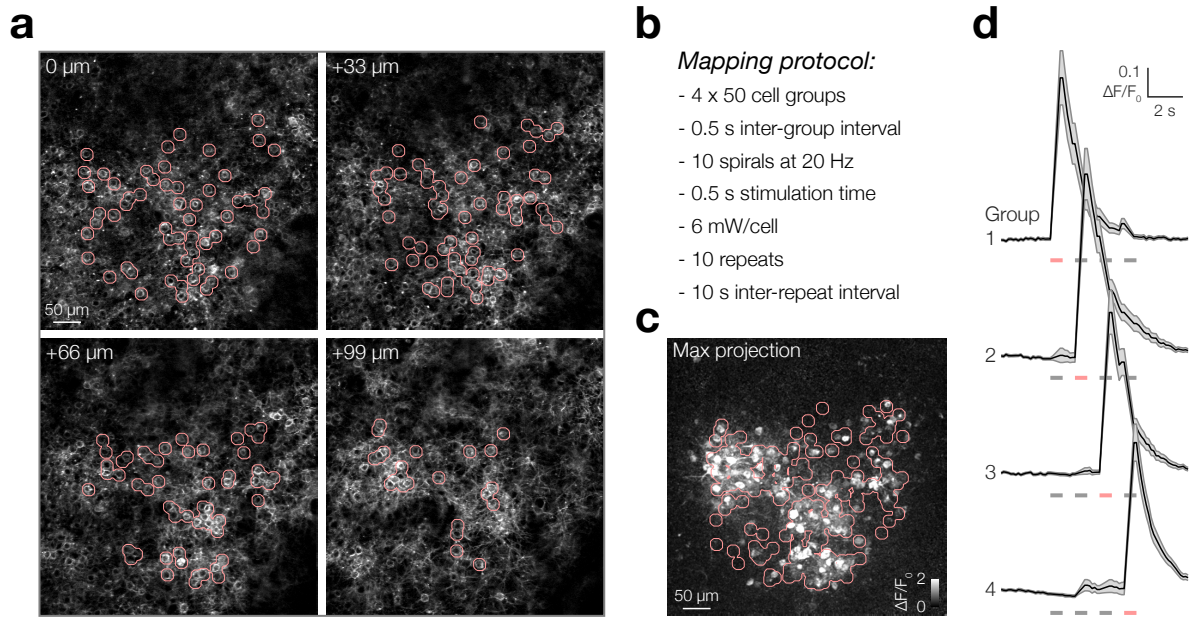


2023
2024
2025
2026
2027
2028
2029
2030

Figure 1 – figure supplement 3 | 1P training protocol.

a, Typical training protocol to transition a naïve mouse to being able to detect two-photon stimulation via a series of one-photon priming phases. Note that exact duration of each component varied by mouse (see **Figure 1 – figure supplement 5f**). **b**, Lick rasters from an example first training session (*left*) and an example low power psychometric curve session (*right*) for a habituated mouse showing first licks on each trial (circles), auto-reward delivery time (blue vertical line) and analysis window (grey shading). Trials were delivered pseudorandomly and are sorted for display only. Hits (black) and misses

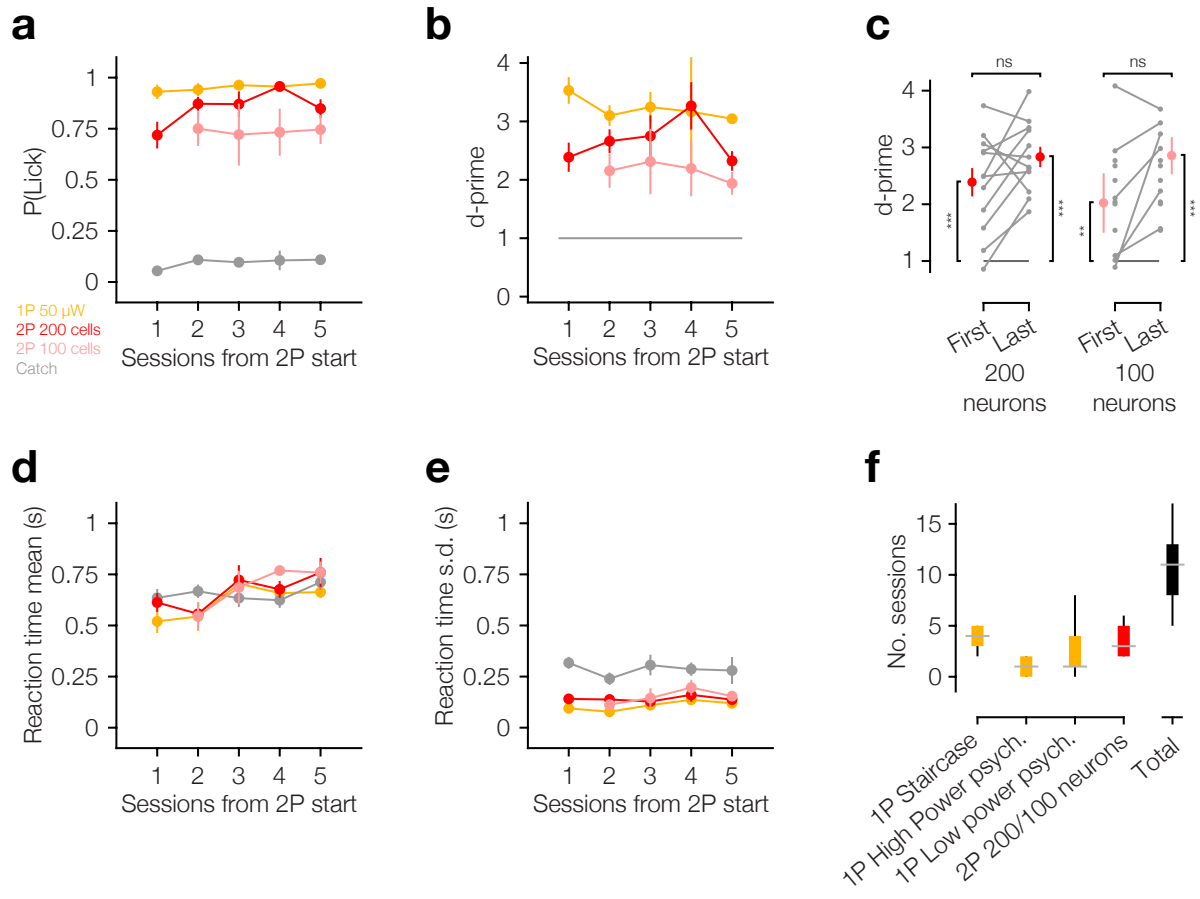
2031 (grey) are indicated as the vertical bar to the right of the raster, followed by coloured boxes indicating
2032 LED power on the far right. **c – e**, Moving average response rate (*c*), average reaction time (*d*) and
2033 standard deviation of reaction time (*e*) for the first 300 LED (amber) and catch (grey) trials using a 20
2034 trial window. **f**, Mean power (*right*) and mean d-prime (*left*) over initial manual power staircase sessions.
2035 **g**, Minimum power used in each session (*right*) and d-prime at that power (*left*) over initial manual
2036 power staircase sessions. **h**, Response rates on three high power psychometric curve sessions. *N* =
2037 22 animals that completed at least one high power psychometric curve session (other animals were
2038 transitioned straight to low power psychometric curves). **i – k**, Response rates (*i*), mean reaction time
2039 (*j*) and standard deviation of reaction time (*k*) on three low power psychometric curve sessions. *N* = 22
2040 animals that completed at least one low power psychometric curve session (other animals were
2041 transitioned straight to subsequent training phases). All error bars are s.e.m. For all group data panels
2042 *N* = 26 mice unless otherwise stated, however some data-points may have fewer *N* as not all animals
2043 completed the same number of sessions (see **Figure 1 – figure supplement 5f** for summary).
2044



2045
 2046
 2047
 2048
 2049
 2050
 2051
 2052
 2053
 2054
 2055
 2056

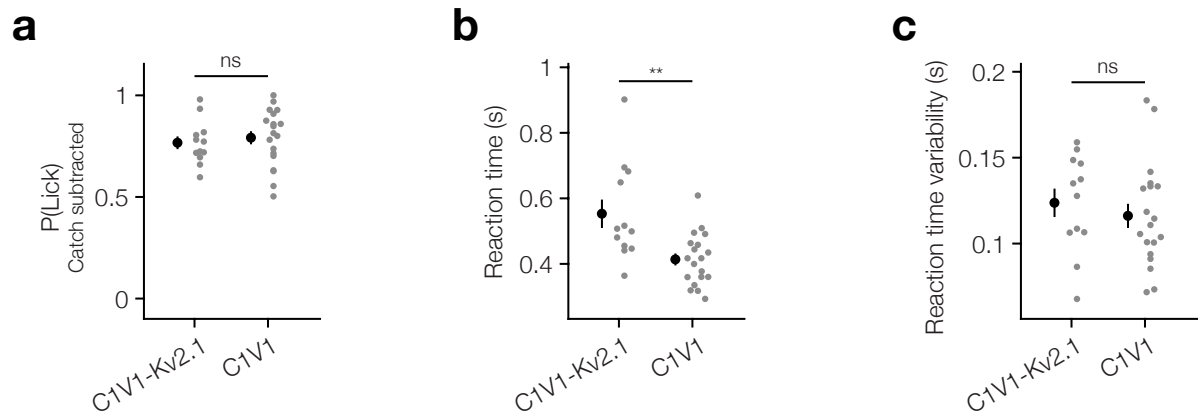
Figure 1 – figure supplement 4 | Example pre-training selection and mapping of 200 neurons in L2/3 barrel cortex.

a, Kv2.1-C1V1-mScarlet expression from an example four-plane imaging volume with stimulation targets overlaid in pink. Neurons are chosen arbitrarily, with the only criteria being that neurons are expressing C1V1 and not too far from FOV centre. Depths relative to most superficial plane (~130 μm below pia). **b**, Pre-training mapping protocol used to assess photostimulatability. Note 200 neurons are mapped in 4 x 50 neuron groups. **c**, Example pixel-wise STA maximum intensity projected across the 4 stimulation groups and the 4 planes with targets overlaid in pink. **d**, Trial-averaged STA traces from ROIs in (c), 50 neurons per group. Note the temporal offset (0.5 s) between activation of each group. Shading denotes s.e.m. $N = 1$ FOV, 1 animal, 200 neurons, 10 trials.



2057
 2058
 2059
 2060
 2061
 2062
 2063
 2064
 2065
 2066
 2067
 2068
 2069
 2070
 2071
 2072

Figure 1 – figure supplement 5 | Rapid transfer learning from 1P to 2P optogenetic stimuli.
a – b Response rates for different 1P and 2P stimulus types from the first session using 2P stimuli, quantified as proportion of trials where animal licked (*a*) and d-prime relative to catch trials (*b*). Note that this includes a combination of Phase 2 (LED/2P/catch trials) and Phase 3 (2P/catch trials) sessions. **c**, Quantification of d-prime relative to our learning criterion (d-prime > 1) for the first and last session using 2P stimuli of different magnitudes. Note that some animals only had 1 session using 2P stimulation of 100 neurons. This session is duplicated in the *First* and *Last* tests against d-prime > 1, but not included in the test for improvement over time. As such these data points appear as grey dots that are not joined by horizontal grey lines. **d – e**, Reaction time mean (*d*) and standard deviation (*e*) for different trial types from the first session using 2P stimuli. Trial types with < 3 responses were excluded from reaction time analyses. **f**, Number of sessions of each step in the training paradigm (coloured bars) and total number of sessions from beginning of 1P training to end of initial 2P training (black bar). For all plots maximum *N* = 12 animals, though individual data-points may have less as not all animals had the same number of training sessions.



2073
 2074
 2075
 2076
 2077
 2078
 2079

Figure 1 – figure supplement 6 | Comparison of behavioural response to somatic and non-somatic C1V1.

a, Animals detect stimulation of somatic and non-somatic C1V1 to similar extents. **b**, Animals response slightly quicker to stimulation of non-somatic C1V1. **c**, Reaction times are similarly consistent across somatic and non-somatic C1V1. All error bars are s.e.m. $N = 12$ C1V1-Kv2.1 mice, 19 C1V1 mice.

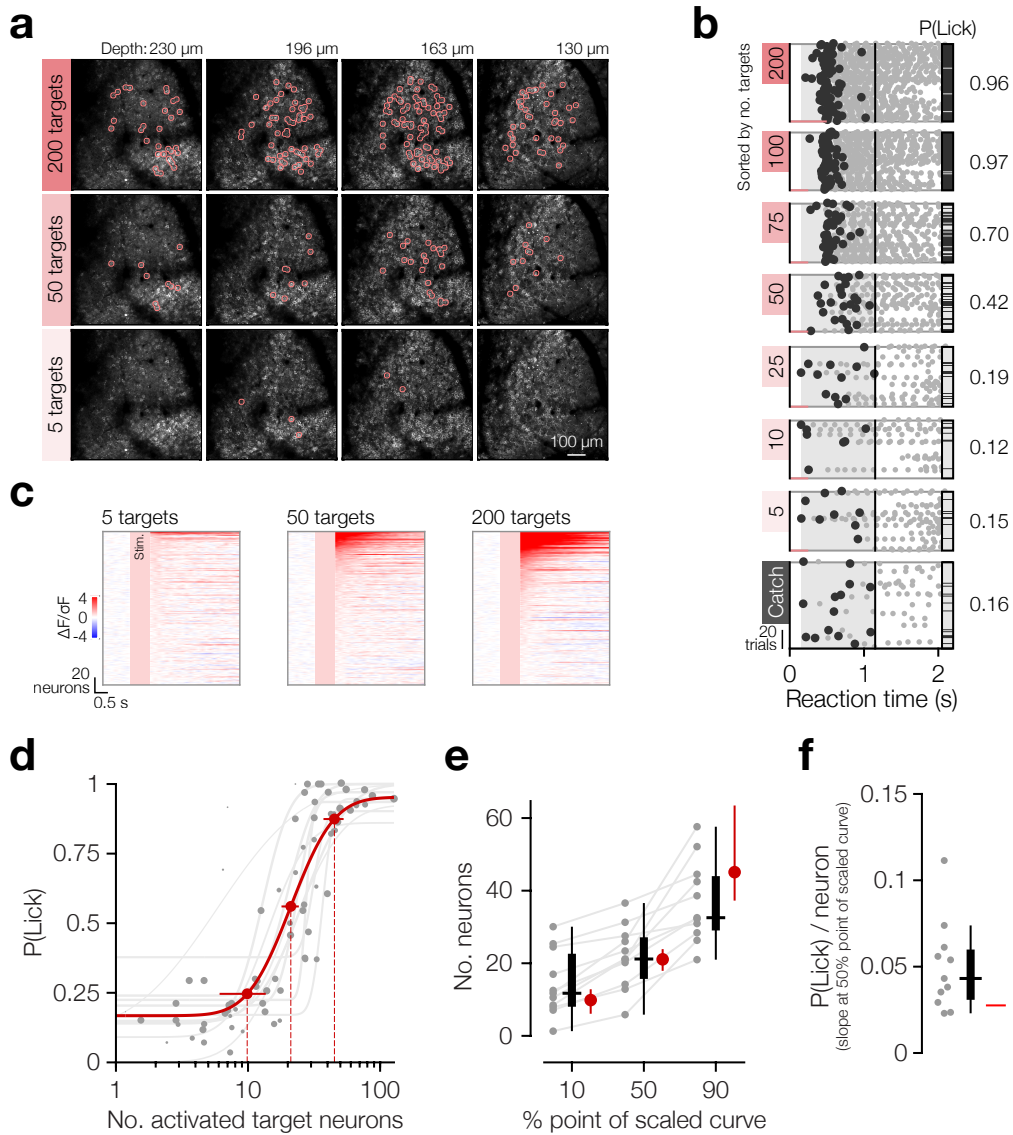


Figure 2 | Animals detect the targeted activation of tens of neurons.

a, Example imaging volumes from an experiment showing 200 (top), 50 (middle) and 5 (bottom) targeted C1V1-expressing neurons. **b**, Example lick raster concatenating an animal's two psychometric curve testing sessions (note data in panels **a** and **c** correspond to the first of these sessions). Trials were delivered pseudo-randomly (see *Methods*) but have been sorted by trial-type for display. Stimulus durations are indicated by coloured bars along the bottom of each raster. Animals respond on more trials and with less variable timing as more neurons are targeted. **c**, Example responses across the top 200 most responsive neurons in the 200 target zones (see *Methods*, **Figure 2 – figure supplement 1**). Neurons have been sorted separately in each plot. Pink boxes indicate the stimulus artefact exclusion epoch which is consistent across all trial-types (see *Methods* for definition). **d**, The psychometric function relating the number of activated target neurons to the behavioural detection rate for all 2P psychometric curve sessions. Individual data (grey dots) are grouped by trial type within session (number of target zones) and plotted as the average number of target neurons activated across all trials of each type. Data point size indicates the number of trials of each type (29 ± 8 trials, range 11 – 44, across data points). Individual psychometric curve fits for each session are plotted (grey lines) weighted by the total number of stimulus trials in the session (202 ± 50 trials, range 97 – 245, across sessions). The aggregate psychometric curve fit across all trial types, all sessions, is plotted in red with the 10%, 50% and 90% points of the scaled curve indicated \pm confidence intervals. The number of activated target neurons required to reach these points are indicated by the red dashed vertical lines. Note that individual curves are often steeper than the aggregate curve. **e**, The number of neurons required to reach the 10%, 50% and 90% points of the scaled psychometric function in **d**.

2102 Grey data points/lines are quantified from individual psychometric curve fits (grey lines in *d*) and
2103 summarized by the black boxplot distributions. Red data points are quantified from the aggregate
2104 psychometric curve fit (red line/dots in *d*) \pm confidence intervals. **f**, The slope at the 50% point of the
2105 scaled curve corresponding to the additional probability of detection (P(Lick)) added per target neuron
2106 activated. Grey data points are quantified from individual psychometric curve fits (grey lines in *d*) and
2107 are summarized by the black boxplot distributions. The red line is quantified from the aggregate
2108 psychometric curve fit (red line in *d*) for which no confidence intervals can be calculated (see *Methods*).
2109 *N* = 11 sessions, 6 mice, 1 – 2 sessions each. All fit parameter error bars are confidence intervals, all
2110 boxplot quantification is median with 25th/75th percentile box and whiskers extending to the last data
2111 points not considered outliers (see *Methods*).
2112

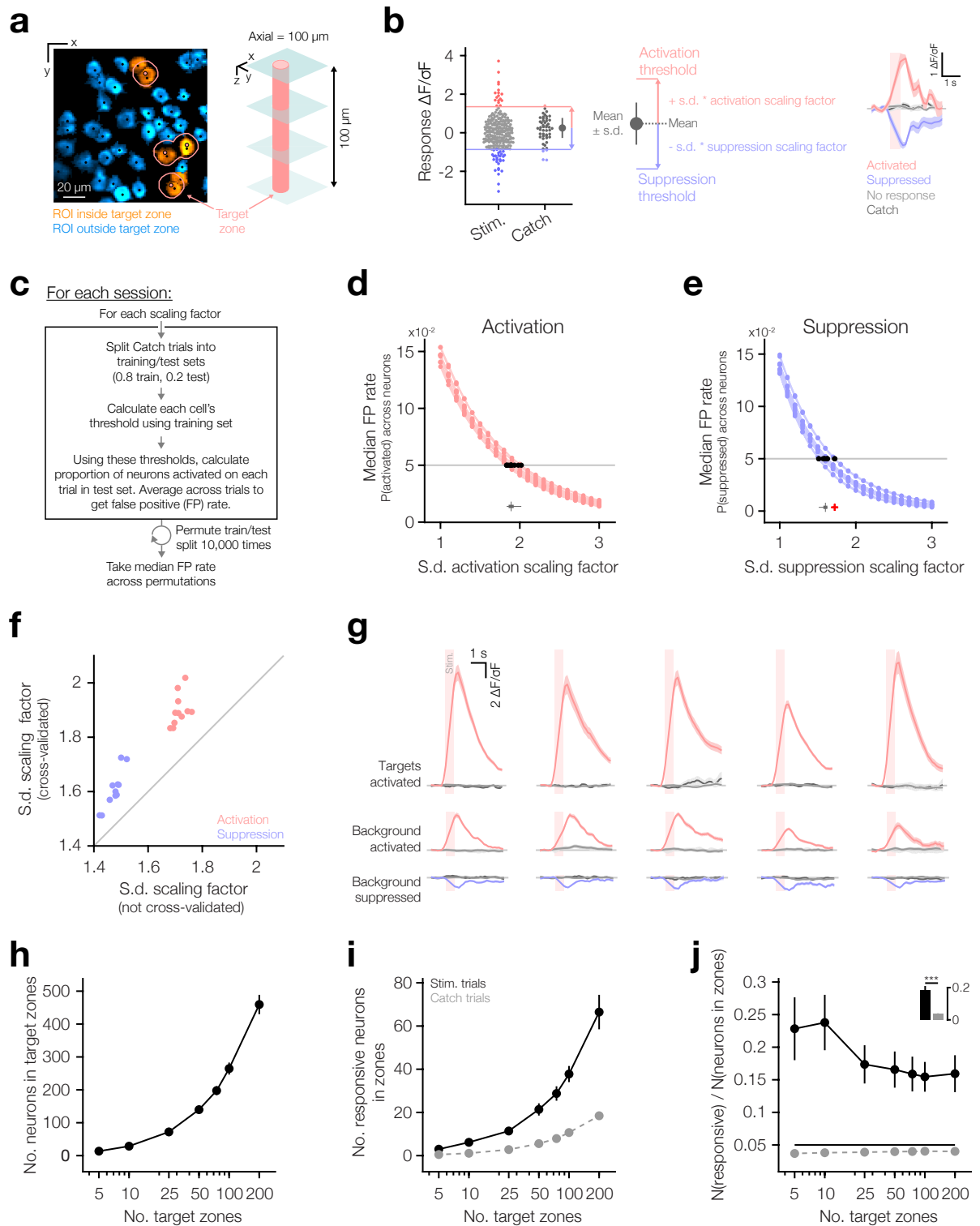
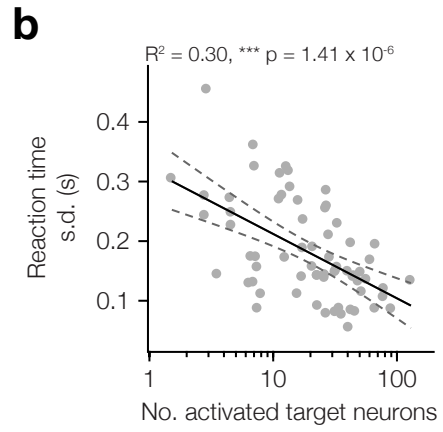
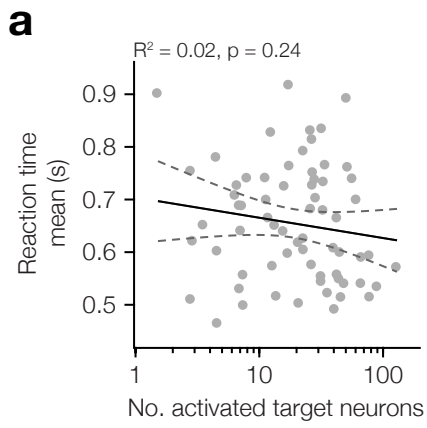


Figure 2 – figure supplement 1 | Quantification of neuronal responses.

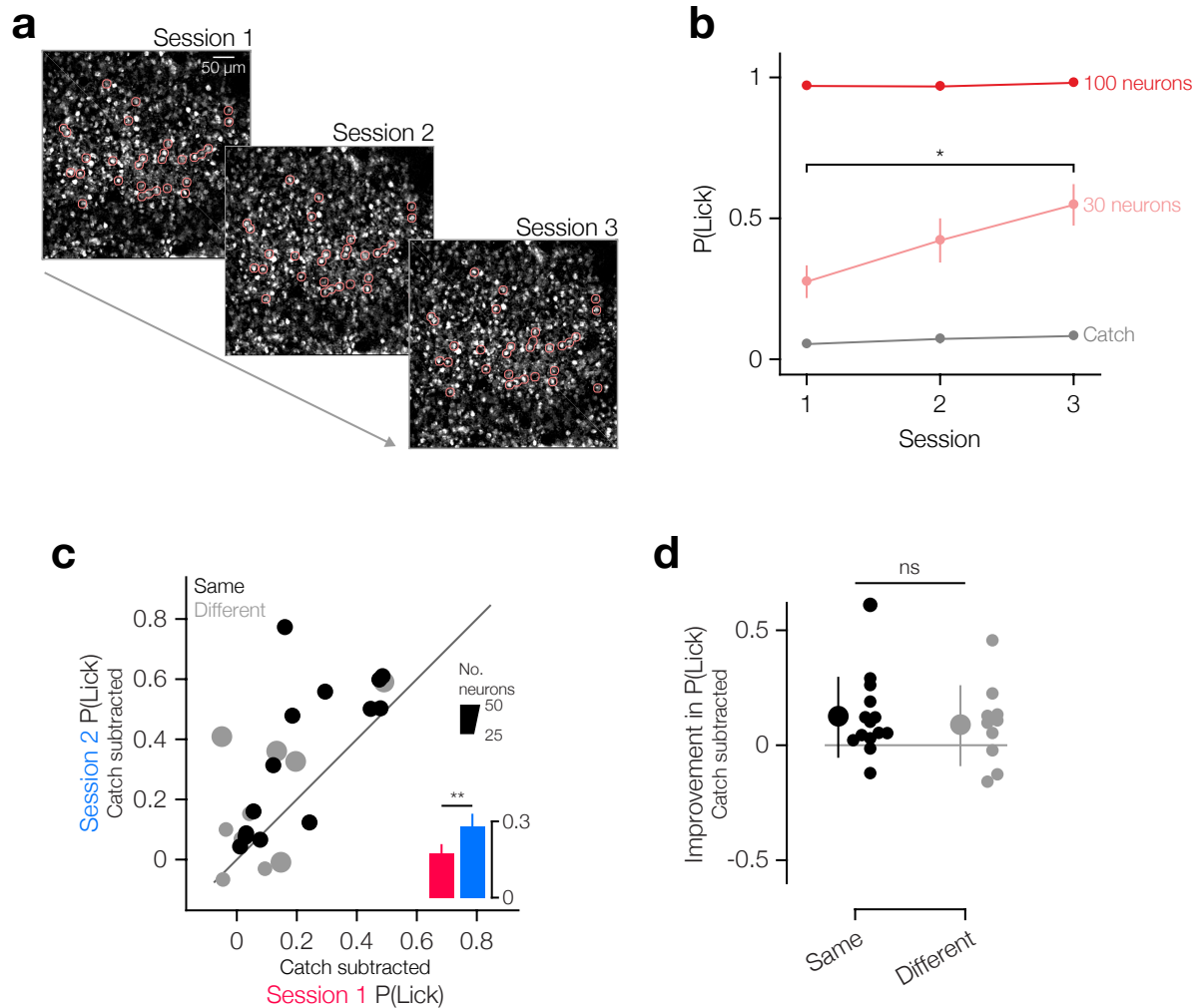
a, Example target zones. *Left*: section of a plane in a volumetric FOV showing Suite2P ROIs (coloured regions), Suite2P centroids (black dots), target co-ordinates (pink dots) and lateral extent of target zone (pink circles; 10 μm radius). ROIs with centroids within the target exclusion zones are considered potential targets (orange ROIs), ROIs outside these regions are considered background neurons (blue ROIs). *Right*: schematic illustrating axial extent of target zone. **b**, Rationale behind activation and suppression thresholds calculated from correct reject (CR) catch trial responses and illustration of the results of our threshold procedure (described in c – e). *Left*: trial-wise responses for a single non-target neuron on stimulus trials of all types and CR catch trials. The mean and standard deviation of

2123 responses on CR catch trials can be used to infer activation and suppression thresholds that separate
2124 stimulus evoked activation (red) and suppression (blue) responses from the majority of CR catch trial
2125 responses. *Middle*: activation and suppression thresholds are computed as the mean + or – the
2126 standard deviation respectively, scaled by a scaling factor (separate scaling factors for activation and
2127 suppression). *Right*: average responses on trials where this neuron was activated (red), suppressed
2128 (blue) or unresponsive (light grey). Catch trials are also included (dark grey). Such a procedure
2129 separates positive and negative going responses from non-responsive trials which should themselves
2130 be indistinguishable from catch trials. **c**, Procedure for inferring cross-validated positive and negative
2131 standard deviation scaling factors that yield a 5% false positive response rate on catch trials for each
2132 session's volumetric FOV. For each session's data, and each threshold type (i.e. activation threshold),
2133 we sweep through a series of scaling factors. For each factor we permute a 80:20 train:test split of
2134 correct reject (CR) catch trials 10,000 times. On each permutation we use the scaling factor and that
2135 permutation's training CR catch trials to calculate each neuron's threshold. Using these neuron-wise
2136 thresholds we then compute the proportion of neurons activated on each testing CR catch trial and
2137 average across trials (false positive rate; FP). We then take the median FP across all permutations at
2138 this scaling factor before moving to the next scaling factor. We can then infer the scaling factor that
2139 yields a 5% FP rate on testing CR catch trials across permutations. **d**, Relationship between standard
2140 deviation scaling factor and FP rate for the activation threshold. Data points are empirically quantified
2141 values, fits are cubic interpolations. The optimal scaling factor for each experiment (horizontal boxplot)
2142 is inferred by finding the scaling factor for which the fitted FP rate is 5% (horizontal line). **e**,
2143 Relationship between the standard deviation scaling factor and FP rate for the suppression threshold.
2144 Data conventions and scaling factor inference the same as *d*. **f**, Scaling factors that yield 5% false
2145 positive rate when all correct reject catch trials are used (not cross-validated, i.e. thresholds inferred
2146 and tested on same trials) compared to those yielded by the cross-validation procedure described in
2147 *c – e*. Cross-validation yields more stringent thresholds. **g**, Example traces from one session for 5
2148 activated target neurons (top row), 5 activated background neurons (middle row) and 5 suppressed
2149 background neurons (bottom row) illustrating responses yielded by our procedure. Averages across
2150 all activated/suppressed trials are shown in red/blue and averages across catch trials/non-responsive
2151 stimulus trials are shown in light and dark grey respectively. Note that neurons in each column are
2152 unrelated. **h**, The number of neurons in all target zones for each trial type (as defined in *a* and *Methods*).
2153 **i**, The number of responsive neurons in all target zones for each trial type on both stimulus trials (black)
2154 and catch trials (grey). **j**, Proportion of responsive neurons in all target zones for each trial type on both
2155 stimulus trials (black) and catch trials (grey) quantified as the number of responsive neurons in target
2156 zones (*i*) divided by the number of neurons in target zones (*h*). *Inset*: Proportion of target zone neurons
2157 that are responsive on stimulus trials compared to catch trials. *N* = 11 sessions, 6 animals, 1 – 2
2158 sessions each for all group data plots. Error bars and shading are mean ± s.e.m.
2159



2160
2161
2162
2163
2164
2165

Figure 2 – figure supplement 2 | Reaction time standard deviation, but not mean, scales with the number of target neurons activated.
a – b, Relationship between mean (a) and standard deviation (b) of reaction time and the number of activated target neurons.



2166
 2167
 2168
 2169
 2170
 2171
 2172
 2173
 2174
 2175
 2176
 2177
 2178

Figure 2 – figure supplement 3 | Detection of small ensembles of neurons improves across days irrespective of whether the same neurons were targeted.

a, FOV from training sessions across 3 consecutive days where we stimulated the same 30 neurons each day **b**, Average behavioural response rates for 100 neuron, 30 neuron and Catch trial conditions for all sessions where we stimulated the same neurons across days ($N = 14$ mice). **c**, Improvement in response rates from session 1 to session 2. Sessions in which we targeted the same neurons are shown in black and sessions where we targeted different neurons in grey. Data-point size denotes number of targeted neurons, scale inset (same neurons group $N = 14$ animals, different neurons group $N = 5$ animals, 2 stim types each). **d**, Sessions targeting the same neurons showed a similar amount of improvement as sessions targeting different neurons (same neurons group $N = 14$ animals, different neurons group $N = 5$ animals, 2 stim types each). All error bars are s.e.m.

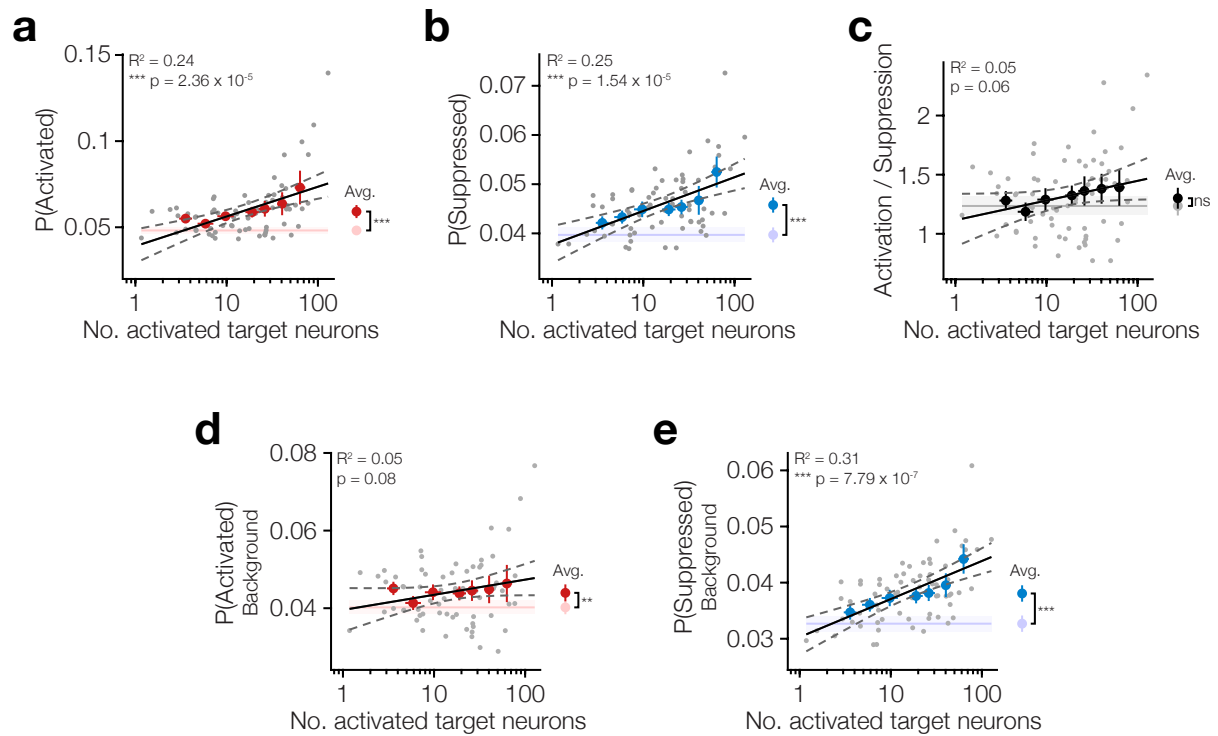
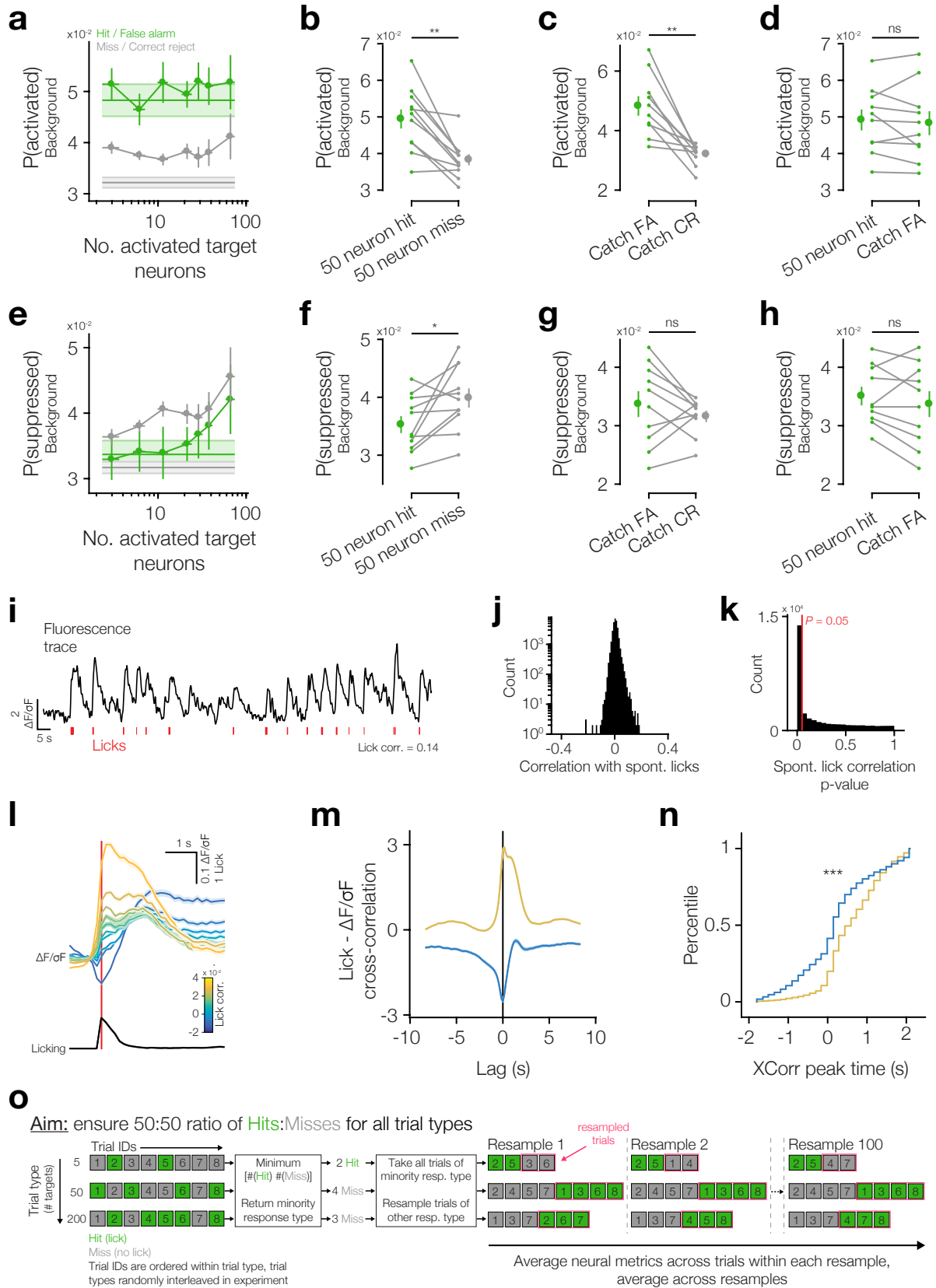


Figure 3 | Increasing target activation is matched by background network suppression.

a, The proportion of neurons activated across all neurons (targets and background) increases as more target neurons are activated. *Inset right*: average activation across all trial types is increased on stimulus trials compared to catch. **b**, The proportion of neurons suppressed across all neurons (targets and background) increases as more target neurons are activated. *Inset right*: average suppression across all trial types is increased on stimulus trials compared to catch. **c**, The ratio of activation and suppression is similar to that observed on catch trials (*inset right*) and isn't strongly modulated by the number of activated target neurons. **d**, Stimulation of target neurons causes mild activation of background neurons (targets excluded; *inset right*) but this is not modulated by the number of target neurons activated. **e**, Stimulation of target neurons causes suppression of background neurons (targets excluded; *inset right*) which increases as more target neurons are activated. All data are hit:miss matched to remove potential lick signals (see **Figure 3 – figure supplement 1** and *Methods*). For all plots $N = 11$ sessions, 6 animals, 1 – 2 sessions each. Some trial types from some sessions are excluded for having too few hits or misses to be able to match the hit:miss ratio. Error bars and shading are mean \pm s.e.m; data points, error bars and linear fits are stimulus trials, shading is catch trials; grey data points: individual trial types, individual sessions; coloured error bars: data averaged within trial type (number of target zones) across sessions; linear fits are to individual data points; fits are reported \pm 95% confidence intervals.

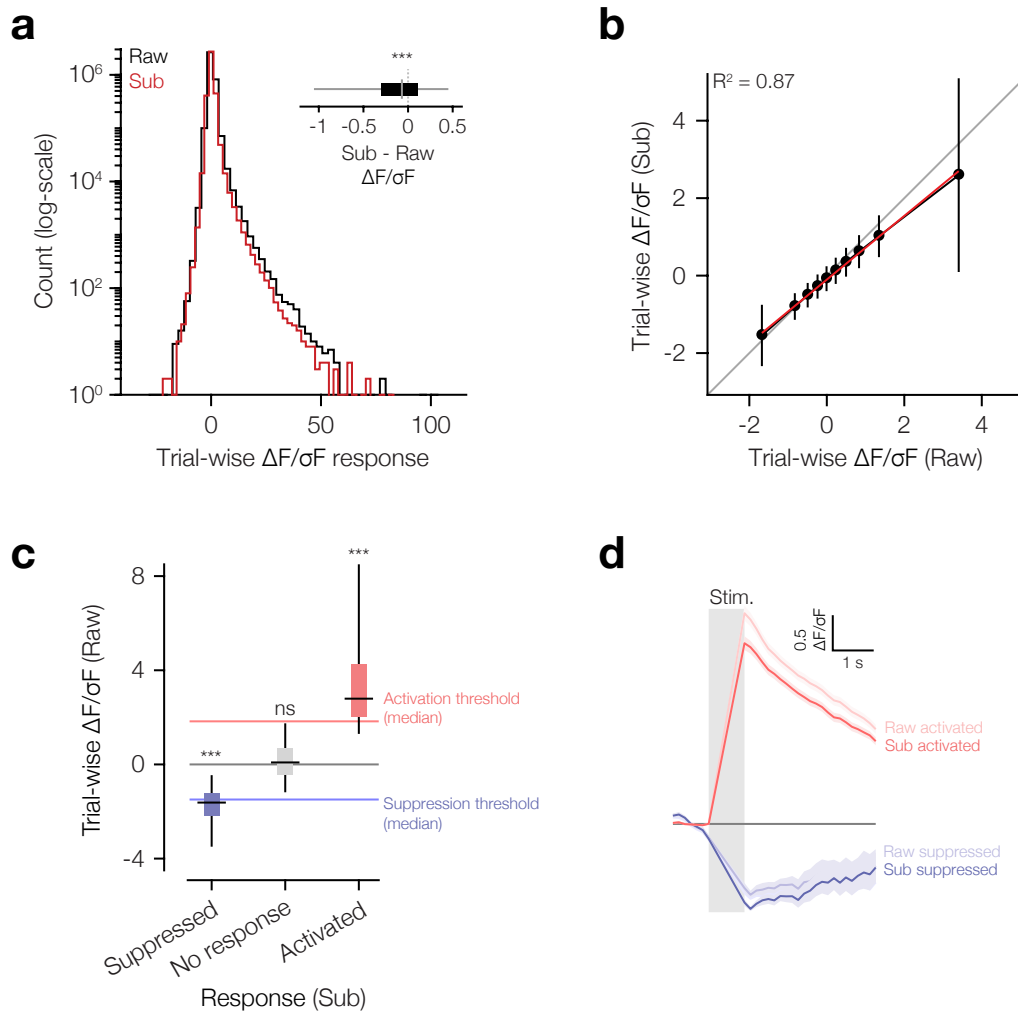


2199
2200
2201
2202
2203
2204

Figure 3 – figure supplement 1 | Comparison of network activity on Hits and Misses for both threshold Go trials and Catch trials in an effort to quantify and account for lick responses.

a, The proportion of background neurons activated when different numbers of target neurons are activated on hits/false alarms (green) and misses/correct rejects (grey) on stimulus trials (error bars) and catch trials (shading). Background neurons become more active on stimulus hits and catch false

2205 alarms and there does not seem to be much modulation of the amount of background activation by
2206 the number of activated target neurons. Note that the background neuron activation response on
2207 stimulus trials overlaps with the response on catch trials across the full range of number of target
2208 neurons activated. **b**, The proportion of activated background neurons is higher on stimulus hit trials
2209 than miss trials. Note that we used the 50 target zone stimulation trial type as it has a roughly equal
2210 number of hits and misses. **c**, The proportion of activated background neurons is greater on catch
2211 false alarms (FA; when animals lick) than on catch correct rejects (CR; when the animal don't lick). **d**,
2212 The proportion of activated background neurons does not differ between 50 target zone stimulus trial
2213 hits and catch trial false alarms raising the concern that this response is due to licking, not
2214 photostimulation. **e**, The proportion of background neurons suppressed when different numbers of
2215 target neurons are activated. Same colour conventions as in *a*. Stimulus hits are associated with
2216 decreased levels of background suppression than misses, and this appears to be somewhat
2217 modulated by the number of activated target neurons. Catch trial false alarms are associated with
2218 marginally more suppression than catch trial correct rejections. **f**, The proportion of suppressed
2219 background neurons is lower on hits than misses. **g**, The proportion of suppressed background
2220 neurons does not differ significantly between false alarms and correct rejects on catch trials. **h**, The
2221 proportion of suppressed background neurons does not differ between 50 target zone stimulus trial
2222 hits and catch trial false alarms. **i**, Fluorescence trace from an example neuron with photostimulation
2223 trial epochs removed (black trace) with licks denoted below (red ticks). This neuron had a lick
2224 correlation of 0.14. The fluorescence trace has been Gaussian smoothed ($\sigma = 1\text{s}$) for display only. **j**,
2225 Distribution correlation values across all neurons recorded. **k**, Distribution of *P*-values for correlation
2226 values reported in *b*. 46 ± 11 % of neurons are lick modulated ($\alpha = 0.05$). **l**, *Top*: Average traces from
2227 neurons binned into 10 equal bins by their lick correlation (trace colours) aligned to the onset of
2228 spontaneous licking (red line). *Bottom*: average across all spontaneous lick bouts. **m**, Lick –
2229 fluorescence cross-correlation for all lick responsive neurons positively modulated (yellow) or
2230 negatively modulated (blue) by licking. **n**, Distribution of the time of maximum |cross-correlation| for
2231 positively modulated (yellow) and negatively modulated (blue) neurons in a 4 s window centred on the
2232 0 time-lag of the cross-correlation. $P = 2.75 \times 10^{-160}$ Mann Whitney U-Test, $N = 9547$ positively lick-
2233 modulated neurons and 4365 negatively modulated neurons. **o**, Schematic illustrating the procedure
2234 used to ensure a 50:50 ratio of hits:misses for each trial type. This is done to remove the effect of
2235 increased recruitment of licking, and thus lick evoked neural responses, by stimulating target
2236 ensembles of increasing size. For a given trial type, say 5 target zones, we find the number of hits and
2237 misses and find the minority response type. For 5 target zone trials, which aren't reliably detected by
2238 animals, this will likely be hits. We then take all hit trials and combine them with random resamples of
2239 miss trials of the same number as hit trials. For example if we only have 2 hits and 6 misses then for
2240 each random resample we would take all 2 hits and 2 random misses. In this way we ensure that we
2241 have an equal number of hit and miss trials. We then calculate neuron response metrics across the
2242 subset of hits and misses in each resample and average these metrics across resamples. All shading
2243 is s.e.m. $N = 11$ sessions, 6 mice, 1 – 2 sessions each.
2244

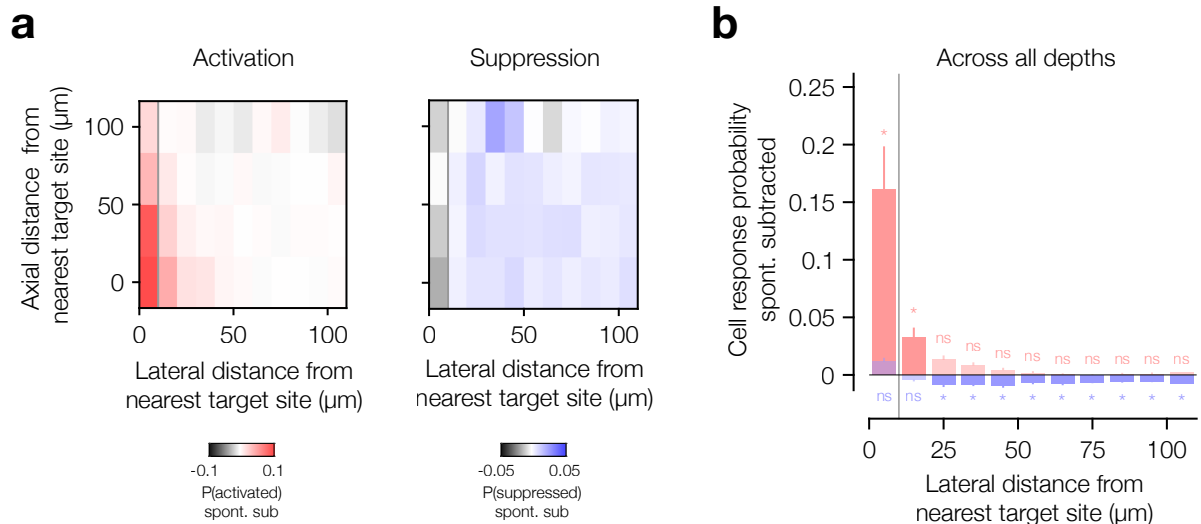


2245
2246
2247
2248
2249
2250
2251
2252
2253
2254
2255
2256
2257
2258
2259
2260
2261
2262
2263
2264
2265
2266
2267
2268
2269
2270

Figure 3 – figure supplement 2 | Neuropil subtraction has a small effect on response amplitude but it is not the sole cause of negative going responses.

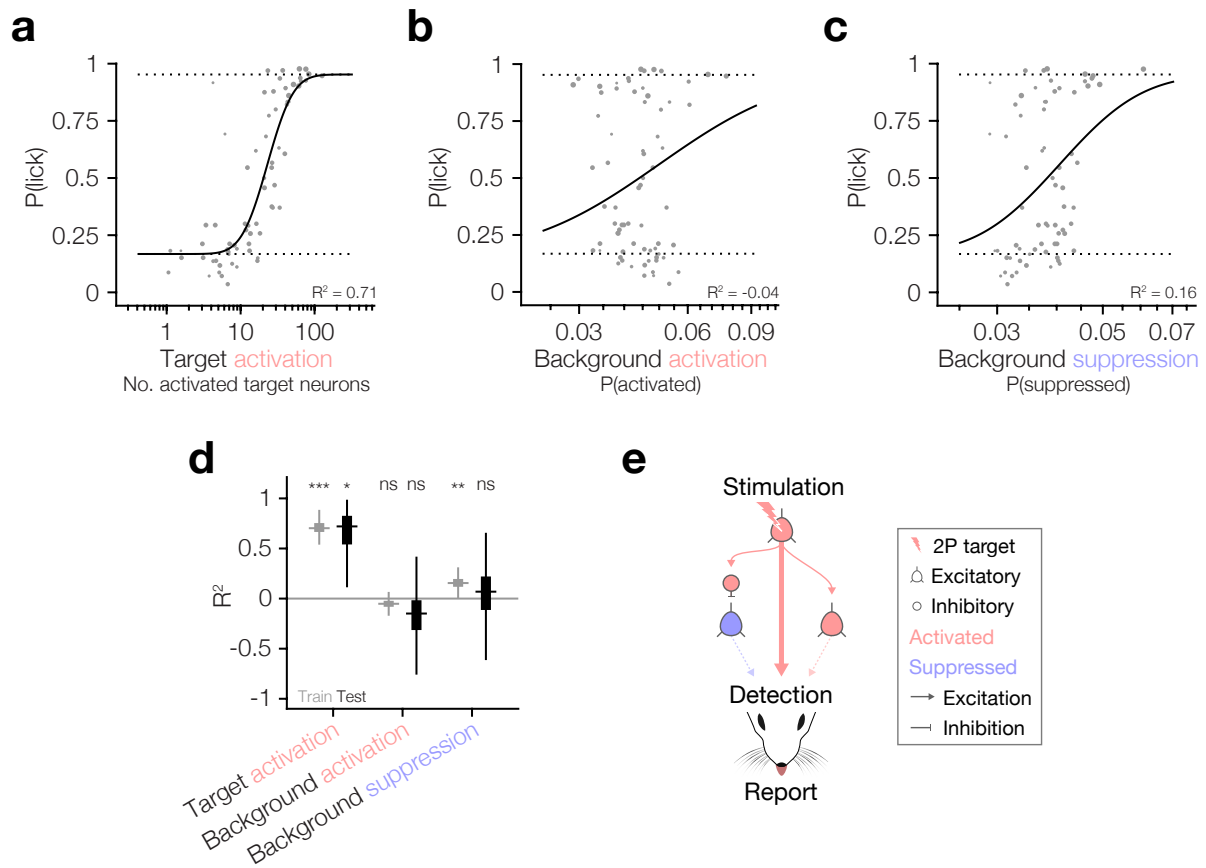
a, Distribution of trial-wise responses on 50+ neuron stimulation trials calculated from raw (Raw; black) and neuropil subtracted (Sub; red) traces ($N = 30,894$ neurons, 1312 trials). A large fraction of negative responses are observed even in raw traces without neuropil subtraction. *Inset*: Difference between each neuron’s trial-wise response when responses were calculated from neuropil subtracted or raw traces (Sub – Raw). Responses are slightly reduced when traces are neuropil subtracted ($-0.16 \pm 0.58 \Delta F/\sigma F$, $P = 0$ Wilcoxon signed-rank test). **b**, Neuropil-subtracted trial-wise responses are highly correlated with raw trial-wise responses ($R^2 = 0.87$, $P = 0$) though slightly reduced ($\beta_0 = -0.10 \pm 5.32 \times 10^{-4}$, $P = 0$) with this reduction mainly limited to large positive going responses ($\beta_1 = 0.82 \times 10^{-1} \pm 3.31 \times 10^{-4}$, $P = 0$). Red: linear fit to data, Black: neuropil-subtracted data binned into deciles by raw trial-wise response and averaged within decile. Data are mean \pm s.d. **c**, Trial-wise responses classified as suppressed, activated and no response using neuropil-subtracted traces also show negative ($-1.75 \pm 1.05 \Delta F/\sigma F$, $P = 0$ Wilcoxon signed-rank test), roughly zero ($0.16 \pm 0.94 \Delta F/\sigma F$, $P = 0$, Wilcoxon signed-rank test) and positive ($3.72 \pm 3.18 \Delta F/\sigma F$, $P = 0$ Wilcoxon signed-rank test) trial-wise responses calculated from raw traces in the same trials. These groups also differed significantly from each other ($P = 0$ Kruskal-Wallis test; Suppressed vs No response, $P = 0$, Suppressed vs Activated, $P = 0$, No response vs Activated, $P = 0$, Bonferroni corrected for multiple comparisons) indicating that our thresholds on neuropil subtracted traces reliably separate different classes of trial-wise responses even in the absence of neuropil-subtraction. **d**, Example raw (light red, light blue) and neuropil-subtracted (dark red, dark blue) traces for neurons reliably activated (red) and suppressed (blue) across trials (using neuropil-subtracted trial-wise magnitudes). Neuropil subtraction slightly decreases response magnitudes in both groups, though doesn’t induce large changes in response time-course. Negative responses can be seen with and without neuropil-subtraction. Shading is mean \pm s.e.m across neurons. Traces have been linearly interpolated across the photostimulation epoch (grey box)

2271 to avoid the photostimulation artefact for display only. All box-plots are median (mid-line) with 25th and
2272 75th percentiles (box) and 5th and 95th percentiles (whiskers). $N = 3.68 \times 10^6$ trial-wise responses, 30894
2273 neurons, 11 sessions, 6 mice, 1 – 2 sessions each.
2274



2275
2276
2277
2278
2279
2280
2281
2282
2283
2284
2285
2286
2287

Figure 3 – figure supplement 3 | Activation and suppression have different spatial profiles.
a, Lateral and axial spatial profile of activation (*left*) and suppression (*right*) relative to nearest target site co-ordinate: for each neuron plot its distance to nearest target site co-ordinate vs the proportion of trials it was activated or suppressed. Bin spatial distances and then average across all neurons in each bin. Average this value across stimulus trial types. **b**, Quantification of spread of activation and suppression with lateral distance, collapsed across all axial planes. All data in all panels are hit:miss matched (see **Figure 3 – figure supplement 1** and *Methods*) and have had catch trial values subtracted. All tests in *b* are Wilcoxon signed-rank tests, Bonferroni corrected for the number of lateral bins. * denotes $P < 0.05$. $N = 10$ sessions, 6 mice, 1 – 2 sessions each. Note one session was excluded as there were no hits on catch trials so we were unable to subtract a hit:miss matched neural response rate on catch trials from the stimulus trial data. Error bars are s.e.m. and spatial bin widths are $10 \mu\text{m}$.



2288
 2289
 2290
 2291
 2292
 2293
 2294
 2295
 2296
 2297
 2298
 2299
 2300
 2301
 2302
 2303
 2304
 2305
 2306
 2307
 2308
 2309

Figure 4 | Behaviour follows the activity of targeted ensembles despite matched suppression in the local network.

a – c, Psychometric curve fits relating behavioural detection to the number of targets activated (**a**), the proportion of the background network activated (**b**) and the proportion of the background network suppressed (**c**). Solid lines: psychometric curve fit; dotted lines: fixed lapse rate (upper) and false alarm rate (bottom) for psychometric fit. Note that all neural data has been hit:miss matched (see *Methods*) so the effective $P(\text{lick})$ for all datapoints is 0.5, however for each datapoint we fit the actual recorded $P(\text{lick})$. The similarity of panel **a**, which is hit:miss matched, to **Figure 2d**, which isn't, demonstrates that the contribution of lick signals to the relationship between target activation and behaviour is negligible. Fits and R^2 values reported are quantified on all data (compared to cross-validated fits in following panels). For these panels $N = 11$ sessions, 6 animals, 1 – 2 sessions each. Some trial types from some sessions are excluded for having too few hits or misses to be able to match the hit:miss ratio. **d**, Variance explained (R^2) by the three predictors in **a – c** during the training (grey) and testing (black) phases of cross-validation (10,000 permutations of 80:20 train:test split). Only target activation strongly and reliably explains behaviour across both training and testing. Background suppression is mildly predictive of behaviour in model training datasets, but this relationship does not generalise to test datasets. Background activation does not explain behaviour. Boxplots are median with 25th/75th percentile boxes and whiskers extending to the most extreme data points not considered outliers (see *Methods*). **e**, Schematic summarising the three tested routes from cortical activation to behavioural report highlighting that only the activity of target neurons has any reliable influence on behaviour despite matched suppression in the local network.